Ratchet phenomena in quantum dissipative systems with spin-orbit interactions

D I S S E R T A T I O N

zur Erlangung des

DOKTORGRADES DER NATURWISSENSCHAFTEN (DR. RER. NAT.)

der Naturwissenschaftlichen Fakultät II - Physik

der Universität Regensburg

vorgelegt von

SERGEY SMIRNOV *aus* ***SKHODNYA,***
MOSKAU REGION, RUSSLAND

im September 2009

Ratchet phenomena in quantum dissipative systems with spin-orbit interactions

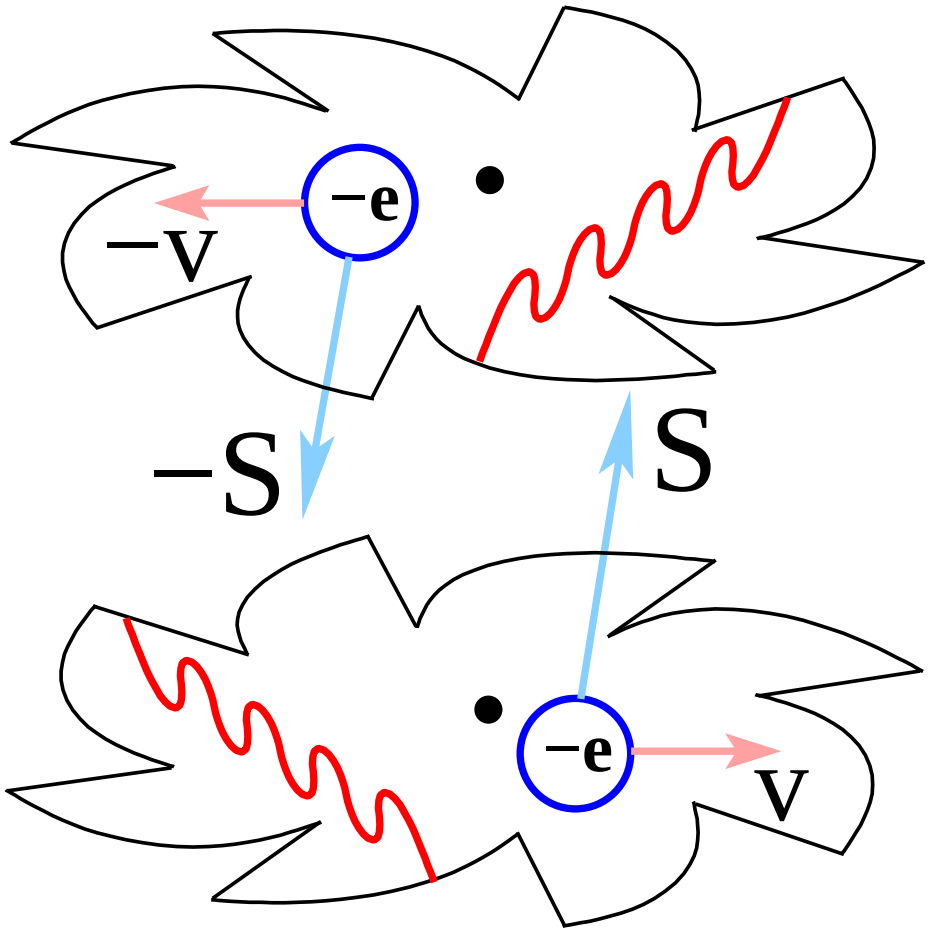

D I S S E R T A T I O N

Promotionsgesuch eingereicht am:	30.06.2009
Die Arbeit wurde angeleitet von:	Prof. Dr. Milena Grifoni
Prüfungsausschuß:	
Vorsitz:	Prof. Dr. Sergey Ganichev
Erstgutachten:	Prof. Dr. Milena Grifoni
Zweitgutachten:	Prof. Dr. Klaus Richter
	Prof. Dr. Vladimir Braun
Datum des Promotionskolloquiums:	25.09.2009

Contents

Chapter 1

Introduction

In this introductory chapter the general concept of a particle ratchet mechanism is introduced. The role of the spatial and time asymmetry is emphasized. The implementation of this concept in classical and quantum systems is described. The spin ratchet concept is presented as a natural generalization of the particle ratchet mechanism. Coherent and dissipative spin ratchets are discussed as two different realizations of the spin ratchet concept. The focus and the structure of the thesis are outlined at the end of the chapter.

1.1 Particle ratchets

1.1.1 General concepts

The particle ratchet mechanism is defined for a system driven by time-dependent external forces with zero time average (also called unbiased forces) and consists in directed particle transport under some asymmetry either in the system or in the driving forces. If the particles involved in the ratchet transport have non-zero charge, the particle ratchet mechanism is also referred to as the charge ratchet mechanism.

Role of the space asymmetry

The term "ratchet" was historically borrowed from the asymmetric toothed wheel. It was believed that in a system driven by unbiased forces directed transport in a given direction was only possible if the system did not have the inversion center in space. A simple example is a windmill. Its asymmetric sails are constructed in such a way that unbiased flow of air is converted into a directed rotation which is subsequently converted into useful work. The particle ratchets with space inversion asymmetry are also called space ratchets.

Role of the time asymmetry

It turns out that even when a system has the inversion center, directed particle transport can still be induced by unbiased forces if these forces are asymmetric in time. The

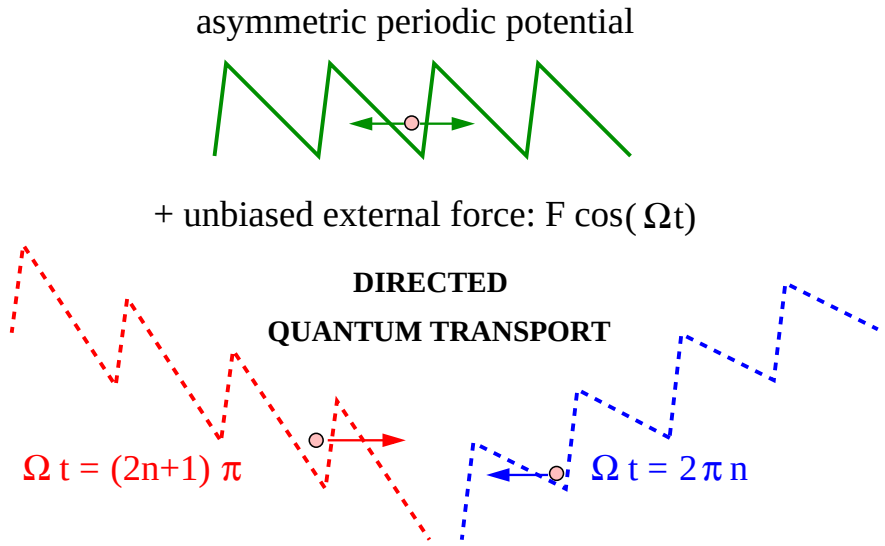

Figure 1.1: The space rocked ratchet based on quantum mechanical tunneling. The two rocking situations at times $t = \pi(2n+1)/\Omega$ and $t = 2\pi n/\Omega$, $n = 0, \pm 1, \pm 2, \ldots$, induce tunneling processes which have different rates in opposite directions.

particle ratchets of this type are usually called time ratchets. Although these class of particle ratchets will not be in the focus of the present thesis, it will be useful below in this introductory chapter to mention some relevant examples in order to later make comparison with the space ratchets.

Rocked ratchets

The ratchet mechanism arising when an external unbiased force rocks the periodic potential is called the rocked ratchet mechanism. This type of ratchets is considered in the present thesis within the quantum mechanical context (see Fig. 1.1). The rocked ratchets should be distinguished from other kinds of ratchets like temperature ratchets or flashing ratchets where the ratchet mechanism appears through either periodic variation of the bath temperature or switching off and on the periodic potential, respectively.

Mechanics

The concept of the particle ratchet mechanism and the roles of space and time asymmetry are general for both classical and quantum mechanics. In particular, space and time ratchet effects can be found in both classical and quantum systems. However, the underlying physical details are much different in classical and quantum cases. Therefore it is convenient to consider the classical and quantum ratchet effects separately. We start with the ratchets based on classical mechanics and then discuss the quantum mechanical ratchets which are in the focus of this thesis.

1.1.2 Ratchets in classical mechanics

To clearly show the essence of the ratchet transport it is better to start with the case of classical mechanics. To simplify the discussion it is convenient to consider a particle in a one-dimensional (1D) space: a particle having mass m moving in a spatially periodic potential $U(x)$ is subject to an unbiased driving force $F(t)$ and interacts with an external environment characterized by viscosity coefficient η and stochastic force $\xi(t)$. The dynamics of this system is described by the classical equation of motion,

$$m\frac{d^2x(t)}{dt^2} + \eta\frac{dx(t)}{dt} + \frac{dU[x(t)]}{dx} = F(t) + \xi(t). \tag{1.1}$$

The particle velocity at time t is $v(t) \equiv dx(t)/dt$. The ratchet effect exists if the averaged particle velocity,

$$v^{\infty} \equiv \lim_{t\to\infty}\frac{1}{t}\int_0^t dt'\, v(t'), \tag{1.2}$$

is not equal to zero.

When $U(x) = 0$ and $F(t) = 0$, Eq. (1.1) describes Brownian motion [1], which was originally observed as a random motion of pollen particles suspended in water.

Brownian motors [2] are the physical systems where work is extracted out of thermal fluctuations. In this case the stochastic force $\xi(t)$ and the friction force $-\eta dx(t)/dt$ result from a coupling to a thermal bath. However, this extraction of work is only possible if the particle is not in thermal equilibrium with the bath as otherwise the second law of thermodynamics would not be respected. The role of the force $F(t)$ in Eq. (1.1) is exactly to break the thermal equilibrium between the particle and thermal bath. If in such a system the thermodynamic equilibrium with the thermal bath to which the system is coupled is broken by an unbiased force, *i.e.*, $\lim_{t\to\infty}\frac{1}{t}\int_0^t dt'\, F(t') = 0$, the corresponding Brownian motor represents a particular realization of the particle ratchet mechanism. However, it is clear that not all Brownian motors are particle ratchets as well as not all particle ratchets are Brownian motors. The ideas of the particle ratchet and Brownian motor mechanisms have a common domain but they also have huge areas which belong only to one of them. The most essential feature of the particle ratchet and Brownian motor mechanisms is that they only make sense out of equilibrium. The impossibility to observe at thermal equilibrium the particle ratchet mechanism implemented as a Brownian motor was proven in an early work by Smoluchowski [3].

A few examples

A classical particle ratchet mechanism when $U(x)$ is asymmetric in space and $F(t)$ is symmetric in time, that is a classical space ratchet, was studied in Ref. [4]. It was shown that the driving force could destroy detailed balance and as a result the second law of thermodynamics.

The rocked ratchet dynamics in a classical system with $\xi(t) = 0$ in Eq. (1.1) and for the case $U(x) \neq U(-x)$ was investigated by Jung *et al.* [5]. The authors examined both the regular and chaotic ratchet mechanisms. In the chaotic case it was found that

deterministically induced chaos can mimic the role of noise. Multiple reversals of the current as a function of the driving amplitude have been predicted. The physical origin of these multiple reversals was revealed by Mateos [6]. It turned out that the current changes its sign because of the bifurcation from chaotic dynamics to periodic one as was clarified comparing the bifurcation diagram of the system with the dependence of the current on the driving amplitude.

Since in the chaotic regime the dynamics is highly sensitive to the initial conditions, the current reversals can even happen without changing a control parameter. The point is that there can coexist several attractors in the phase space of a dynamical system. For the rocked ratchet model a chaotic and periodic attractors can coexist [7]. The periodic attractor generates current in one direction and the chaotic one generates current in the opposite direction. Even a small deviation in the initial conditions will change the dynamics from one attractor to another one and the current will change sign. This effect finds applications in particle selections from ensembles of particles whose initial conditions have some distributions in phase space.

The role played by the viscosity coefficient η in the classical rocked ratchet was studied by Borromeo *et al.* [8]. The numerical results showed that there is a critical value η_c below which the dynamics becomes chaotic and the ratchet current monotonically goes to zero. Above the critical value the ratchet efficiency reaches its maximum close to η_c.

When the stochastic force is present, $\xi(t) \neq 0$ in Eq. (1.1), the classical particle rocked ratchets acquire new features. The dynamics suffers essential changes. This can already been seen in the case of the symmetric in space periodic potential $U(x)$ and symmetric in time driving force $F(t)$. Although in this case the ratchet effect does not appear, the dynamics has qualitatively changed. This can be detected by additionally applying a constant force. Surprisingly, in the case of thermal equilibrium fluctuations, zero-mean Gaussian white noise, $\langle \xi(t) \rangle = 0$, $\langle \xi(t)\xi(t') \rangle = \delta(t - t')$, particles start moving against this constant force: the phenomenon of absolute negative mobility has a pure noise origin [9].

The optimization of the classical rocked ratchet efficiency in the presence of stochastic force was numerically performed in Ref. [10] for the case of zero-mean Gaussian white noise and symmetric periodic driving. At very weak noise and large driving frequencies the ratchet velocity was maximized and its fluctuations were minimized for some values of the driving amplitude. In the work of Marchesoni *et al.* [11] it was shown that the behavior of the classical rocked ratchets is extremely different at very close physical conditions: in the absence of noise and at vanishingly low noise level. In the first case the dynamics is chaotic and unpredictable leading to small ratchet currents for heavy particles. In the second case the dynamics is stable, the ratchet currents are large and can be optimized by varying the viscosity coefficient.

The classical ratchet mechanism with zero stochastic force, $\xi(t) = 0$, was studied in Ref. [12]. The dynamical evolution was both periodic and chaotic. It was found that when the periodic potential $U(x)$ is symmetric in space and the unbiased driving force $F(t)$ is asymmetric in time, a non-zero stationary particle current exists, that is the time ratchet mechanism described above is realized in this classical system.

There are other types of classical ratchets. They are based on electronic systems. When the wave nature of electrons does not play any role in the ratchet mechanism, it is in fact the classical particle ratchet mechanism. Below a few examples of such an implementation of the classical particle ratchet mechanism are given.

The experiments on an antidot lattice showed that the classical space rocked particle ratchet mechanism could appear in two-dimensional (2D) electronic systems [13]. In these experiments the electronic system was used in an antidot array based on a GaAs/AlGaAs heterostructure. The temperature was 4.2 K. The antidot lattice had a square shape with a triangular basis resulting in a 2D system without an inversion center in space. The lattice period was 0.5 μm while the antidots had the base width 0.3 μm and the height 0.2 μm. The sample was illuminated by modulated far-infrared (wavelength 119 μm) radiation. As a result of this irradiation a lateral photovoltage appeared. The sign of this photovoltage depended on the magnitude of the magnetic field perpendicular to the plane of the antidot lattice.

The antidot experiments mentioned above were also done under irradiation with linearly polarized microwaves and at higher temperatures [14]. The 2D antidot array was based on a high mobility two-dimensional electron gas (2DEG) formed in a GaAs/AlGaAs heterostructure. The antidots had the semidisk geometry with the radius 0.5 μm. The lattice period was 1.5 μm. The temperature range in the experiments was 1-100 K. At 1.5 K the electron mean-free path was 15-30 μm which was much larger than the antidot spacing. A net charge current was found to be finite. Its direction depended on the polarization of the microwave irradiation. The ratchet current vanished at 70K. At this temperature isotropic phonon scattering became dominant, the electron mean-free path was 1.7 μm which was comparable with the lattice period. In this case the electrons did not feel the antidot lattice anymore and the ratchet effect disappeared. The effect of electron-electron interactions on the ratchet behavior in a semidisk antidot lattice was theoretically studied in Ref. [15] within the semiclassical Boltzmann formalism. It was predicted that the ratchet mechanism existed in the interacting case and that the interactions in the system could enhance the ratchet effect.

The classical particle ratchet mechanism based on the Seebeck effect was predicted by Blanter *et al.* [16]. The Seebeck effect is an effect of classical electrodynamics. It consists in the appearance of an electrical current in a circuit composed of two conductors made from different materials when the junctions between these conductors have different temperatures. The circuit is equivalent to a 1D periodic system in which the potential and temperature variation have the same period. As it was noticed in Ref. [16], the crucial role in the appearance of the ratchet current was in the phase shift between the periodic potential and periodic variation of the temperature. Even when the periodic potential was symmetric in space the ratchet current was still finite for a finite value of the phase shift. This result demonstrated that a temperature modulation was equivalent to an external driving force. The ratchets based on the presence of both periodic potential and periodic temperature variation are termed as Seebeck ratchets. These ratchets and their close relatives were theoretically considered in Ref. [17].

The Seebeck ratchet effect was experimentally observed by Olbrich *et al.* [18]. In

these experiments gratings of 0.5 μm width and period 2.5 μm were used to create a 1D superlattice in a 2DEG located in an n-type GaAs/AlGaAs quantum well structure. Technically the periodic potential was formed by means of grooves the shape of which could be varied in order to control the symmetry of the periodic potential. The ratchet effect was induced by electromagnetic radiation. The appearance of an electric current in this case is usually called photogalvanic effect. This effect can appear due to either the microscopic spatial inversion asymmetry or macroscopic one related to the superlattice structure. The GaAs/AlGaAs heterostructure used in the experiment was grown along the (001) direction and therefore it had C_{2v} point-group symmetry. This symmetry forbids in-plane photogalvanic effect under normal incidence. Therefore, Olbrich and colleagues used the normal incidence to exclude the microscopic photogalvanic effect in order to study the photocurrents induced by the superlattice potential. The electromagnetic radiation played two different roles. The first role was just the role of driving. In this case the classical particle ratchet mechanism was detected when the periodic potential was asymmetric in space. To remove this space rocked ratchet effect the periodic potential was made spatially symmetric. The second role of the electromagnetic radiation consisted in creating a periodic temperature variation. Due-to near-field effects in the grooved superlattice the distribution of the electric field in the superlattice was inhomogeneous. The electric field became periodic. Its period was equal to the period of the superlattice. The decisive circumstance was that the periodic potential and periodic radiation intensity being of the same period had a finite relative phase shift. The periodic radiation intensity induced without any phase shift a periodic variation of the local non-equilibrium temperature. This periodic temperature variation had the same period as the radiation intensity, *i.e.*, it was equal to the period of the superlattice. As a result the periodic potential and periodic temperature variation had the same period and a finite phase shift. In this way the Seebeck ratchet was experimentally implemented and the corresponding finite ratchet currents were detected even for the case of a spatially symmetric superlattice potential.

Other important examples of the classical particle ratchet mechanism involve the biological realm, transport in nanopores, microfluidics. The detailed description of these and other sundry physical implementations of the classical particle ratchet mechanism can be found in the reviews by Jülicher *et al.* [19] and Hänggi *et al.* [20].

1.1.3 Ratchets in quantum mechanics

General view

As mentioned earlier the general concept of the particle ratchet mechanism and symmetry considerations are independent of the mechanics governing the particle dynamics. Therefore in quantum systems the particle ratchet effects are also expected under the space or time asymmetry. Since the presence of asymmetry in space or time is only a necessary condition for the particle ratchet mechanism but not sufficient, the two fundamental questions naturally arise: 1) What is the ratchet behavior of the quan-

tum counterparts of classical particle ratchets? 2) Are there quantum particle ratchets having no classical analogs?

The main qualitative difference which one immediately observes between classical and quantum particle ratchets comes from the quantum mechanical tunneling of a particle through a potential barrier when the particle's energy is lower than the barrier height and the quantum mechanical reflection of a particle from a barrier when the particle's energy is larger than the barrier height. These phenomena have no analogs in classical mechanics.

To travel in the periodic potential $U(x)$ the energy of a classical particle must be larger than the potential barrier height $\Delta U = \max[U(x)] - \min[U(x)]$. This can happen due to the thermal activation resulting from the energy exchange with the bath which has temperature T. The probability P_c to overcome the barriers decays exponentially when ΔU increases or when T decreases,

$$P_c = A \exp\left[-\frac{\Delta U}{k_{\mathrm{Boltz}} T}\right], \tag{1.3}$$

where k_{Boltz} is the Boltzmann constant. As the probability goes to zero when the temperature decreases, it is obvious that no classical particle ratchet mechanism is possible at zero temperature, $T = 0$.

In a quantum system in addition to the classical probability P_c to travel above the barriers with the help of the thermal activation there also exists the probability P_q to travel trough these barriers with the help of the quantum mechanical tunneling. In the quasi-classical case the tunneling probability P_q reads as

$$P_q = \exp\left\{-\frac{2}{\hbar}\int_{x_a}^{x_b} dx \sqrt{2m[U(x) - E]}\right\}, \tag{1.4}$$

where E is the particle energy and x_a and x_b are the classical turning points, where the classical velocity is equal to zero. The distance $|x_a - x_b|$ gives the effective barrier width. As one can see from Eq. (1.4), the tunneling probability is independent of the bath temperature and depends only on the periodic potential geometry and particle energy. Therefore when $T = 0$, one has $P_c = 0$ and $P_q \neq 0$. The particle transport is still possible and based only on quantum mechanics. The particle ratchet mechanism could thus survive and represent in this case a pure quantum mechanical particle ratchet. Such quantum ratchet mechanisms were indeed found both theoretically [21] and experimentally [22]. When $T \neq 0$, one has $P_c \neq 0$ and $P_q \neq 0$ and both classical and quantum mechanics govern the ratchet transport. The dependence of the particle current on the temperature is thus highly non-trivial. In particular, the current can change its direction as a function of the temperature [21]. This fact is indeed confirmed experimentally [23].

When $T \neq 0$, the particle ratchet can also be of pure quantum nature. This happens for example at low temperatures in systems where particles populate energy levels deep below the barriers, the case studied in this thesis. In this case the particle ratchet effect takes place due to the tunneling processes and interaction with the thermal bath. This complicated dynamics may lead to changing the current direction not only as a function

of the temperature but also as a function of the amplitude of the driving force or as a function of the parameters characterizing the interaction between the system and bath [24–29].

Coherent and incoherent quantum ratchets

In the quantum mechanical case there is an additional possibility to classify the particle ratchet mechanism. It is based on such a notion of quantum mechanics as coherence. In general quantum particle transport can be described by the density matrix formalism [30]. Transport in a quantum system is called coherent if the contributions of non-diagonal elements of the density matrix to the transport properties of the system are dominant. In the opposite case transport is of incoherent nature. Since the form of the density matrix depends on the basis chosen to describe quantum transport, the notion of coherent/incoherent quantum transport is basis dependent. To classify the transport as coherent or incoherent the energy basis is very often assumed. We will follow the same convention.

The particle ratchet mechanism based on quantum incoherent transport is classified as the quantum incoherent particle ratchet mechanism.

In this thesis we will work with infinite open quantum systems strongly coupled to external environments [31] and consider the weak tunneling limit. It is usually believed that the quantum coherence of the particles in such systems is quickly lost: the non-diagonal elements of the density matrix are much smaller than the diagonal ones. As a consequence, transport in such systems has incoherent nature.

However, the quantum particle ratchet mechanism can also originate through coherent transport. This means that in the appearance of the quantum particle ratchet mechanism non-diagonal elements of the density matrix play the decisive role. Such a ratchet mechanism is then classified as the quantum coherent particle ratchet mechanism.

The coherent type of the quantum particle ratchet mechanism can, for example, result from the complex energy spectra of some systems. In such systems the density of states (DOS) has non-monotonic character resulting in highly non-linear dynamical behavior. This non-linear dynamics can appear even at low driving fields and become asymmetric when either the periodic potential is not symmetric in space or the driving force is not symmetric in time.

To describe the coherent quantum transport phenomena in a system the Landauer-Büttiker formalism [32] is a popular tool. Since in this approach the transport properties of a system attached to leads are derived from a quantum state representing a linear combination of the eigenstates of the system+leads Hamiltonian, the corresponding density matrix is essentially non-diagonal. Therefore the Landauer-Büttiker formalism automatically includes the coherent contributions to the transport properties of the system to which it is applied.

In practice it is not always possible to clearly distinguish between quantum coherent and incoherent particle ratchets because both coherent and incoherent contributions can be comparable and play equally important role in the appearance of the ratchet

behavior. Examples of quantum coherent and incoherent particle ratchets will be given at the end of this subsection.

Caldeira and Leggett model

Since a particle interacting with a thermal bath represents an open system, the energy-conserving quantum mechanical description of the particle ratchet mechanism should be applied to the system-plus-bath complex. Within such a description the total energy is conserved and one is able to analyze the energy exchange between the system and bath. This energy exchange leads to the appearance of a stochastic force, which was modeled in the classical case by the function $\xi(t)$, as well as dissipation which entered Eq. (1.1) through the friction term with the viscosity coefficient η. This approach was used in Ref. [33] and is adopted in the present thesis. It is useful at this stage to discuss the application of this so-called Caldeira and Leggett approach to the quantum rocked particle ratchets because it represents a building block in the analysis of the quantum rocked spin ratchets being the central issue of the thesis. We will only consider space ratchets. The application of the Caldeira and Leggett approach to the time particle ratchet mechanism can be found in Refs. [34, 35] for the rocked case.

For simplicity we will consider 1D dynamics. Let us start with the full Hamiltonian of the system-plus-bath complex. It can be written as the sum,

$$\hat{H}_{\mathrm{P}}(t) = \hat{H}_0^{1\mathrm{D}} + \hat{H}_{\mathrm{B}} + \hat{H}_{\mathrm{D}}(t). \tag{1.5}$$

In Eq. (1.5) $\hat{H}_0^{1\mathrm{D}}$ is the system Hamiltonian representing a particle of mass m moving in an asymmetric periodic potential $U(x)$ with period L, $U(x) \neq U(-x)$, $U(x+L) = U(x)$, that is

$$\hat{H}_0^{1D} = \frac{\hat{p}^2}{2m} + U(\hat{x}). \tag{1.6}$$

The second term in Eq. (1.5) describes the interaction between the system and bath as well as the bath itself,

$$\hat{H}_{\mathrm{B}} = \frac{1}{2}\sum_{\alpha=1}^{N_{\mathrm{O}}}\left[\frac{\hat{p}_\alpha^2}{m_\alpha} + m_\alpha\omega_\alpha^2\left(\hat{x}_\alpha - \frac{c_\alpha}{m_\alpha\omega_\alpha^2}\hat{x}\right)^2\right]. \tag{1.7}$$

This term represents the Caldeira and Leggett model of a bath of N_{O} harmonic oscillators with masses m_α and frequencies ω_α. The coordinates $\hat{x}_\alpha$ of these oscillators couple bilinearly with coupling constants c_α to the particle coordinate $\hat{x}$. This coupling is the source of dissipative processes in the system. As will become clear soon, the effect of the bath will always appear through its spectral density

$$J(\omega) = \frac{\pi}{2}\sum_{\alpha=1}^{N_{\mathrm{O}}}\frac{c_\alpha^2}{m_\alpha\omega_\alpha}\delta(\omega - \omega_\alpha). \tag{1.8}$$

We will only use an Ohmic spectral density, that is a linear dependence of $J(\omega)$ on ω at low values of the frequency ω. Since the bath cannot instantaneously react to changes

in the system state, a cutoff frequency should be introduced to avoid divergences in dynamical quantities [31]. We will assume an exponential cutoff,

$$J(\omega) = \eta\omega \exp\big(-\frac{\omega}{\omega_c}\big), \tag{1.9}$$

where ω_c is the cutoff frequency. The coefficient η is identified (see below) with the viscosity coefficient introduced earlier in the classical description of the particle ratchet mechanism, Eq. (1.1).

The last term in Eq. (1.5) describes the driving by a time-dependent unbiased force,

$$\hat{H}_{\mathrm{D}}(t) = -F(t)\hat{x}. \tag{1.10}$$

In this thesis we will use the following unbiased and symmetric driving

$$F(t) = F\cos(\Omega t), \tag{1.11}$$

where F and Ω are the driving amplitude and frequency, respectively.

Let us now look whether the classical limit of the Caldeira and Leggett model makes physical sense. The Heisenberg equations of motion are

$$\begin{aligned}
&m\frac{d\hat{x}(t)}{dt} = \hat{p}(t),\\
&\frac{d\hat{p}(t)}{dt} = \sum_{\alpha=1}^{N_{\mathrm{O}}} c_\alpha\left[\hat{x}_\alpha(t) - \frac{c_\alpha}{m_\alpha\omega_\alpha^2}\hat{x}(t)\right] - \frac{dU(x)}{dx}\bigg|_{x\to\hat{x}(t)} + F(t)\hat{1},\\
&m_\alpha\frac{d\hat{x}_\alpha(t)}{dt} = \hat{p}_\alpha(t),\\
&\frac{d\hat{p}_\alpha(t)}{dt} = \hat{x}(t)c_\alpha - \hat{x}_\alpha(t)m_\alpha\omega_\alpha^2,
\end{aligned} \tag{1.12}$$

where the operators are written in the Heisenberg representation with respect to the Hamiltonian $\hat{H}_{\mathrm{P}}(t)$. From Eq. (1.12) one finds the equation for $\hat{x}(t)$ which describes the system dynamics. It has the form

$$m\frac{d^2\hat{x}(t)}{dt^2} + m\int_0^t dt'\gamma(t-t')\frac{d\hat{x}(t')}{dt'} + \frac{dU(x)}{dx}\bigg|_{x\to\hat{x}(t)} = F(t)\hat{1} + \hat{\xi}(t) \tag{1.13}$$

and is called quantum Langevin equation. Here t_0 is the initial time. In this equation

$$\gamma(t) = \frac{2}{\pi m}\int_0^\infty d\omega\frac{J(\omega)}{\omega}\cos(\omega t) \tag{1.14}$$

is the damping kernel and

$$\hat{\xi}(t) = \sum_{\alpha=1}^{N_{\mathrm{O}}} c_\alpha\left\{\left[\hat{x}_\alpha(0) - \frac{c_\alpha\hat{x}(0)}{m_\alpha\omega_\alpha^2}\right]\cos(\omega_\alpha t) + \frac{\hat{p}_\alpha(0)}{m_\alpha\omega_\alpha}\sin(\omega_\alpha t)\right\} \tag{1.15}$$

is the force which becomes stochastic when $N_{\mathrm{O}} \to \infty$. In the classical limit $\hat{x}(t)$ is replaced with $x(t)$ and one arrives at the equation similar to Eq. (1.1) but with the friction term non-local in time. The local friction, $\eta dx(t)/dt$, is recovered if we consider the Ohmic spectral density (1.9) with $\omega_c \to \infty$. In this case the damping kernel has no memory effects,

$$\gamma(t) = \frac{2\eta}{m}\delta(t). \tag{1.16}$$

Therefore as mentioned above η is really identified with the viscosity coefficient from the classical dynamics described by Eq. (1.1).

The stochastic force $\xi(t)$ in Eq. (1.15) depends on the initial (*i.e.*, at time $t = 0$) preparation of the thermal bath. For the initial preparation in which the bath is in thermal equilibrium with the system at temperature T the bath density matrix has the form ($\beta \equiv 1/k_{\mathrm{Boltz}}T$)

$$\hat{\rho}_{\mathrm{B}} = \frac{\exp\{-\beta\hat{H}_{\mathrm{B}}[x(0)]\}}{\mathrm{Tr}_{\mathrm{B}}\exp\{-\beta\hat{H}_{\mathrm{B}}[x(0)]\}}, \tag{1.17}$$

where Tr_{B} stands for the trace over the bath degrees of freedom and $x(0)$ is the initial coordinate of the particle,

$$x(0) = \mathrm{Tr}_{\mathrm{S}}[\hat{\rho}(0)\hat{x}], \tag{1.18}$$

where Tr_{S} stands for the trace over the system degrees of freedom and $\hat{\rho}(0)$ is the initial density matrix of the system. In this case one obtains [31]

$$\mathrm{Tr}_{\mathrm{B}}[\hat{\rho}_{\mathrm{B}}\hat{\xi}(t)] = 0, \tag{1.19}$$

$$\mathrm{Tr}_{\mathrm{B}}[\hat{\rho}_{\mathrm{B}}\hat{\xi}(t)\hat{\xi}(t')] = \hbar L(t-t'), \tag{1.20}$$

where $L(t)$ is the bath correlation function:

$$L(t) = \frac{1}{\pi}\int_0^\infty d\omega J(\omega)\left[\coth\left(\frac{\hbar\omega\beta}{2}\right)\cos(\omega t) - \mathrm{i}\sin(\omega t)\right]. \tag{1.21}$$

Eq. (1.19) shows that the average value of the stochastic force is zero. In the limit of high temperatures and large cutoff frequencies Eq. (1.20) gives

$$\mathrm{Tr}_{\mathrm{B}}[\hat{\rho}_{\mathrm{B}}\hat{\xi}(t)\hat{\xi}(t')] = 2\eta k_{\mathrm{Boltz}}T\delta(t-t'). \tag{1.22}$$

This result is consistent with the local friction obtained above: the stochastic force $\xi(t)$ originates from a heat reservoir with zero memory time. Therefore we conclude that the model of Caldeira and Leggett is a reasonable approach to describe quantum open systems because in the classical limit it leads to the proper dynamics of the corresponding classical open systems.

Discrete variable representation

For practical calculations of the ratchet current one usually restricts the Hilbert space $\mathcal{H}$ to a subspace $\mathcal{S}$. Physically it is natural to make this restriction using the Bloch basis of the Hamiltonian of the isolated system, $\hat{H}_0^{1D}$, Eq. (1.6). The restriction is based on the physical assumption that at low temperatures and not too strong driving fields only a few Bloch bands contribute to transport. Such a situation can be realized in different physical systems. For example, in semiconductors these bands could be the lowest conduction bands, in metals the Bloch bands with the energy range containing the Fermi energy are the most important ones in transport phenomena. Therefore one usually keeps only the Bloch states corresponding to a few relevant Bloch bands and further works only within the subspace $\mathcal{S}$ generated by those states. In the subspace $\mathcal{S}$ the coordinate operator $\hat{x}$ has a discrete spectrum instead of the continuous one which it has in $\mathcal{H}$. The space integrals are replaced with space sums:

$$\int dx \to \sum_x .$$

Here x under the summation denotes a complete set of quantum numbers characterizing the discrete spectrum of $\hat{x}$. The actual quantum numbers over which the summation is performed, *i.e.*, the quantum numbers which determine the discrete eigenstates of the coordinate operator, are not important for the moment and will be detailed in the following chapters.

The eigenstates of the coordinate operator restricted to the subspace $\mathcal{S}$ constitute a basis of $\mathcal{S}$. This basis is called discrete variable representation (DVR) basis. Such a basis was first introduced by Harris *et al.* in Ref. [36]. Let us denote the DVR basis states through $\{|x\rangle\}$. In the DVR basis the Hamiltonian $\hat{H}_0^{1D}$ is written as

$$\hat{H}_0^{1D} = \sum_x \varepsilon_x |x\rangle\langle x| + \sum_{x\neq y} \Delta_{xy} |x\rangle\langle y|, \tag{1.23}$$

where

$$\varepsilon_x \equiv \langle x|\hat{H}_0^{1D}|x\rangle \tag{1.24}$$

are the DVR on-site energies and

$$\Delta_{xy} \equiv \langle x|\hat{H}_0^{1D}|y\rangle, \quad x \neq y, \tag{1.25}$$

are the DVR hopping matrix elements. The DVR tight-binding model can be obtained in the usual way taking into account only the hopping matrix elements between the DVR states corresponding to neighboring discrete eigenvalues of $\hat{x}$.

Ratchet current

As in the classical case in order to determine whether the particle ratchet mechanism exists one has to calculate the averaged particle velocity,

$$v^\infty \equiv \lim_{t\to\infty} \frac{1}{t} \int_0^t dt' \, \langle \hat{v} \rangle (t'), \tag{1.26}$$

where $\langle\hat{v}\rangle(t)$ is the quantum mechanical average of the particle velocity at time t. This quantity is provided through the reduced density matrix $\hat{\rho}(t)$ that is the full one $\hat{W}(t)$ traced over the bath degrees of freedom,

$$\hat{\rho}(t) = \mathrm{Tr}_{\mathrm{B}}\hat{W}(t). \tag{1.27}$$

The quantum mechanical average of the particle velocity at time t is expressed through the reduced density matrix as

$$\langle\hat{v}\rangle(t) = \frac{d}{dt}\langle\hat{x}\rangle(t), \tag{1.28}$$

where $\langle\hat{x}\rangle(t)$ is

$$\langle\hat{x}\rangle(t) = \mathrm{Tr}_{\mathrm{S}}[\hat{x}\hat{\rho}(t)]. \tag{1.29}$$

The quantum particle ratchet mechanism exists if Eq. (1.26) gives non-zero result. It is obvious from Eq. (1.29) that using the eigenstates of the coordinate operator one only needs the diagonal elements of the density matrix to find the quantum mechanical average of the particle velocity,

$$\langle\hat{x}\rangle(t) = \sum_x x\langle x|\hat{\rho}(t)|x\rangle = \sum_x xP(x,t), \tag{1.30}$$

$$\langle\hat{v}\rangle(t) = \sum_x x\frac{dP(x,t)}{dt}, \tag{1.31}$$

where the diagonal matrix elements of the reduced density matrix,

$$P(x,t) \equiv \langle x|\hat{\rho}(t)|x\rangle, \tag{1.32}$$

are the populations of states $|x\rangle$. Therefore the ratchet velocity can be found from the dynamics of the averaged populations:

$$v^{\infty} = \lim_{t\to\infty}\sum_x x\frac{d\bar{P}(x,t)}{dt}, \tag{1.33}$$

where

$$\bar{P}(x,t) \equiv \frac{1}{t}\int_0^t dt'\, P(x,t'). \tag{1.34}$$

For the specific case of a periodic force with period T the average in Eq. (1.26) reduces to the stationary limit of the average over one period of the force,

$$v^{\infty} = \lim_{t\to\infty}\frac{1}{T}\int_t^{t+T} dt'\,\langle\hat{v}\rangle(t'). \tag{1.35}$$

In this case v^{∞} is obtained from Eq. (1.33) in which $\bar{P}(x,t)$ is given as

$$\bar{P}(x,t) \equiv \frac{1}{T}\int_t^{t+T} dt'\, P(x,t'). \tag{1.36}$$

Master equation

For the periodic driving given by Eq. (1.11) it has been shown [31,37,38] that when the driving frequency Ω is much bigger than all other relevant time scales in the dynamics of the system-plus-bath complex, the time evolution of the averaged populations $\bar{P}(x,t)$, Eq. (1.36) with $T = 2\pi/\Omega$, is governed by the averaged master equation which at long times has the Markovian form (*i.e.*, it is local in time):

$$\frac{d\bar{P}(x,t)}{dt} = \sum_{y\neq x} \bar{\Gamma}_{xy}\bar{P}(y,t) - \sum_{y\neq x} \bar{\Gamma}_{yx}\bar{P}(x,t), \tag{1.37}$$

where $\bar{\Gamma}_{xy}$ is the averaged transition rate from $|y\rangle$ to $|x\rangle$. The expressions for the averaged transition rates were found in [31,37,39] within the second order in the DVR hopping matrix elements (1.25):

$$\bar{\Gamma}_{xy} = \frac{|\Delta_{xy}|^2}{\hbar^2}\int_{-\infty}^{\infty} dt\, \exp\left[-\frac{(y-x)^2}{\hbar}Q(t) + \mathrm{i}\frac{\varepsilon_y - \varepsilon_x}{\hbar}t\right] J_0\left[\frac{2F(y-x)}{\hbar\Omega}\sin\left(\frac{\Omega t}{2}\right)\right], \tag{1.38}$$

where J_0 is the Bessel function of zero order. The function $Q(t)$ is the twice-integrated bath correlation function [31] defined through the bath correlation function $L(t)$, Eq. (1.21),

$$\frac{d^2Q(t)}{dt^2} \equiv L(t), \tag{1.39}$$

and is required to satisfy the additional conditions:

$$Q(0) = 0, \quad Q(-t) = Q^*(t). \tag{1.40}$$

One finds that

$$Q(t) = \frac{1}{\pi}\int_0^{\infty} d\omega \frac{J(\omega)}{\omega^2}\left\{\coth\left(\frac{\hbar\omega\beta}{2}\right)[1-\cos(\omega t)] + \mathrm{i}\sin(\omega t)\right\}. \tag{1.41}$$

Examples of quantum ratchets involving Brownian motion

The quantum incoherent particle ratchet mechanisms in an infinite 1D system was theoretically predicted by Reimann *et al.* in Ref. [21]. Here the dissipation was taken into account through the model of Caldeira and Leggett described above. The periodic potential was asymmetric in space. The driving force was symmetric in time and represented an unbiased bistable force switching between the two values $\pm F$. The adiabatic limit was considered: the switching rate of the bistable force was much slower than any time scale of the system. It was found that there was a crossover temperature above which the particle ratchet mechanism had the classical nature dominated by the over-barrier transport. However, below the crossover temperature the transport was mostly governed by the tunneling processes. A net current was detected. Strikingly, in the low temperature limit it changed its direction and remained finite at zero temperature, *i.e.*, the quantum incoherent space rocked particle ratchet mechanism was realized in this system.

Another interesting feature of an infinite open periodic quantum system driven symmetrically was investigated in Ref. [28] within the Caldeira and Leggett approach. It was discovered that even for a periodic potential asymmetric in space the quantum incoherent space rocked particle ratchet mechanism could only arise when the particles in the system populated more than one Bloch band. In its dependence on the driving amplitude the ratchet current had multiple reversals.

The quantum incoherent time rocked particle ratchet mechanism was studied by Goychuk *et al.* [34, 40] in a infinite open periodic system. The dissipation was again taken into account using the model of Caldeira and Leggett for the Ohmic case. The periodic potential was symmetric in space but the driving force was asymmetric in time and it represented an unbiased harmonic mixing signal. The finite ratchet current was predicted. As a function of the driving amplitude the current reversed its direction. In general the time ratchet behavior of this system took place in presence of any unbiased asymmetric driving and finite dissipation [41]. No current appeared without interaction with an external environment: directed transport in this system was a highly nonlinear cooperative effect of the asymmetric driving and quantum dissipation.

Another kind of the quantum incoherent space particle ratchet mechanism was experimentally found in a double quantum dot system [42] prepared on a GaAs/AlGaAs heterostructure containing a 2DEG. In this experiment a double quantum dot was electrostatically coupled to a quantum point contact. The double quantum dot system was not biased while the quantum point contact was dc biased. The current through the double quantum dot was measured. It turned out that this current could be finite depending on the double quantum dot ground state configuration. This phenomenon was explained in terms of inelastic tunneling as follows. The highest energy electron localized in one of the dots could resonantly absorb an energy quantum and tunnel to the other dot. This energy quantum was taken from the electrostatic coupling to the dc biased quantum point contact. The resonance condition required that the energy quantum was equal to the absolute value of the asymmetry energy, that is to the energy difference between the two charge configurations. Via the dot-lead tunneling of electrons the system relaxed back to the ground state: the excited electron escaped to the lead attached to the dot to which the inelastic tunneling process had been made whereas another electron entered from the lead attached to the dot from which this process had occurred. This resulted in the net current through the double quantum dot system observed in this experiment. It was pointed out that other more probable inelastic processes involving ionization of one of the two quantum dots towards its adjacent lead followed by recharging from the same lead did not result in a net current. When the asymmetry energy was equal to zero the current through the double quantum dot vanished, *i.e.*, an internal asymmetry of the double quantum dot was needed for a dc current resulting from single electron tunneling processes between quantized energy levels. This demonstrated that the double quantum dot system considered in this experiment was a quantum ratchet driven by the electrostatic coupling to a dc biased quantum point contact playing the role of a non-equilibrium energy source. Note that in this example the equilibrium between the system and environment was broken by external fields applied to the environment and not to the system.

Examples of quantum ratchets without Brownian motion

In a finite system coupled to fermionic reservoirs a current reversal upon a reduction of the temperature of the fermionic reservoirs was experimentally found and theoretically investigated by Linke *et al.* [23] for the case where Brownian motion was inessential. This current reversal is an analog of the current reversal from the first example of quantum ratchets involving Brownian motion. In the present example any Brownian motion between the fermionic reservoirs was absent. The ratchet was implemented using an electronic system and the particle current was therefore identified with the charge

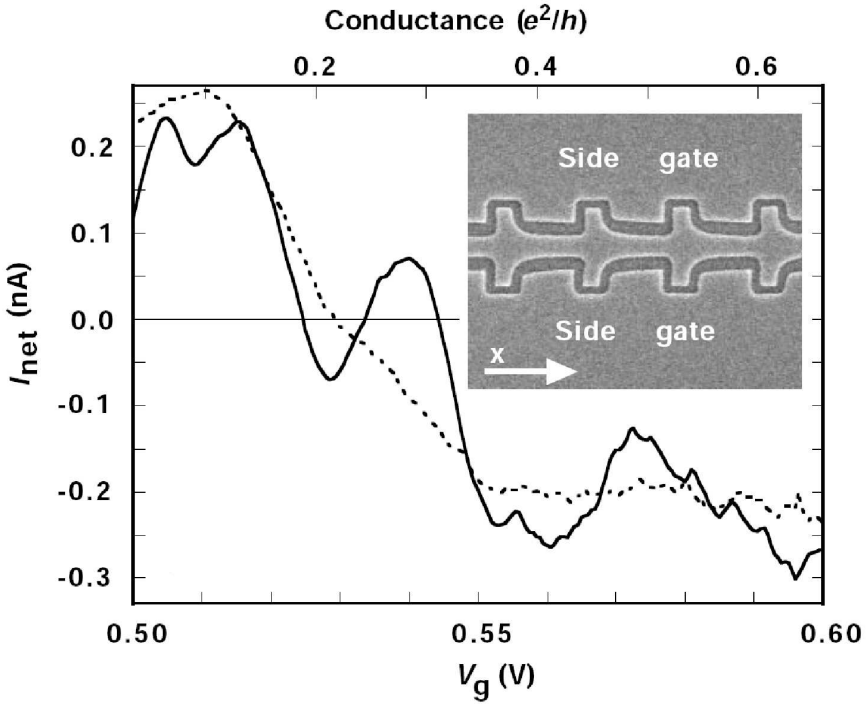

Figure 1.2: Net current versus side-gate voltage V_g (bottom axis) for a structure with 10 barriers at 0.4 K (solid curve) and 4 K (dotted curve), driving amplitude $U_0 = 1$ meV. The top axis is the measured device conductance as a function of V_g. (Inset) Scanning electron micrograph of a periodic ratchet, showing four repeated ratchet cells [23].

current. A quasi-1D system having 10 barriers was prepared in a two-dimensional electron gas located parallel to the surface of a GaAs/AlGaAs heterostructure. An asymmetry of the corresponding 1D potential having 10 periods was created by a periodic variation of the width of the channel (see Fig. 1.2). It was demonstrated that in this system the classical and quantum contributions to the ratchet current, *i.e.*, the overbarrier and tunneling contributions, respectively, flowed in opposite directions. The temperature range was from 0.2 K to 4.2 K. The electron transport could have both coherent and incoherent nature. The experiments showed that the ratchet current reversed its direction as a function of the temperature. The simplified theoretical explanation of this phenomenon was based on the Landauer-Büttiker formalism. As discussed above this formalism automatically takes into account the coherent contributions to the transport properties of the system to which it is applied. It was shown that

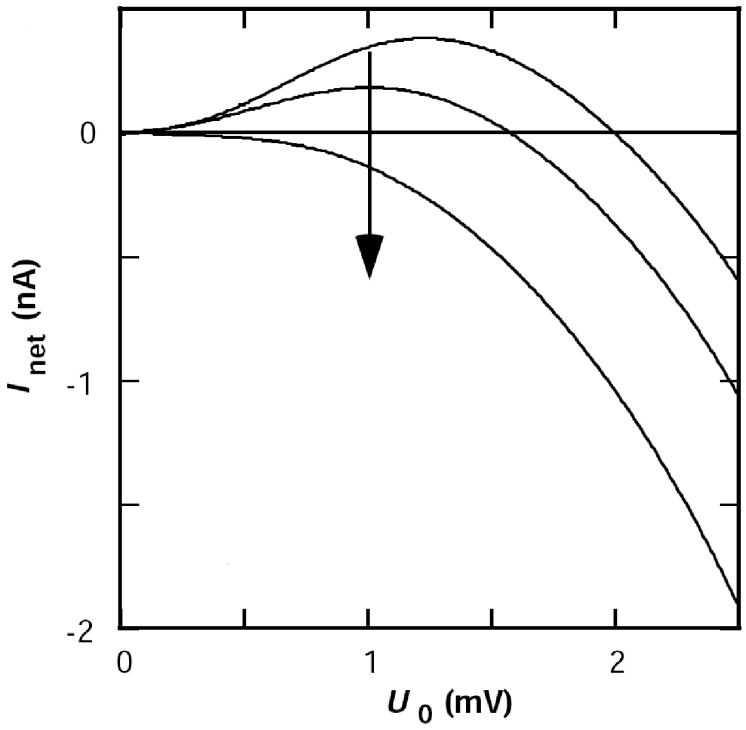

Figure 1.3: Net current versus driving amplitude for a structure with 1 barrier, gate voltage $V_g = -0.74$ V, temperature (from top) 0.6, 2, and 4 K [23].

the Landauer-Büttiker model used by Linke *et al.* was able to qualitatively describe the ratchet behavior observed experimentally. In particular, the current reversals were present in the model (see Fig. 1.3). Therefore, the coherent component could play an essential role in the ratchet behavior of the present example.

The quantum particle ratchet mechanism in a triple quantum dot system was explored in Ref. [43]. The system was based on a GaAs/AlGaAs heterostructure. The temperature in the experiments was 0.38 K. The contacts were attached to two quantum dots. One of these two contact dots was coupled to the remaining third dot so that tunneling between them was possible. The trapping ratio for this tunneling was estimated using the orthodox theory of the Coulomb blockade. The current through the system was proportional to this trapping ratio. The orthodox theory is an incoherent transport model. Therefore in this work it was assumed that the incoherent contribution to the transport properties of the system was of relevance. The current-voltage characteristics obtained experimentally and theoretically revealed a non-linear dependence on the static bias. The most important feature of these characteristics was their asymmetry with respect to the bias. The ratchet effect in the system was a consequence of this asymmetry.

A quantum coherent particle ratchet mechanism in a triangular quantum dot was explored experimentally and theoretically in Ref. [44]. In that work the quantum dot was made in a 2DEG formed in a GaAs/AlGaAs semiconductor heterostructure. The temperature was fixed at 0.3 K. Measuring the linear-response resistance as a function of the gate voltage revealed a non-monotonic structure of DOS inside the dot. Due to

this non-monotonic structure of DOS the differential resistance behaved non-linearly and depended on the current direction. Such an asymmetry, caused by quantum interference inside the dot, gave rise to a net charge (or, equivalently, particle) current when the dot was driven by unbiased symmetric ac voltage $U_0 \sin(\omega t)$. Therefore this system represented a quantum rocked particle ratchet. Due to the triangular spatial geometry an inversion center was absent and thus this ratchet was of space type. As a function of the driving amplitude U_0 the charge current changed its direction, *i.e.*, current reversals were detected.

In the previous three examples the quantum space rocked particle ratchet mechanism was implemented using semiconductor heterostructures. In the present example the quantum coherent space and time rocked particle ratchet mechanisms based on molecular wires are considered. They were suggested and theoretically explored by Lehmann *et al.* [26,45]. The space ratchet in Ref. [26] consisted of a chain of asymmetric in space molecular groups. This asymmetry resulted from an asymmetric in space level structure of the orbital energies. This system, called molecular wire, had a finite length and was weakly coupled to two fermionic reservoirs which were in equilibrium. The reservoirs had the same chemical potential, *i.e.*, no dc bias was present. The system was driven by a strong laser field which was unbiased and symmetric in time. A finite ratchet current through the molecular wire was obtained. This current as a function of the amplitude of the driving laser field had multiple zero current points where its direction changed to the opposite one. In the time ratchet in Ref. [45] the molecular wire consisted of a symmetric in space molecular groups, *i.e.*, the level structure of the orbital energies was symmetric in space. This molecular wire was driven by an unbiased laser field asymmetric in time. This asymmetry was modeled by mixing of different harmonics. A finite ratchet current was found. However, the reversals of the ratchet current were not predicted for this time ratchet.

The quantum coherent and incoherent space ratchet behavior in a rocked Luttinger liquid [46, 47], a prototype for interacting electrons in 1D systems, was studied in Ref. [48]. The system represented a 1D wire with strong electron-electron interactions. This wire was coupled to two non-interacting leads. The potential profile was spatially asymmetric. This asymmetry was modeled by a two-impurity asymmetric potential. The driving was symmetric: an unbiased bistable force of low frequency. The total current was given as a sum of the current injected from the non-interacting leads and the current backscattered off the asymmetric potential. The former component was described by the Landauer formula while the latter one contained a contribution to the ratchet effect. A finite ratchet current was found. It turned out that strong repulsive electron interactions enhance the ratchet effect which was strong even for a weak asymmetric potential.

Other important examples of the quantum particle ratchet mechanism include quasi-1D Josephson arrays where the ratchet effect takes place for vortices induced by a magnetic field perpendicular to the array [22] and quantum Hamiltonian systems where the quantum dynamics is strictly Hamiltonian and directed transport can appear

in absence of any dissipation the role of which in these systems can be played by either quantum coherence or quantum chaos as well as by their interplay when both of them are essential in the dynamical behavior [49–55]. These and other examples of concrete realizations of the quantum particle ratchet mechanism are discussed in the modern review by Hänggi *et al.* [20].

1.2 Spin ratchets

1.2.1 Spin ratchet concept

In the previous section the classical and quantum particle ratchet mechanisms have been introduced and classified. Having understood the particle ratchet mechanism one naturally arrives at the notion of the spin ratchet mechanism. It is clear that the spin ratchet mechanism can only be of quantum nature. This is related to the fact that the spin degree of freedom of a particle does not have analogs in classical mechanics. Since the notion of the particle ratchet mechanism is based on the notion of the particle flow, it is quite natural to relate the spin ratchet concept to the spin flow. Assuming that a spin flow has been defined one can employ in a straightforward way the classification of the particle ratchets introduced in the previous section to classify the spin ratchets. For example, space, time, rocked, coherent, incoherent and other types of the spin ratchet mechanism are introduced in complete analogy with the corresponding types of the particle ratchet mechanism.

A consistent investigation of the spin ratchet mechanism is not possible without a comprehensive understanding of the corresponding particle ratchet mechanism for the same system. In other words, when exploring the spin ratchet mechanism in a given system one always tries to connect it to the corresponding quantum particle ratchet response of the system. In the previous section, devoted to the particle ratchet mechanism, the crucial role of space-time symmetries of a system in the appearance of particle ratchet currents in this system has been emphasized. A fundamental question is then whether the spin ratchet mechanism respects the spatial and temporal symmetries of a given system in the same way as the quantum particle ratchet mechanism does for the same system. Another question which is important from the practical point of view is whether a spin ratchet current can appear in the *absence* of a particle (charge) ratchet current. Reformulating the last question we are interested in the generation of pure spin currents by means of the spin ratchet mechanism.

As it has been seen from the previous section, an important feature of the particle transport is that it is characterized by a flow of a quantity (like mass or charge) which is single-valued. In contrast, the spin degree of freedom is a multi-valued quantity for a particle with a non-zero spin. It is also important to realize that such a notion as spin of a particle in quantum mechanics is an additional (to the spatial coordinates of this particle) degree of freedom while such properties as mass or charge characterizing the particle flow are not degrees of freedom of the particle. When a particle moves in real space its mass and charge are assumed to be independent of the transport conditions. However, the spin degree of freedom of the same particle can depend on

the transport conditions. This dependence can result in switching the particle spin between its multiple values. Therefore, a proper definition of the spin flow becomes a non-trivial point. Below we present two definitions of the spin current used to study spin transport.

1.2.2 Spin current definitions

We start with the definition of the spin current operator which is the product of the quantum mechanical spin and velocity operators. This definition, so-called conventional spin current operator, historically appeared as the first one and many important results on spin transport were obtained using the conventional spin current operator. One can arrive at the definition of the conventional spin current operator by deriving for a given system the quantum mechanical continuity equation [56] for the spin density,

$$\frac{\partial S_i(\vec{r},t)}{\partial t} + \nabla \cdot \vec{J}_i^{(\mathrm{s})}(\vec{r},t) = \mathcal{T}_i(\vec{r},t). \tag{1.42}$$

In Eq. (1.42)

$$S_i(\vec{r},t) = \psi^\dagger(\vec{r},t)\hat{s}_i\psi(\vec{r},t), \tag{1.43}$$

is the spin density in a spinor state $\psi(\vec{r},t)$. Here $\hat{s}_i$ $(i = x, y, z)$ is the i-th component of the spin operator. The vector $\vec{J}_i^{(\mathrm{s})}(\vec{r},t)$ in Eq. (1.42) is the spin current density polarized along the i-th direction:

$$\vec{J}_i^{(\mathrm{s})}(\vec{r},t) = \mathrm{Re}\left[\psi^\dagger(\vec{r},t)\frac{1}{2}\{\hat{s}_i,\hat{\vec{v}}\}\psi(\vec{r},t)\right], \tag{1.44}$$

where $\hat{\vec{v}}$ is the velocity operator and the curly brackets mean the anticommutator operation. Finally, the quantity in the right hand side of Eq. (1.42) represents the spin torque density for the spin polarization along the i-th direction:

$$\mathcal{T}_i(\vec{r},t) = \mathrm{Re}[\psi^\dagger(\vec{r},t)\hat{\tau}_i\psi(\vec{r},t)], \tag{1.45}$$

where $\hat{\tau}_i$ is the spin torque operator for the polarization along the i-th direction. It is defined as

$$\hat{\tau}_i \equiv \frac{d\hat{s}_i}{dt} = -\frac{\mathrm{i}}{\hbar}[\hat{s}_i,\hat{H}], \tag{1.46}$$

where $\hat{H}$ is the Hamiltonian of the system.

The spin current operator corresponding to the form (1.42) of the continuity equation for the spin density reads as

$$\hat{J}_{ij}^{(\mathrm{s})} = \frac{1}{2}\{\hat{s}_i,\hat{v}_j\}, \tag{1.47}$$

where the index i stands for the polarization of the spin current and the index j denotes the direction in which the spin current flows. Therefore, the conventional spin current operator is associated with the continuity equation for the spin density written in the form of Eq. (1.42).

The definition of the spin current operator (1.47) is a reasonable choice for systems where the spin degree of freedom represents a good quantum number, *i.e.*, in systems where there is no spin flipping,

$$\frac{d\hat{s}_i}{dt} = 0. \tag{1.48}$$

However, for systems with spin flipping (caused, *e.g.*, by spin-orbit interactions considered in the next chapter), *i.e.*, for systems where

$$\frac{d\hat{s}_i}{dt} \neq 0, \tag{1.49}$$

the definition of the spin current operator given by Eq. (1.47) turns out to be unsatisfactory. As it was discussed by Rashba [57], in non-centrosymmetric 2D systems the conventional definition (1.47) resulted in non-vanishing spin currents at thermodynamic equilibrium. Although from a general symmetry point of view this conclusion was not entirely surprising, it was pointed out that such background currents present in the absence of in-plane external fields were non-transport currents. To study spin transport in a system these background currents should be eliminated because they do not describe any real transport of electron spins and cannot result in spin injection or accumulation. A proposal on how to measure such equilibrium spin currents using a flexible substrate as a cantilever was described by Sonin in Ref. [58].

Another drawback of the conventional spin current, *i.e.*, the spin current calculated using the conventional spin current operator, Eq. (1.47), is that this current is not conserved. Indeed, in systems with spin flipping the right hand side in Eq. (1.42) does not identically vanish due to Eq. (1.49). This means that in such systems there may be microscopic spin generation and therefore for a given elementary volume the spin flowing in may not compensate the spin flowing out.

As it was pointed out by Shi *et al.* [59] the conventional spin current could even be finite in insulators with localized eigenstates only. Therefore it is highly questionable whether this current is relevant for describing real spin transport. In particular, the spin ratchet mechanism being a transport phenomena would be present in insulators which is physically unlikely.

An attempt to improve the conventional spin current operator was made in Refs. [59, 60] where the authors defined an alternative spin current operator. The spin current based on the alternative spin current operator, the alternative spin current, is physically appealing because it is absent in insulators and for many important cases it is conserved. However, the alternative spin current operator does not allow to automatically eliminate the equilibrium spin currents and therefore their manual elimination suggested in Ref. [57] is still necessary.

One can come to the alternative spin current operator of Ref. [59] as follows. For systems where the average spin torque density vanishes in the bulk, one can write the the spin torque density as a divergence of a spin torque dipole density,

$$\mathcal{T}_i(\vec{r}, t) = -\nabla \cdot \vec{P}_i(\vec{r}, t). \tag{1.50}$$

The continuity equation for the spin density is then rewritten as

$$\frac{\partial S_i(\vec{r},t)}{\partial t} + \nabla\cdot\big(\vec{J}_i^{\,(\mathrm{s})}(\vec{r},t) + \vec{P}_i(\vec{r},t)\big) = 0. \tag{1.51}$$

The advantage of the form (1.51) of the continuity equation for the spin density is that it is sourceless. The spin current density corresponding to the form (1.51) of the continuity equation is the alternative spin current density which was introduced in Ref. [59]. It has the form

$$\vec{J}_i^{\,(\mathrm{s,a})}(\vec{r},t) = \vec{J}_i^{\,(\mathrm{s})}(\vec{r},t) + \vec{P}_i(\vec{r},t) \tag{1.52}$$

From Eq. (1.51) it follows that the alternative spin current related to the alternative spin current density (1.52) is conserved. This current is not yet completely defined because the spin torque density in Eq. (1.50) is not unique. The spin torque density can be fixed by the physical constraint which comes from the fact that this quantity is a material property and thus it should vanish outside the sample. Therefore, one obtains

$$\int dV\,\vec{P}_i(\vec{r},t) = -\int dV\,\vec{r}\big(\nabla\vec{P}_i(\vec{r},t)\big) = \int dV\,\vec{r}\,\mathcal{T}_i(\vec{r},t). \tag{1.53}$$

Upon bulk average the effective alternative spin current density may be written in the form

$$J_{ij}^{(\mathrm{s,a})}(\vec{r},t) = \mathrm{Re}[\psi^{\dagger}(\vec{r},t)\hat{J}_{ij}^{(\mathrm{s,a})}\psi(\vec{r},t)], \tag{1.54}$$

where

$$\hat{J}_{ij}^{(\mathrm{s,a})} = \frac{d(\hat{s}_i\hat{x}_j)}{dt} \tag{1.55}$$

is the alternative spin current operator introduced in Ref. [59]. As one can see, in comparison with the conventional spin current operator, Eq. (1.47), the alternative spin current operator in Eq. (1.55) contains an additional term. This term reads as

$$\vec{r}\frac{d\hat{s}_i}{dt}$$

and it takes into account the contribution from the spin torque.

Since the alternative spin current operator, Eq. (1.55), is a time derivative, the alternative spin current must vanish in localized states. Therefore, it cannot flow in insulating systems. It was shown [59] that the alternative spin current vanishes in such systems even in the presence of a weak electric field.

After a proper measure for the spin flow in a given system has been chosen, the spin ratchet mechanism in this system can be subject to an analysis in the same way as the particle ratchet mechanism discussed in the previous section.

It is clear that in a system where spin flip processes do not take place and the spin degree of freedom is not coupled to both orbital degrees of freedom and external driving fields the spin ratchet mechanism is just a clone of the charge ratchet mechanism in this system. Indeed, under such circumstances a spin state of a particle will not change and it will not create any asymmetry in the orbital motion of this particle. In this case

the spin degree of freedom is similar to such single-valued particle properties as its mass or charge and therefore a ratchet spin flow of particles having the same spin state is equivalent to the ratchet flow of these particles.

Non-trivial implementations of the spin ratchet mechanism are thus those ones where the multi-valued nature of the spin degree of freedom plays a crucial role in the appearance of the spin ratchet effect. Below we consider some examples of such implementations.

1.2.3 Coherent spin ratchets

In this subsection we will give some examples of coherent spin ratchets. These spin ratchets are divided into three sets. In the first set the ratchet potential has a magnetic nature, in the second set it is electrostatic and in the third set it is a proper combination of both.

Magnetic ratchet potential

The coherent space rocked spin ratchet mechanism was investigated in Ref. [61]. The system represented a 2DEG connected to two non-magnetic leads. The Hamiltonian for the 2DEG had the form,

$$\hat{H} = \frac{\hat{p}_x^2 + \hat{p}_y^2}{2m} + \frac{g\mu_{\mathrm{B}}}{2} H_y(\hat{x})\hat{\sigma}_y + V(\hat{y}), \tag{1.56}$$

where m and g were the effective mass and the effective electron spin g-factor, respectively, $\hat{\sigma}_y$ the Pauli spin operator, $H_y(x)$ a non-uniform magnetic field along the y-direction perpendicular to the transport direction which was along the x-axis, $V(y)$ the transverse confinement and μ_{B} the Bohr magneton. The driving was symmetric in time: an unbiased bistable force with the two values $\pm U_0$. The adiabatic limit was assumed. A static non-uniform magnetic field introduced in Eq. (1.56) was chosen as,

$$H_y(x) = H_0\left[-\sin\left(\frac{2\pi}{l}x\right) + \alpha\sin\left(\frac{4\pi}{l}x\right)\right], \tag{1.57}$$

where H_0 and l were the amplitude and period of the magnetic field, respectively, and α was an asymmetry parameter. The magnetic field (1.57) played a double role: 1) it produced asymmetry in space along the transport direction; 2) it coupled, through the Zeeman term, the spin degree of freedom with an orbital one, namely with the coordinate along the transport direction. An important feature of this magnetic field was that it did not cause any spin flipping. Therefore, as analyzed above, a non-trivial spin ratchet behavior in this setup could only result through the magnetic field induced coupling between the spin degree of freedom and the coordinate along the transport direction. Such a magnetic field could be experimentally realized using the fringe fields of ferromagnetic stripes patterned on top of a 2DEG and magnetized in the plane direction perpendicular to the transport one. The Landauer-Büttiker approach [32] was employed for the numerical calculations. As mentioned in the previous section on the

particle ratchet mechanism this approach is often used when coherence plays an important role in transport phenomena. Since processes which could lead to switching between the two spin states of the electrons in the 2DEG were absent, the equality Eq. (1.48) was fulfilled. The conventional spin current was conserved because the continuity equation (1.42) was sourceless. The conventional and alternative spin current operator definitions, Eqs. (1.47) and (1.55), respectively, were equivalent. Since different transverse modes were not coupled, only the lowest sub-band was taken into account. Because of the absence of spin flipping, the transmission and reflection coefficients between different spin states were equal to zero. In this case the conventional definition of the spin current operator, Eq. (1.47), results in the following expression for the spin current polarized along the y-axis,

$$I_{\mathrm{S}} = \frac{1}{4\pi}\int_0^\infty dE[f(E,\mu_1) - f(E,\mu_2)][T_{+,+}(E) - T_{-,-}(E)], \tag{1.58}$$

where $T_{+,+}(E)$ and $T_{-,-}(E)$ are the spin diagonal elements of the transmission matrix for an electron whose energy is equal to E and $f(E,\mu_{1,2})$ is the Fermi-Dirac distribution for the two leads which have the chemical potentials equal to $\mu_{1,2}$. The expression for the charge (or equivalently particle) current is

$$I_{\mathrm{C}} = -\frac{e}{h}\int_0^\infty dE[f(E,\mu_1) - f(E,\mu_2)][T_{+,+}(E) + T_{-,-}(E)]. \tag{1.59}$$

In this system it does not matter in which lead the spin flow is measured because the spin current is conserved. Therefore, Eqs. (1.58) and (1.59) are valid for the both leads. For the case of the magnetic field (1.57) the commutation relations ($\hat{R}_x$ is the x-axis inversion operator)

$$[\hat{H}, \hat{\sigma}_x\hat{R}_x] = 0, \quad [\hat{H}, \hat{\sigma}_z\hat{R}_x] = 0 \tag{1.60}$$

take place when the longitudinal size of the system is a multiple of the magnetic field period. The commutation relations (1.60) lead to the following relation between the spin diagonal elements of the transmission matrix,

$$T_{\sigma,\sigma}(+U_0) = T_{-\sigma,-\sigma}(-U_0), \quad \sigma = +,-. \tag{1.61}$$

As a result the ratchet spin current in Ref. [61] was given as

$$\langle I_{\mathrm{S}}\rangle \equiv \frac{1}{2}[I_{\mathrm{S}}(+U_0) + I_{\mathrm{S}}(-U_0)] = I_{\mathrm{S}}(+U_0) \tag{1.62}$$

while the ratchet charge current was absent,

$$\langle I_{\mathrm{C}}\rangle \equiv \frac{1}{2}[I_{\mathrm{C}}(+U_0) + I_{\mathrm{C}}(-U_0)] = 0. \tag{1.63}$$

The numerical results obtained in Ref. [61] showed that indeed when the system size was a multiple of the magnetic field period, the charge ratchet current was absent

while the spin ratchet current was finite. For an arbitrary value of the system size both the charge and spin ratchet currents were finite and had multiple zero current points where the currents reversed their directions.

In the example described above we see that a coupling between the spin degree of freedom and an asymmetric periodic potential may be enough for the existence of the spin ratchet mechanism. We also see how the presence of the spin degree of freedom broadens our understanding of the role of different symmetries in the appearance of the particle ratchet mechanism. Indeed, according to our discussion of the particle ratchet mechanism in the previous section we know that if in a periodic system with Hamiltonian $\hat{H}$ the periodic potential is asymmetric and not coupled to the spin degree of freedom, the particle ratchet current may be finite. In this case $[\hat{H}, \hat{R}_x] \neq 0$. However, from the example of the spin ratchet mechanism described above we have learnt that if the periodic potential is asymmetric, *i.e.*, $[\hat{H}, \hat{R}_x] \neq 0$, and coupled to the spin degree of freedom, the particle ratchet mechanism does not exist if the commutation relations $[\hat{H}, \hat{\sigma}_{x/z}\hat{R}_x] = 0$ are satisfied.

In Ref. [62] the authors extended the above discussed model in two respects: 1) all three components of the magnetic field were considered; 2) the magnetic field was non-uniform in both of the in-plane directions. The Hamiltonian of the 2DEG therefore becomes (the 2DEG is in the $x - y$ plane)

$$\hat{H} = \frac{\left(\hat{\vec{p}} - e\vec{A}(\hat{x}, \hat{y})\right)^2}{2m} + \frac{g\mu_{\mathrm{B}}}{2}\vec{H}(\hat{x}, \hat{y}) \cdot \hat{\vec{\sigma}} + V(\hat{y}), \tag{1.64}$$

where $\vec{H}(x, y)$ is the magnetic field vector and $\hat{\vec{\sigma}}$ the vector of the Pauli matrices.

In connection with our preliminary analysis it is clear that a non-trivial spin ratchet content of the considered system could be due to both the coupling of the spin degree of freedom to the spatial coordinates and the spin flipping. These two effects are both induced by the non-uniform magnetic field with an arbitrary spatial orientation.

In this setup the inequality (1.49) takes place and the spin current based on the conventional spin current operator (1.47) is not in general conserved in the 2DEG because the continuity equation (1.42) may have a non-zero source term. However, in Ref. [62] the spin current was measured in the leads where there was not any magnetic field and as a result the conventional (1.47) and alternative (1.55) spin current operators were equivalent. Due to the presence of the spin flip processes the spin currents in the two leads were different and thus one had to fix the lead in order to analyze the spin ratchet behavior.

Two cases were studied. In the first case there were two in-plane ferromagnetic stripes perpendicular to the transport direction which was along the x-axis. The stripes were magnetized along the y-axis in opposite directions. Therefore, the y-component of the vector potential was absent, $A_y(x, y) = 0$. The x and y-components of the magnetic field were odd functions of x, $H_x(x, y) = -H_x(-x, y)$, $H_y(x, y) = -H_y(-x, y)$ while the z-component was an even function of x, $H_z(x, y) = H_z(-x, y)$. To get such a magnetic field the x-component of the vector potential was chosen as an even function of x, $A_x(x, y) = A_x(-x, y)$. It is obvious that in this situation the commutation relations from the previous example, $[\hat{H}, \hat{\sigma}_{x/z}\hat{R}_x] = 0$, are not valid anymore. In Ref. [62] it was

assumed that the orbital effects due to the out-of-plane component of the magnetic field were negligible and thus the commutation relation $[\hat{H}, \hat{\sigma}_z \hat{R}_x] = 0$ took place under this assumption. It turned out that under this symmetry the charge ratchet mechanism did not exist in the system. At the same time the spin ratchet current was finite. In the second case there was a single ferromagnetic stripe magnetized in the $x - z$ plane. The y-component of the magnetic field was absent, $H_y(x, y) = 0$. The x-component of the magnetic field was chosen to be an odd function of x, $H_x(x, y) = -H_x(-x, y)$ and the z-component was an even function of x, $H_z(x, y) = H_z(-x, y)$. The corresponding vector potential had only the y-component which was an odd function of x, $A_y(x, y) = -A_y(-x, y)$. It is easy to see that for this configuration of the magnetic field the commutation relation $[\hat{H}, \hat{\mathcal{C}}\hat{R}_x\hat{\sigma}_z] = 0$ is satisfied. Here the complex conjugation operator $\hat{\mathcal{C}}$ is introduced in order to change the sign of $\hat{p}_y$. As it has been demonstrated in Ref. [62], when this new symmetry is present, the charge ratchet mechanism does not appear whereas the spin ratchet mechanism coexists with this symmetry.

Electrostatic ratchet potential

The two examples described above have a common feature: the spin flipping and/or coupling of the spin degree of freedom to orbital coordinates were induced by an external magnetic field which at the same time played the role of a ratchet potential. In this sense on can say that those spin ratchet mechanisms are of extrinsic nature. Now let us consider another example where a non-trivial spin ratchet behavior originates from intrinsic spin-orbit interactions. The example is based on the Rashba spin-orbit interaction (RSOI) [63]. This interaction and its spintronic applications will be reviewed in the next chapter. Here we describe an RSOI based implementation of the spin ratchet mechanism just from the general point of view of its non-trivial roots. This spin ratchet effect was studied in Ref. [64]. The setup differs from the previous two examples in three details: 1) there are no ferromagnetic stripes on the surface of the 2DEG anymore and as a result there is not any external magnetic field; 2) RSOI is present in the 2DEG; 3) as in the case of the particle ratchet mechanism from the previous section an external non-magnetic (*e.g.*, electrostatic) potential which is periodic in the transport direction has been included. The Hamiltonian of the 2DEG (in the $x - z$ plane) reads

$$\hat{H} = \frac{\hat{\vec{p}}}{2m} - \frac{\hbar k_{\text{so}}}{m}(\hat{\sigma}_x\hat{p}_z - \hat{\sigma}_z\hat{p}_x) + U(\hat{x}, \hat{z}), \tag{1.65}$$

where the term proportional to the spin-orbit coupling constant k_{so} is so-called Rashba Hamiltonian and $U(x, z)$ is a non-magnetic potential which describes a transverse confinement along the z-axis as well as a periodic potential along the x-axis (transport direction). Again from our general preliminary discussion we see that in this system there are convincing reasons for a non-trivial spin ratchet behavior. First of all there are spin flip processes because both $\hat{\sigma}_x$ and $\hat{\sigma}_z$ operators enter the Hamiltonian (1.65). The second important point is that the spin degree of freedom is coupled to the both orbital degrees of freedom, however, this time not through the coordinate operators as in the

previous cases with an external magnetic field but through the momentum operators. And, finally, the third important moment is that the periodic potential is not coupled to the spin operators as it was the case in the first example. What we would expect from our experience with the particle ratchet mechanism from the previous section is that since the periodic potential is not coupled to the spin operators, an asymmetry of the periodic potential must be crucial for the charge ratchet current. The charge ratchet mechanism must be absent when $U(x) = U(-x)$. However, no such conclusion can be made concerning the spin ratchet mechanism. This is exactly what was found in Ref. [64]. As one can see, the Hamiltonian (1.65) has the same symmetry as in the previous example, *i.e.*, $[\hat{H}, \hat{\mathcal{C}}\hat{R}_x\hat{\sigma}_z] = 0$, if the periodic potential is an even function, $U(x) = U(-x)$. In Ref. [64] it was shown that this commutation relation resulted in zero charge ratchet current and could coexist with a finite spin ratchet current. This means that the spin ratchet mechanism in this system is insensitive to the symmetry of the periodic potential and is present even when $U(x) = U(-x)$.

Magnetic and electrostatic ratchet potentials

An implementation of the coherent spin ratchet mechanism using resonant tunneling was proposed in Ref. [65]. In this implementation the Hamiltonian is similar to the Hamiltonian of the second example, Eq. (1.64), but the transverse confinement (non-magnetic potential) had an additional dependence on the x-coordinate (transport direction),

$$\hat{H} = \frac{\left(\hat{\vec{p}} - e\vec{A}(\hat{x}, \hat{y})\right)^2}{2m} + \frac{g\mu_{\mathrm{B}}}{2}\vec{H}(\hat{x}, \hat{y}) \cdot \hat{\vec{\sigma}} + V(\hat{x}, \hat{y}). \tag{1.66}$$

This additional x-dependence represented a resonant tunneling structure: two quantum wells (equivalently two quantum dots) separated by a potential barrier. The first case from the second example was considered, *i.e.*, there were two in-plane ferromagnetic stripes perpendicular to the x-axis. The stripes were magnetized along the y-axis in opposite directions and each of them was placed on the top of each of the two quantum wells. Therefore the energy levels in the two quantum wells had opposite Zeeman spin splitting. As a result the resonances for the spin-up and spin-down states took place in opposite transport directions resulting in a finite spin ratchet current and zero charge ratchet current (see Fig. 1.4). Here we see an additional concrete illustration of the general idea that in the presence of a symmetric potential not coupled to the spin degree of freedom (*i.e.*, $V(x, y)$, $V(x, y) = V(-x, y)$) the particle (or charge in the present context) ratchet mechanism cannot appear while the spin ratchet mechanism may exist.

1.2.4 Dissipative spin ratchets and this thesis

Above we have seen some concrete non-trivial examples where the spin ratchet mechanism was implemented through coherent electron transport. In those implementations electrons did not interact during their travelling process with any external environment. Thus travelling electrons did not lose any energy as well as did not gain any

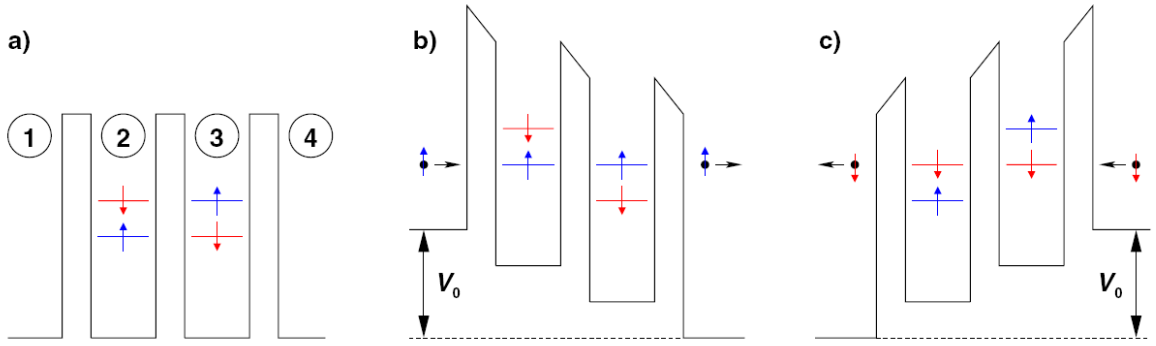

Figure 1.4: Illustration of the working principle of a resonant tunneling-based spin ratchet. a, System divided into four regions R1 to R4 through three barriers. A magnetic field, oriented in opposite directions in regions R2 and R3, splits the levels of spin-up and spin-down electrons (one representative level shown). b, c, Upon application of a positive or negative bias voltage, $\pm V_0$, the transmission probability is resonantly enhanced for spin-up or spin-down electrons, respectively [65].

energy from an external environment. Equivalently, there was not any dissipation or stochastic force responsible for an energy flow outside or inside the electronic system. Therefore, those spin ratchets cannot represent Brownian motors, the notion of which was introduced at the beginning of Section 1.1 devoted to the particle ratchet mechanism. The specific feature of the Brownian motor mechanism is that it requires a coupling of a given system to a thermal bath in order to have a possibility to extract work from the thermal fluctuations induced by this coupling. These fluctuations manifest through a particle's random walk, called Brownian motion. In the spin ratchet effects described above any Brownian motion between the fermionic reservoirs, to which the corresponding systems were coupled, was absent and hence it could not be converted into a finite spin ratchet current. The spin ratchet effects described above resulted from an interplay between the external driving fields, applied to the systems, and the coupling of the systems to their fermionic reservoirs. A characteristic feature of this interplay was that it did not induce any thermal fluctuations inside the systems and thus no subsequent conversion of any Brownian motion inside the systems into spin currents could take place.

A natural question is then whether the spin ratchet mechanism can be implemented as a Brownian motor. This is exactly the question which will be explored in the present thesis. From the discussion presented in this chapter it is now clear that in order to perform this investigation one needs to consider a system where a non-trivial spin-ratchet behavior is expected, couple this system to an external environment to induce Brownian motion in the system and apply unbiased driving fields.

In this thesis we employ a 2DEG with RSOI as a system which can support a non-trivial spin ratchet dynamics and couple it to an external environment described by the model of Caldeira and Leggett. In other words, the full Hamiltonian in our case is given by Eq. (1.5) where the Hamiltonian of the isolated system, Eq. (1.6), is replaced with the Hamiltonian (1.65) of an RSOI superlattice. We will consider both asymmetric and symmetric RSOI superlattices, *i.e.*, asymmetric and symmetric

periodic potentials in Eq. (1.65).

Moreover, we will also include a magnetic driving field. From the examples of the coherent spin ratchets we have seen that the driving was only electric. However, in our general discussion on a possibility for a given system to have a non-trivial spin ratchet behavior we mentioned a coupling of the spin degree of freedom to external driving fields. So far this additional aspect has not been studied at all. To answer the fundamental questions about the spin ratchet mechanism in a given system and to study an impact of the spin degree of freedom on the particle ratchet mechanism in the same system one has to also include a coupling of the spin degree of freedom to external fields. Thus, in addition to an electric driving field, which will be symmetric in time and have the form of Eq. (1.11), we will also include a magnetic driving field. It will be coupled to the spin degree of freedom through the Zeeman term and have the same time dependence (1.11), *i.e.*, the magnetic driving will be also symmetric in time.

We will be interested in the stationary dynamics of the above described driven open quantum system. As it was mentioned in Subsection 1.1.3, transport in such open quantum systems has incoherent nature at long times. We can therefore classify what we are going to investigate as incoherent space rocked charge (particle) and spin ratchet mechanisms implemented as Brownian charge and spin motors.

It will be demonstrated that under electric driving the spin ratchet mechanism is present when the RSOI superlattice [66] is asymmetric and that the charge ratchet mechanism is absent when the electrons in the superlattice populate only one Bloch band [67]. With this a possibility of a dissipative pure spin ratchet [68] will be established. An in-plane stationary magnetic field will be taken into account. It will be proven that such a magnetic field does not break the existence conditions of the spin ratchet mechanism but it can significantly enhance or reduce the spin ratchet current [69]. Finally, a magnetic driving field will be involved and it will be shown that the charge ratchet mechanism appears in this case just because of the Rashba spin flip processes in the isolated system and that this charge ratchet mechanism exists even when the periodic potential of the RSOI superlattice is spatially symmetric [70].

This thesis is organized as follows. Chapter 2 is a short overview of RSOI and its spintronic applications. In Chapter 3 a quasi-1D superlattice with RSOI is described and its energy spectrum is analyzed. A tight-binding model employed in our transport calculations is developed in Chapter 4. The main results of the thesis are obtained in Chapter 5 where we perform an analytical and numerical investigation of the existence of the charge and spin ratchet mechanisms in a dissipative system with RSOI.

Chapter 2

Rashba spin-orbit interaction

2.1 Introduction

In this chapter an overview of the theoretical and experimental aspects related to Rashba spin-orbit interaction is presented in order to gain physical insight as well as support the understanding of the results obtained in the following three chapters.

In the late fifties and early sixties of the twentieth century a new, at that time, type of band structure was investigated in semiconductors with wurtzite lattice. The characteristic feature of that band structure was that it had an extremum not at isolated points of the Brillouin zone but over a whole curve (extremum loop) - a periphery whose center lied on the axis of symmetry. To study absorption of radio waves in such semiconductors Rashba in 1960 introduced a spin-orbit term which gave rise to transitions involving a change in spin due to the Lorentz force [63]. This term got the name of Rashba, Rashba spin-orbit interaction. We will abbreviate it RSOI as in the previous chapter.

During the eighties RSOI took a new life. The point was that during this period a set of experimental data on the combined resonance (*i.e.*, electric dipole spin resonance) and the cyclotron resonance of a 2DEG at the interfaces of GaAs-$Al_xGa_{1-x}As$ heterojunctions were reported in the papers of Stein *et al.* [71] and Stormer *et al.* [72]. The experiments showed that the spin degeneracy was lifted in the inversion layer. The theory developed by Rashba in 1960 enabled Bychkov and Rashba [73] to describe this experimental data using a spin-orbit interaction term in the total Hamiltonian. This spin-orbit part of the total Hamiltonian was RSOI. Bychkov and Rashba wrote it in the following form:

$$\hat{H}_{\rm so} = \alpha[\hat{\vec{\sigma}} \times \hat{\vec{k}}] \cdot \vec{n}. \tag{2.1}$$

In Eq. (2.1) $\vec{n}$ is a unit vector perpendicular to the layer and $\hat{\vec{p}} \equiv \hbar\hat{\vec{k}}$, $\alpha \equiv \hbar^2 k_{\rm so}/m$. Other notations are the same as in Chapter 1. Like the momentum operator $\hat{\vec{p}}$ and its eigenvalue $\vec{p}$, called momentum, we will call $\hat{\vec{k}}$ and $\vec{k}$ as momentum operator and momentum, respectively. The spin-orbit operator $\hat{H}_{\rm so}$ in Eq. (2.1) lifts the twofold spin degeneracy at momenta $\vec{k} \neq 0$ and results in a spin-orbit band slitting near zero momentum, $\vec{k} = 0$.

2.2 Two-Dimensional Electron Gas

In semiconductor technology based on planar integrated circuit design, quantum confinement can be realized in two different ways: 1) through the growth of inhomogeneous layered structures where the dynamics is quantized in the growth direction; 2) through lateral patterning using ultrafine lithography techniques. Historically, a system where quantum size effects played an important role was first implemented using the growth approach. It was done in Ref. [74] where quantum size effects were experimentally detected in the inversion layer of a SiMOS structure. In this system, quantization of the carrier motion is essential at the Si/SiO_2 interface where a narrow potential well results from the band bending induced by the gate voltage. Later, with the development of precision epitaxial growth techniques such as molecular beam epitaxy and metal organic chemical vapor deposition, high-quality lattice-matched heterojunction systems could be realized. In these systems 2D layers formed at the heterointerfaces exhibited quantum size effects which were more pronounced than the ones in the SiMOS system. This happens because the surface state density at the heterointerface of the lattice-matched materials, such as GaAs and $Al_xGa_{1-x}As$, is lower and also because the conduction band mass is usually smaller.

To understand why a 2D layer is formed at the heterointerface let us consider the conduction and valence bands along the z direction. Before joining the two semiconductors (Fig. 2.1a) the Fermi energy E_f in the widegap n-AlGaAs layer is higher than in the narrowgap GaAs layer. Consequently, electrons come out from the n-AlGaAs leaving positively charged donors. This space charge gives rise to an electric field that causes the bands to bend as shown in Fig. 2.1b. In the equilibrium the Fermi energy must be constant in the whole structure. Thus the electron density is sharply peaked near the n-AlGaAs/GaAs interface forming a thin conduction 2D layer that is a 2DEG. The carrier concentration in a 2DEG typically ranges from $2 \cdot 10^{11}\text{cm}^{-2}$ to $2 \cdot 10^{12}\text{cm}^{-2}$ and can be varied by applying a voltage to a metallic gate deposited on the surface. Usually a 2DEG is confined in layers of thickness of about 100 Å. This corresponds to a bulk concentration of 10^{18}cm^{-3}. In structures of this kind the electron mobility is very high, up to 10^6 $\text{cm}^2/(\text{V} \cdot \text{s})$. Such large values are reached because of the spatial separation between the donor atoms in the n-AlGaAs layer and the conduction electrons in the 2D layer formed at the heterointerface. As a result the cross-section due to the impurity scattering is extremely low.

2.3 Rashba effect in a 2DEG

It is well known that spin-orbit coupling in a 2DEG may have two distinct sources. The first source is due to the inversion asymmetry of the zinc-blende crystal structure of the bulk host material. The corresponding contribution to the Hamiltonian was obtained in Refs. [75, 76] in the lowest order in the momentum k. This contribution has the form,

$$\hat{H}_{k^3} = \gamma[\hat{\sigma}_x\hat{k}_x(\hat{k}_y^2 - \hat{k}_z^2) + \hat{\sigma}_y\hat{k}_y(\hat{k}_z^2 - \hat{k}_x^2) + \hat{\sigma}_z\hat{k}_z(\hat{k}_x^2 - \hat{k}_y^2)], \tag{2.2}$$

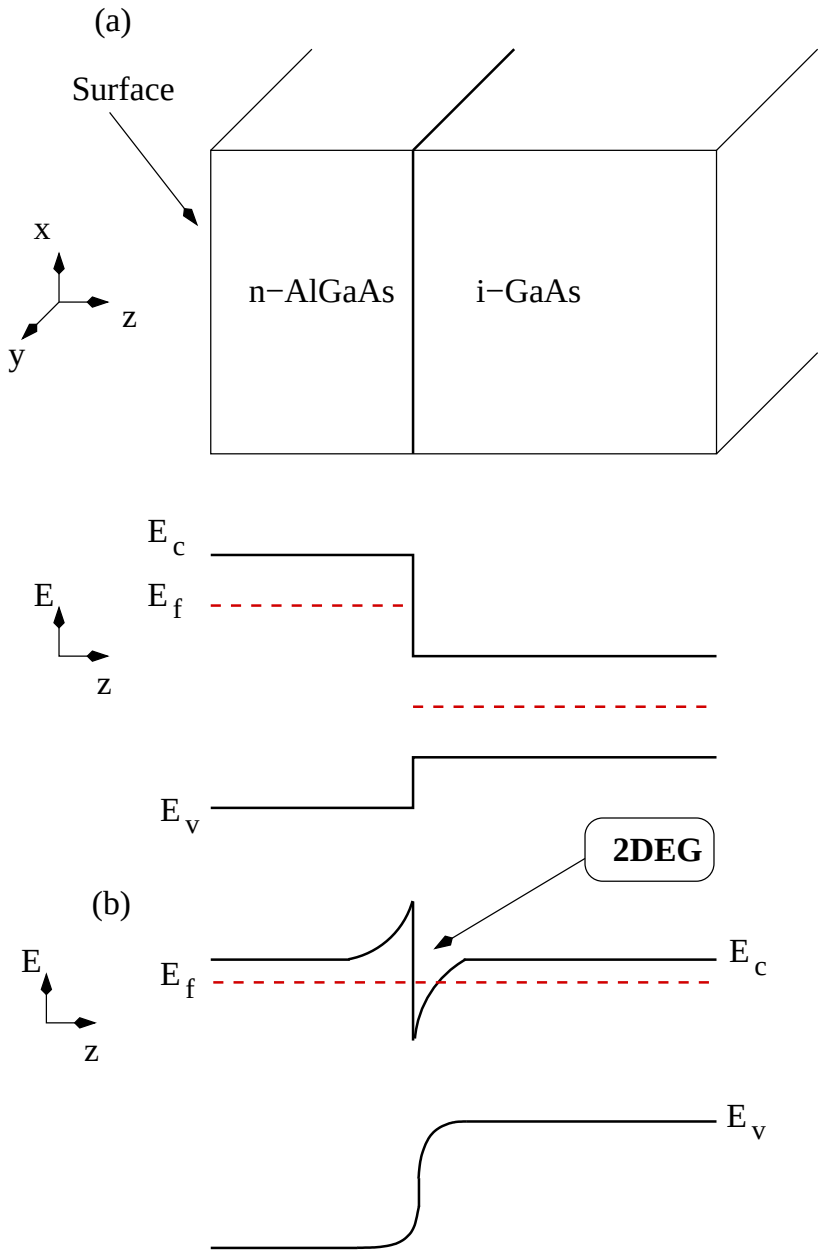

Figure 2.1: The conduction and valence bands along the growth direction (which is along the z-axis) in a vicinity of the heterojunction between an n-type AlGaAs and intrinsic GaAs. a, The semiconductor layers joined along the growth direction and the band structure which would take place without the charge redistribution. b, The band structure after the charge redistribution which is responsible for the 2DEG formation.

where γ is a material constant and the coordinate axes are along the crystallographic ones. In a sufficiently narrow quantum well grown along the [001] direction it is possible to replace the operators $\hat{k}_z$ and $\hat{k}_z^2$ by their expectation values $\langle\hat{k}_z\rangle$, $\langle\hat{k}_z^2\rangle$. This leads to the following two contributions to spin-orbit coupling resulting from the bulk inversion asymmetry: the Dresselhaus term,

$$\hat{H}_{\mathrm{D}} = \beta(\hat{\sigma}_x\hat{k}_x - \hat{\sigma}_y\hat{k}_y), \tag{2.3}$$

linear in the momentum operators with $\beta = -\gamma\langle\hat{k}_z^2\rangle$ and the cubic term,

$$\hat{H}_{\mathrm{D}}^{(3)} = \gamma(\hat{\sigma}_x\hat{k}_x\hat{k}_y^2 - \hat{\sigma}_y\hat{k}_y\hat{k}_x^2). \tag{2.4}$$

The magnitude of $\langle\hat{H}_{\mathrm{D}}^{(3)}\rangle$ compared to $\langle\hat{H}_{\mathrm{D}}\rangle$ is given by the ratio between the Fermi energy E_{F} and the kinetic energy of the quantized degree of freedom corresponding to the growth direction. For typical values of E_{F} (about 10 meV) and not too wide quantum wells this ratio is small. Therefore, the Dresselhaus cubic term is usually neglected.

The second source of spin-orbit coupling in a 2DEG is due to the Rashba effect. In contrast to the Dresselhaus effect, RSOI is not related to bulk properties. It has been demonstrated by de Andrada e Silva *et al.* [77] that RSOI is only present in semiconductor heterostructures where there is a lack of inversion symmetry along the growth direction.

Let us consider what is the essential difference between RSOI and the linear Dresselhaus spin-orbit interaction (LDSOI). Since LDSOI comes from bulk properties of a semiconductor, the corresponding coupling constant β is fixed and cannot be tuned. However, RSOI depends on the shape of the confining potential. Its coupling constant α can be tuned by means of a metallic gate voltage because the confining potential can be modified by an electric field (see Fig. 2.2). This feature can be verified experimentally. One possible experiment is based on studying beat patterns in the Shubnikov-de Haas (SdH) oscillations [78–80]. The idea is that the magnetoconductance of a 2DEG (in the $x-y$ plane to be definite) at $T=0$ is given by

$$\sigma_{xx} \propto \sum_{n,\sigma}\left(n+\frac{\sigma}{2}\right)\exp\left\{-\frac{(E_F - E_{n,\sigma})^2}{\Gamma^2}\right\}, \tag{2.5}$$

where $E_{n,\sigma}$ is the energy of the n-th Landau level corresponding to the out-of-plane spin projection $\sigma = \pm 1$ and Γ is the Landau level broadening which is assumed to be constant. In a magnetic field $\vec{B} = (0,0,B)$ the energy spectrum is quantized and the corresponding Landau levels [56] are

$$\begin{aligned} E_{0,\sigma} &= \frac{1}{2}\hbar\omega_c, \\ E_{n,\sigma} &= \hbar\omega_c\left[n + \frac{\sigma}{2}\sqrt{\left(1-\frac{gm}{2}\right)^2 + n\frac{\Delta_R^2}{E_F\hbar\omega_c}}\right], \quad n>0, \end{aligned} \tag{2.6}$$

where ω_c is the cyclotron frequency, $\omega_c = eB/m$, and g the effective electron spin

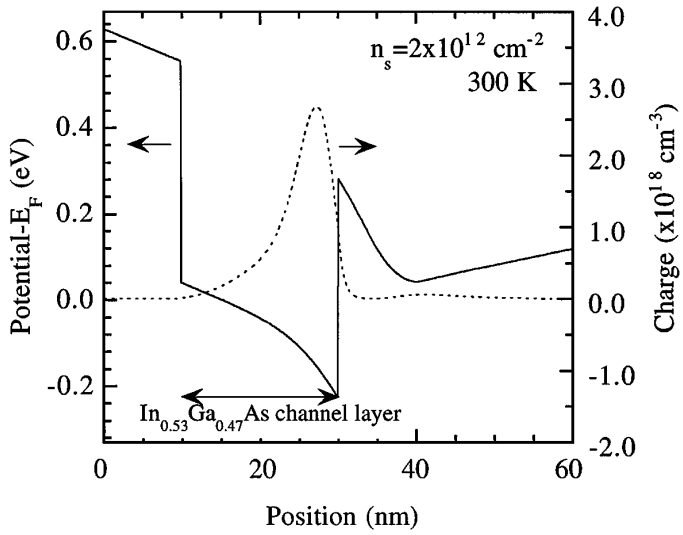

Figure 2.2: Calculated conduction band profile and electron density [78].

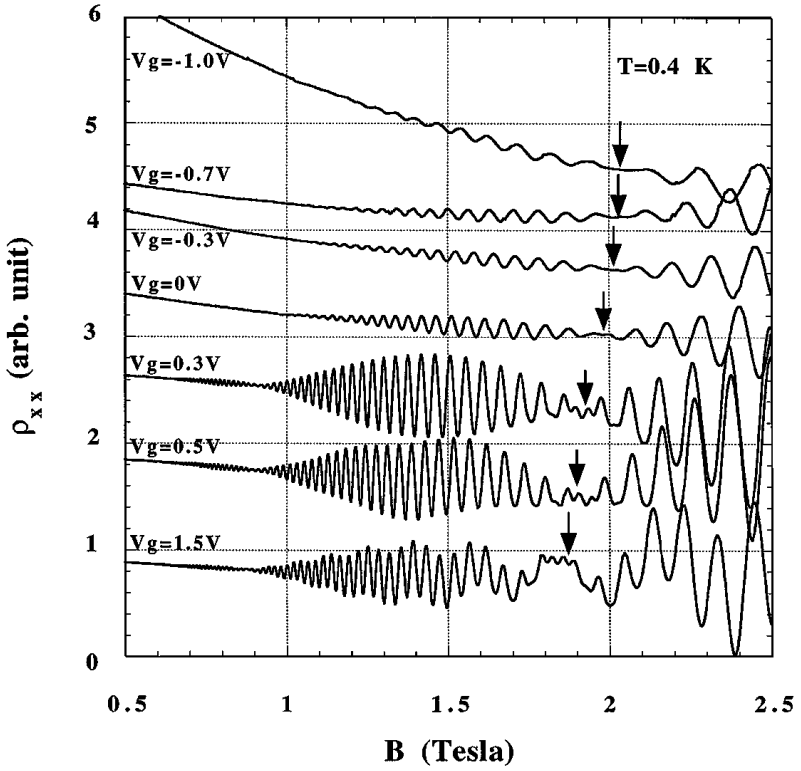

Figure 2.3: Shubnikov-de Haas oscillations as a function of the applied gate voltage. [78]. Here ρ_{xx} denotes the magnetoresistance.

g-factor. In Eq. (2.6) the information related to RSOI is kept in the term $\Delta_R = 2k_F\alpha$ where k_F is the Fermi momentum.

In Fig. 2.3 the SdH oscillations as a function of the applied gate voltage are shown

in an $In_{0.53}Ga_{0.47}As/In_{0.52}Al_{0.48}As$ heterostructure at the temperature 0.4 K. The presence of the beat patterns clearly demonstrates the existence of two closely spaced SdH oscillation frequency components with similar amplitudes. Increasing the positive gate voltage from $V_g = 0$ V to $V_g = 0.3$ V enhances the beat pattern. Above $V_g = 0.5$ V a different low SdH oscillation frequency component becomes visible due to the occupation of the second Landau sub-band. For more negative V_g the oscillation frequency becomes lower because of the decrease in the carrier concentration. From this experiment Nitta and colleagues [78] obtained a variation of α in the range between $0.6 \cdot 10^{-11}$ and $0.95 \cdot 10^{-11}$ eV·m.

In another experiment the possibility to tune the strength of RSOI is measured taking into account the fact that the conductivity of low-dimensional systems shows signatures of quantum interference which is sensitive to a magnetic field and spin-orbit coupling [81]. In particular, constructive backscattering associated with pairs of time-reversed closed-loop electron trajectories in the absence of significant spin-orbit interactions leads to negative magnetoresistance effects known as weak localization. On the contrary, when significant spin-orbit interactions are present, the backscattering becomes destructive and positive magnetoresistance effects are observed indicating anti-weak localization.

It has been demonstrated by Miller *et al.* [82] that changing the spin-orbit coupling strength by a top-gate voltage in a moderately high-mobility 2DEG formed in a GaAs/AlGaAs heterostructure one can induce a crossover from weak localization to weak anti-localization (see Fig. 2.4).

The two experimental techniques described above are not able to estimate the relation between the strengths of RSOI and LDSOI. To measure this relation one may resort to an experiment [83] exploring the angular dependence of the spin-galvanic photocurrent [84]. The spin-galvanic effect in semiconductor heterostructures is induced by a non-equilibrium, but uniform spatial distribution of electron spins. The microscopic origin of this effect is the presence of a relative shift in the momentum space between the unequally populated energy sub-bands (see Fig. 2.5) describing electronic states with opposite spins. There is an inherent asymmetry in the spin-flip scattering events between the two sub-bands. This scattering asymmetry leads eventually to an asymmetry in the population of the sub-bands and thus to a spin-galvanic photocurrent. The spin-galvanic photocurrent is driven by the average in-plane electron spin $\vec{S}_\parallel$ according to

$$\vec{j}_{\mathrm{SGE}} \propto \begin{pmatrix} \beta & -\alpha \\ \alpha & -\beta \end{pmatrix} \vec{S}_\parallel. \tag{2.7}$$

The main idea [83] is that the spin-galvanic photocurrent $\vec{j}_{\mathrm{SGE}}$ for a certain direction of $\vec{S}_\parallel$ consists of RSOI and LDSOI induced photocurrents, $\vec{j}_{\mathrm{R}}$ and $\vec{j}_{\mathrm{D}}$. Their magnitudes are $j_{\mathrm{R}} \propto \alpha|\vec{S}_\parallel|$ and $j_{\mathrm{D}} \propto \beta|\vec{S}_\parallel|$, and their ratio is

$$\frac{j_{\mathrm{R}}}{j_{\mathrm{D}}} = \frac{\alpha}{\beta}. \tag{2.8}$$

For $\vec{S}_\parallel$ oriented along one of the crystallographic axes it follows from Eq. (2.7) that

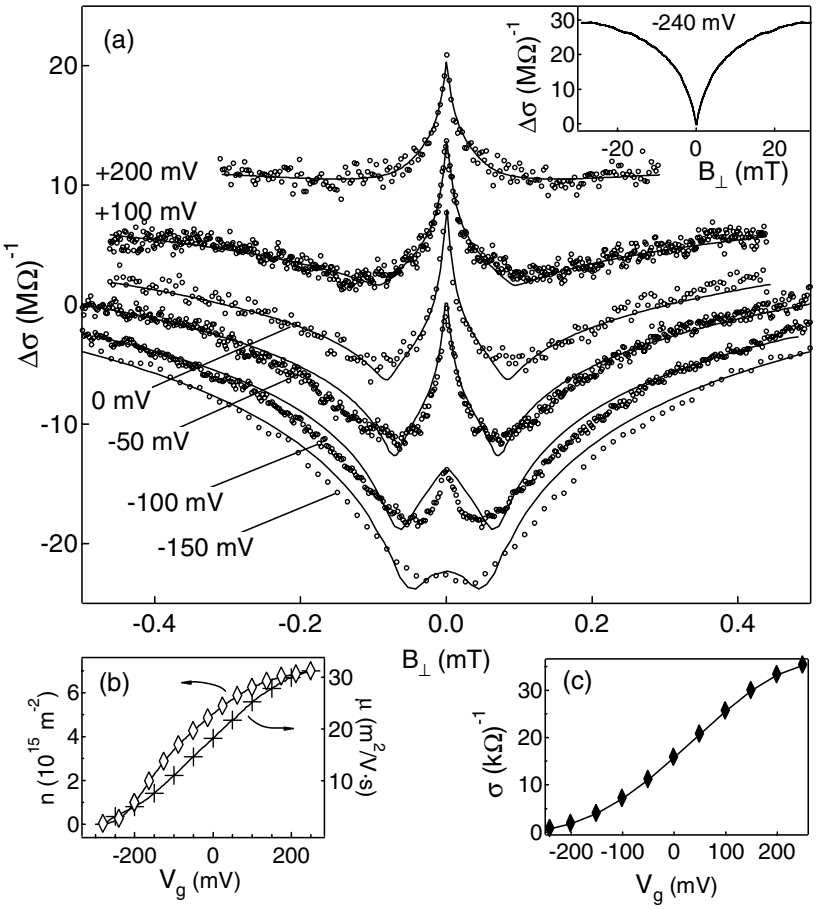

Figure 2.4: a, Experimental magnetoconductance, $\Delta\sigma = \sigma(B) - \sigma(0)$ (circles), offset for clarity, along with three-parameter fits (solid line) for several gate voltages. Inset: Experimental magnetoconductance data for the most negative gate voltage, showing pure weak localization. b, Density and mobility as function of V_g, extracted from longitudinal and Hall voltage measurements. c, Experimental conductivity, showing strong dependence on V_g [82].

the photocurrents flowing along and perpendicular to $\vec{S}_{\|}$ are equal to j_{D} and j_{R}, respectively, yielding experimental access to determine α/β.

The experiment of Ganichev *et al.* [83] was performed using an $\mathrm{InAs/Al_{0.3}Ga_{0.7}Sb}$ n-type heterostructure. The growth direction was [001]. The width of the quantum well was 15 nm, the density of free carriers about $1.3 \cdot 10^{12}$ cm^{-2} and the carrier mobility at room temperature $\sim 2 \cdot 10^4$ cm^2/(V $\cdot$ s). The ratio between the RSOI and LDSOI photocurrents was found to be equal to $j_{\mathrm{R}}/j_{\mathrm{D}} = 2.15 \pm 0.25$ in a good agreement with the value of the ratio α/β from theoretical results predicting that in InAs quantum wells RSOI dominates over LDSOI.

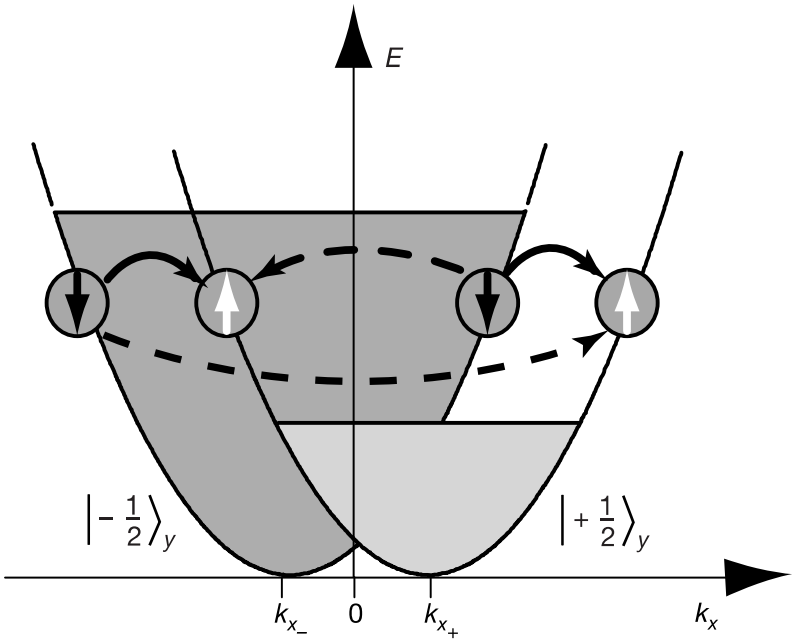

Figure 2.5: Microscopic origin of the spin-galvanic current in the presence of $\vec{k}$-linear terms in the electron Hamiltonian. If one spin sub-band is preferentially occupied (*e.g.*, by spin injection), then asymmetric spin-flip scattering processes (dashed arrows) yield a finite x-component of the charge current. This happens because such scattering results in an asymmetric occupation of the two sub-bands.

2.4 Persistent spin helix

In the previous section we have considered three spin-orbit interactions: RSOI, Eq. (2.1), LDSOI, Eq. (2.3), and the Dresselhaus cubic spin-orbit interaction, Eq. (2.4). We have also discussed the relative importance of these spin-orbit interactions in a 2DEG. It is instructive to reconsider the roles of $\hat{H}_{\rm so}$, $\hat{H}_{\rm D}$ and $\hat{H}_{\rm D}^{(3)}$ from the point of view of the SU(2) symmetry. The generators of the SU(2) group are given through the spin operators. Therefore, the Hamiltonians $\hat{H}_{\rm so}$, $\hat{H}_{\rm D}$ and $\hat{H}_{\rm D}^{(3)}$ cannot be invariant with respect to spin rotations, *i.e.*, the SU(2) symmetry is broken. According to the basics of quantum mechanics [56] breaking of the spin rotational symmetry of a system means that in this system the total spin is not conserved. The absence of the spin conservation shows its face in experiments dealing with spins lifetimes in systems in which the SU(2) symmetry is broken: an initially spin polarized system quickly goes to a state in which it has no net spin. As discussed in the previous section, the RSOI coupling strength can be varied by a gate voltage and the situation with $\alpha = \beta$ can be realized. This situation can also be realized by changing the width of a quantum well since in this case β will change. When in a system $\alpha = \beta$, the SU(2) symmetry of this system is recovered [85] in the presence of both RSOI and LDSOI. As a result the spin lifetime in this system gets infinite giving rise to a persistent spin helix. From the practical point of view this means that for $\alpha = \beta$ the spin lifetime in this system must significantly increase in the presence of both RSOI and LDSOI which have no impact on the spin

lifetime anymore and thus other mechanisms for spin decay must become relevant. A persistent spin helix was detected experimentally [86, 87] in GaAs quantum wells. Approaching the symmetry point $\alpha = \beta$ a spin lifetime enhancement of two orders of magnitude was observed and the Dresselhaus cubic spin-orbit interaction, Eq. (2.4), was identified as the main term violating the SU(2) symmetry.

2.5 Eigenenergies and eigenstates of a 2DEG with RSOI

Let us find the eigenenergies and eigenstates of an electron in a 2DEG with RSOI. The total Hamiltonian of the system is the sum of the kinetic energy and the spin-orbit term (2.1),

$$\hat{H} = \frac{\hbar^2 \hat{\vec{k}}^2}{2m} + \alpha[\hat{\vec{\sigma}} \times \hat{\vec{k}}] \cdot \vec{n}. \tag{2.9}$$

From Eq. (2.9) one can immediately see that RSOI violates the spatial inversion symmetry. Another feature is that none of the operators $\hat{\vec{\sigma}}_i$, $i = x, y, z$, commutes with the Hamiltonian (2.9). Therefore, none of the spin projections is a good quantum number. On the other side, the chirality operator,

$$\hat{R} \equiv [\hat{\vec{\sigma}} \times \hat{\vec{e}}\,] \cdot \vec{n}, \tag{2.10}$$

with

$$\hat{\vec{e}} \equiv \frac{\hat{\vec{k}}}{|\hat{\vec{k}}|} \tag{2.11}$$

being the operator of the momentum direction, commutes with the Hamiltonian (2.9) and momentum operator. Since the momentum operator commutes with the Hamiltonian (2.9), we come to the conclusion that in a 2DEG with RSOI an electron state is described by an eigenvalue of the chirality operator, λ, and by an eigenvalue of the momentum operator, *i.e.*, it has the label $(\vec{k}, \lambda)$.

To be definite let us consider Eq. (2.9) in the $x - y$ plane. In the plane wave basis $|\vec{k}, \sigma\rangle$ the chirality operator is

$$\langle \vec{k}', \sigma' | \hat{R} | \vec{k}, \sigma \rangle = \delta_{\vec{k}', \vec{k}} \begin{pmatrix} 0 & -\mathrm{i}e^{\mathrm{i}\phi_{\vec{k}}} \\ \mathrm{i}e^{-\mathrm{i}\phi_{\vec{k}}} & 0 \end{pmatrix}, \tag{2.12}$$

where $\phi_{\vec{k}}$ is the angle between the electron momentum $\vec{k}$ and the x-axis. In Eq. (2.12) and below in this section we use the spinorial notations [56]. The eigenvalues λ and eigenvectors $|\vec{k}, \lambda\rangle$ of the chirality operator are easily found from the diagonalization of the matrix in Eq. (2.12). One obtains,

$$\langle \vec{k}', \sigma | \vec{k}, \lambda \rangle = \delta_{\vec{k}', \vec{k}} \frac{1}{\sqrt{2}} \begin{pmatrix} 1 \\ \lambda \mathrm{i}e^{-\mathrm{i}\phi_{\vec{k}}} \end{pmatrix}, \quad \lambda = \pm 1. \tag{2.13}$$

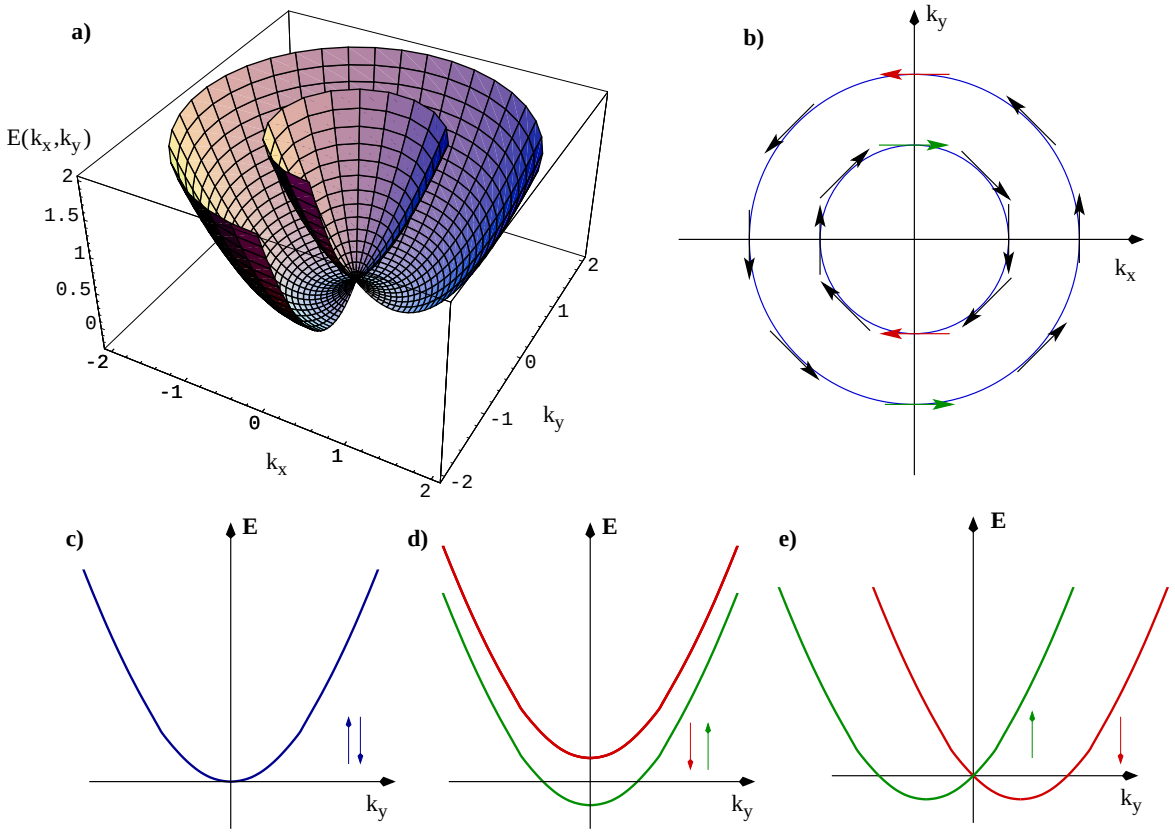

Figure 2.6: Rashba energy spectrum. a, Energy spectrum of the Hamiltonian (2.9). b, The Fermi contours and the average spin in the corresponding eigenstates. c, Cross-section of the energy spectrum for a free 2D electron. d, Cross-section of the energy spectrum for a 2D electron in the presence of a magnetic field (Zeeman slitting). e, Cross-section of the energy spectrum for a 2D electron in the presence of RSOI.

Since the eigenvectors of the chirality operator are also the eigenvectors of the Hamiltonian (2.9), we get the following eigenenergies and eigenstates of an electron in a 2DEG with RSOI,

$$\epsilon_\lambda(\vec{k}) = \frac{\hbar^2\vec{k}^2}{2m} + \alpha|\vec{k}|\lambda = \frac{\hbar^2}{2m}(|\vec{k}| + \lambda k_{\rm so})^2 - \Delta_{\rm so}, \tag{2.14}$$

$$\langle\vec{r},\sigma|\vec{k},\lambda\rangle = e^{{\rm i}\vec{k}\cdot\vec{r}}\frac{1}{\sqrt{2}}\begin{pmatrix}1\\ \lambda{\rm i}e^{-{\rm i}\phi_{\vec{k}}}\end{pmatrix}, \tag{2.15}$$

where $|\vec{r},\sigma\rangle$ is the eigenvector of the coordinate operator and $\Delta_{\rm so} \equiv \hbar^2 k_{\rm so}^2/2m$. The energy spectrum is graphically depicted in Fig. 2.6a. The expectation value $\langle\vec{k},\lambda|\hat{\vec{\sigma}}|\vec{k},\lambda\rangle$ is shown in Fig. 2.6b. Note that $\langle\vec{k},\lambda|\hat{\sigma}_z|\vec{k},\lambda\rangle = 0$ and the average spin is always perpendicular to the momentum.

In Fig. 2.6c-e the cross-sections of the electron energy spectra in a 2DEG are shown under different physical conditions. Fig. 2.6c is the spectrum of a free electron in a 2DEG. In this case the spin degeneracy is present. In the presence of a magnetic field $\vec{B}$ (see Fig. 2.6d) the spin degeneracy is removed by the Zeeman effect and the relative shift (along the energy axis) between the two energy branches is equal to $g\mu_{\rm B}|\vec{B}|$ where g is the the effective electron spin g-factor and $\mu_{\rm B}$ is the Bohr magneton. When RSOI is present, Fig. 2.6e, the spin degeneracy is removed except the zero momentum point, $\vec{k} = 0$. Additionally, in contrast to the Zeeman effect, where the energy branches are shifted along the energy axis, the RSOI shifts the energy branches along the momentum axis.

2.6 Conclusion

In this chapter a 2DEG with spin-orbit interactions has been considered. We have started with a short reminder on a 2DEG formation. After this the roles of RSOI, LDSOI and the Dresselhaus cubic spin-orbit interaction have been discussed. At this point it has been emphasized that the most essential feature for spintronic applications of RSOI is the possibility to control its strength by means of a gate voltage. Due to this fact $k_{\rm so}$ becomes an important variable and thus in Chapter 5, when exploring the spin ratchet mechanism, we will also investigate the corresponding spin ratchet current as a function of the RSOI coupling strength. Finally, at the end of this chapter the eigenenergies and eigenstates of a 2DEG with RSOI have been presented. The energy spectrum of this system is a basis in understanding the Bloch bands of the RSOI superlattice studied in Chapter 3.

Chapter 3

Energy spectrum of a spin-orbit superlattice

In collaboration with D. Bercioux and M. Grifoni, Ref. [66].

3.1 Introduction

In this chapter we consider a 2DEG with RSOI and two in-plane potentials superimposed along directions perpendicular to each other. The first of these potentials is assumed to be a general periodic potential while the second one is totally arbitrary. A general form for the Bloch amplitude is found and an eigenvalue problem for the band structure of the system is derived. We apply the general result to the two particular cases in which either the second potential represents a harmonic in-plane confinement or it is zero. We find that for a harmonic confinement regions of the Brillouin zone with high polarizations are associated with the ones of large group velocity.

From Chapter 2 we know that in a 2DEG, formed in a semiconductor heterostructure by an asymmetric confining potential, RSOI, Eq. (2.1), plays an important role. It is very attractive for applications in electronic devices because the spin-orbit coupling strength can be controlled by an external gate voltage. Other spin-orbit mechanisms such as LDSOI, Eq. (2.3), or the spin-orbit interaction which is cubic in momentum, Eq. (2.4), can be relevant. In this thesis, for simplicity, we focus on the effects of RSOI since the LDSOI term can be treated in full analogy. Additionally, when externally enhanced, RSOI may become stronger than other spin-orbit interactions as it was mentioned in Section 2.3. In this case the Hamiltonian has the form of Eq. (2.9) which we write here for the $x-z$ plane, *i.e.*, in Eq. (2.9) $\vec{n}=(0,1,0)$:

$$\hat{H}_0^{\mathrm{2D}}=\frac{\hbar^2\hat{\vec{k}}^2}{2m}-\frac{\hbar^2 k_{\mathrm{so}}}{m}\big(\hat{\sigma}_x\hat{k}_z-\hat{\sigma}_z\hat{k}_x\big). \tag{3.1}$$

According to Eq. (2.15) the eigenstates of the Hamiltonian (3.1) have a 2D spinorial part $\phi_\lambda^{\mathrm{2D}}(\sigma)$ where λ is an eigenvalue of the chirality operator (2.10), $\lambda=\pm1$, and σ is an eigenvalue of $\hat{\sigma}_z$, $\sigma=\pm1$. The eigenenergies split into two branches

$\varepsilon_\lambda^{2\mathrm{D}}(k_x, k_z)$ described by Eq. (2.14). Systems with such energy spectrum can be exploited to study spin-dependent transport in different semiconductor heterostructures, especially in III-V compounds because of the large values of the spin-orbit coupling strength. As mentioned above they are also used to build both 2D and essentially 1D electronic devices. One such device, called spin transistor, was proposed in Ref. [88] for the case of a quasi-1D system with RSOI. It is obtained from a 2DEG described by Eq. (3.1), where by further confinement along, *e.g.*, the z-direction, a quasi-1D wire is formed. These quasi-1D systems were investigated for the case of a harmonic z-confinement [89–91] and for an infinite square well z-confinement [92]. In general one can conceive a situation where an arbitrary potential $V(z)$ along the z-direction is present. We would like to emphasize that $V(z)$ must not necessarily be a confinement. In this case the Hamiltonian is written as:

$$\hat{H}_z^{2\mathrm{D}} = \frac{\hbar^2 \hat{\vec{k}}^2}{2m} + V(\hat{z}) - \frac{\hbar^2 k_{\mathrm{so}}}{m}\big(\hat{\sigma}_x \hat{k}_z - \hat{\sigma}_z \hat{k}_x\big). \tag{3.2}$$

The Hamiltonian $\hat{H}_z^{2\mathrm{D}}$ assumes that the spin-orbit interaction caused by $V(z)$ is much weaker than RSOI induced by an asymmetric confinement forming the 2DEG. For a given system this means that the out-of-plane electric field should be much stronger than the in-plane one.

In systems described by (3.2) RSOI removes the spin degeneracy of each energy branch and splits them into two ones. The splitting is also accompanied by a deviation from the quadratic dependence on the momentum. For example in the case of a harmonic z-confinement, if only the first two transverse sub-bands are considered, there are four 1D dispersion relations $\varepsilon_\chi^{1\mathrm{D}}(k_x)$, $\chi = 1, 2, 3, 4$. The eigenstates have a four-dimensional spinorial part $\phi_{k_x,\chi}^{1\mathrm{D}}(\sigma, j)$ where $j = 0, 1$ is the transverse mode index. It turns out that for this model the energy spectrum can be found in analytic form [91] from the diagonalization of Hamiltonian (3.2).

Structures where a periodic modulation $U(x)$ is additionally present have recently been investigated by various authors. For the case $U(x) \neq 0$, $V(z) = 0$ the Bloch band energies have been found in Ref. [93] within the tight-binding approximation. In Ref. [94] the same problem has been investigated numerically. In the presence of an external homogeneous magnetic field the so-called magnetic Bloch states are discussed in Ref. [95] for the case $U(x) \neq 0$ and $V(z)$ being periodic as well. However, analytic relations between the eigenvalues of those problems and the ones of their corresponding truly 1D problems without RSOI have not been provided so far and this is one of the topics of the present chapter.

In this chapter we consider two potentials $U(x)$ and $V(z)$, where the potential $U(x)$ is a periodic potential while the shape of the potential $V(z)$ is arbitrary. First, a general structure of the Bloch amplitude is educed. Next, we formulate the eigenvalue problem. As an example we apply the general approach to the particular case of a harmonic confinement and, as a consequence, taking into account only the first two transverse modes, we generalize the analytical results obtained in Ref. [91] to the case of a periodic potential along the wire. Finally, setting $V(z) = 0$ we analytically solve the problem examined numerically in [94]. Since in the latter case transverse modes

do not exist, we do not need to make any approximation restricting ourselves to a few first transverse modes. In this sense the problem with $V(z) = 0$ is solved exactly.

3.2 A periodic structure with RSOI

In this section we consider a system described by the Hamiltonian $\hat{H}_z^{2\mathrm{D}} + U(\hat{x})$ where the 1D periodic potential $U(x)$ has the period L:

$$U(x + L) = U(x). \tag{3.3}$$

That is, the total Hamiltonian of the problem is

$$\hat{H} = \frac{\hbar^2 \hat{\vec{k}}^2}{2m} + V(\hat{z}) - \frac{\hbar^2 k_{\mathrm{so}}}{m}\left(\hat{\sigma}_x \hat{k}_z - \hat{\sigma}_z \hat{k}_x\right) + U(\hat{x}). \tag{3.4}$$

Before considering the full problem it is instructive to refresh the Bloch theorem for a truly 1D periodic structure without RSOI.

3.2.1 A truly 1D periodic structure

As it is known [96], a system described by the Hamiltonian

$$\hat{H}_0^{1\mathrm{D}} = \frac{\hbar^2 \hat{k}_x^2}{2m} + U(\hat{x}) \tag{3.5}$$

has eigenenergies $\varepsilon_{l,\sigma}^{(0)}(k_{\mathrm{B}})$ and eigenstates $|l, k_{\mathrm{B}}, \sigma\rangle$, with

$$\hat{H}_0^{1\mathrm{D}} |l, k_{\mathrm{B}}, \sigma\rangle = \varepsilon_{l,\sigma}^{(0)}(k_{\mathrm{B}}) |l, k_{\mathrm{B}}, \sigma\rangle, \tag{3.6}$$

characterized by Bloch's quasi-momentum k_{B}, running over a discrete set of values in the first Brillouin zone, and the band index l. The eigenenergies are degenerate with respect to the spin index, $\varepsilon_{l,+1}^{(0)}(k_{\mathrm{B}}) = \varepsilon_{l,-1}^{(0)}(k_{\mathrm{B}}) \equiv \varepsilon_l^{(0)}(k_{\mathrm{B}})$. In the coordinate representation the eigenstate is related to Bloch's amplitude $u_{l,k_{\mathrm{B}},\sigma}(x, \sigma')$ by

$$\begin{aligned} &\langle x, \sigma' | l, k_{\mathrm{B}}, \sigma\rangle = \frac{1}{\sqrt{L_0}} e^{\mathrm{i}k_{\mathrm{B}}x} u_{l,k_{\mathrm{B}},\sigma}(x, \sigma'), \\ &u_{l,k_{\mathrm{B}},\sigma}(x, \sigma') = \delta_{\sigma',\sigma} u_{l,k_{\mathrm{B}}}(x), \\ &u_{l,k_{\mathrm{B}}}(x) = u_{l,k_{\mathrm{B}}}(x + L), \end{aligned} \tag{3.7}$$

where L_0 is the size of the system along the x-axis. Here the spinorial structure of the Bloch amplitude is trivial.

3.2.2 Influence of a transverse potential and RSOI

The transverse potential $V(z)$ together with RSOI change the Bloch spinors $|l, k_{\mathrm{B}}, \sigma\rangle$. We denote the new spinors through $|l, k_{\mathrm{B}}, \eta\rangle$:

$$\hat{H}|l, k_{\mathrm{B}}, \eta\rangle = \varepsilon_{l,\eta}(k_{\mathrm{B}})|l, k_{\mathrm{B}}, \eta\rangle. \tag{3.8}$$

As a result the Bloch amplitude acquires a new spinorial structure:

$$\begin{aligned} &\langle x, j, \sigma|l, k_{\mathrm{B}}, \eta\rangle = \frac{1}{\sqrt{L_0}} e^{\mathrm{i}k_{\mathrm{B}}x} u_{l,k_{\mathrm{B}},\eta}(x; j, \sigma), \\ &u_{l,k_{\mathrm{B}},\eta}(x; j, \sigma) = u_{l,k_{\mathrm{B}},\eta}(x + L; j, \sigma), \end{aligned} \tag{3.9}$$

where $|j\rangle$ is an eigenvector corresponding to an eigenvalue ε_j^z and both are found from the Schrödinger equation:

$$\left[\frac{\hbar^2 \hat{k}_z^2}{2m} + V(\hat{z})\right]|j\rangle = \varepsilon_j^z |j\rangle. \tag{3.10}$$

It is convenient to represent the total Hamiltonian (3.4) as the sum $\hat{H} = \hat{H}' + \hat{H}''$, where $\hat{H}'$ and $\hat{H}''$ are given by

$$\begin{aligned} &\hat{H}' \equiv \frac{\hbar^2}{2m}\left(\hat{k}_x + \hat{\sigma}_z k_{\mathrm{so}}\right)^2 + U(\hat{x}) + \frac{\hbar^2 \hat{k}_z^2}{2m} + V(\hat{z}) - \frac{\hbar^2 k_{\mathrm{so}}^2}{2m}, \\ &\hat{H}'' \equiv -\frac{\hbar^2 k_{\mathrm{so}}}{m} \hat{\sigma}_x \hat{k}_z. \end{aligned} \tag{3.11}$$

The eigenenergies and eigenstates of $\hat{H}'$ are easily found and related to $\varepsilon_l^{(0)}(k_{\mathrm{B}})$ and $u_{l,k_{\mathrm{B}}}(x)$ as follows:

$$\begin{aligned} &\hat{H}'|l, k_{\mathrm{B}}, j, \sigma\rangle = \varepsilon'_{l,j,\sigma}(k_{\mathrm{B}})|l, k_{\mathrm{B}}, j, \sigma\rangle, \\ &\varepsilon'_{l,j,\sigma}(k_{\mathrm{B}}) = \varepsilon_l^{(0)}(k_{\mathrm{B}} + \sigma k_{\mathrm{so}}) - \frac{\hbar^2 k_{\mathrm{so}}^2}{2m} + \varepsilon_j^z, \\ &\langle x, j', \sigma'|l, k_{\mathrm{B}}, j, \sigma\rangle = \frac{\delta_{j',j}\delta_{\sigma',\sigma} e^{\mathrm{i}k_{\mathrm{B}}x}}{\sqrt{L_0}} u_{l,k_{\mathrm{B}}+\sigma k_{\mathrm{so}}}(x). \end{aligned} \tag{3.12}$$

Let us denote through $\theta_{l,k_{\mathrm{B}},\eta}(j, \sigma)$ the Bloch spinors in the $\{l, k_{\mathrm{B}}, j, \sigma\}$ representation, that is, $\theta_{l,k_{\mathrm{B}},\eta}(j, \sigma) \equiv \langle l, k_{\mathrm{B}}, j, \sigma|l, k_{\mathrm{B}}, \eta\rangle$. Then

$$\langle l', k'_{\mathrm{B}}, j, \sigma|l, k_{\mathrm{B}}, \eta\rangle = \delta_{l',l}\delta_{k'_{\mathrm{B}},k_{\mathrm{B}}}\theta_{l,k_{\mathrm{B}},\eta}(j, \sigma). \tag{3.13}$$

We can make a general statement concerning Bloch's amplitude $u_{l,k_{\mathrm{B}},\eta}(x; j, \sigma)$. From the identity

$$\frac{1}{\sqrt{L_0}} e^{\mathrm{i}k_{\mathrm{B}}x} u_{l,k_{\mathrm{B}},\eta}(x; j, \sigma) \equiv \sum_{l',k'_{\mathrm{B}},j',\sigma'} \langle x, j, \sigma|l', k'_{\mathrm{B}}, j', \sigma'\rangle\langle l', k'_{\mathrm{B}}, j', \sigma'|l, k_{\mathrm{B}}, \eta\rangle \tag{3.14}$$

and using (3.12) and (3.13) it follows

$$u_{l,k_{\rm B},\eta}(x;j,\sigma) = u_{l,k_{\rm B}+\sigma k_{\rm so}}(x)\theta_{l,k_{\rm B},\eta}(j,\sigma). \tag{3.15}$$

The last equation clearly shows that the spinorial part of the Bloch amplitude $u_{l,k_{\rm B},\sigma}(x,\sigma')$ in Eq. (3.7) transforms from $\delta_{\sigma',\sigma}$ into the spinor $\theta_{l,k_{\rm B},\eta}(j,\sigma)$ when the potential $V(z)$ and RSOI are involved.

The spinors $\theta_{l,k_{\rm B},\eta}(j,\sigma)$ can be found from Eq. (3.8) which in $\{l,k_{\rm B},j,\sigma\}$ representation takes the form:

$$\begin{aligned}&\sum_{j',\sigma'}\big[\langle l',k'_{\rm B},j,\sigma|\hat{H}'|l,k_{\rm B},j',\sigma'\rangle + \langle l',k'_{\rm B},j,\sigma|\hat{H}''|l,k_{\rm B},j',\sigma'\rangle\big]\theta_{l,k_{\rm B},\eta}(j',\sigma') = \\ &= \varepsilon_{l,\eta}(k_{\rm B})\delta_{l',l}\delta_{k'_{\rm B},k_{\rm B}}\theta_{l,k_{\rm B},\eta}(j,\sigma).\end{aligned} \tag{3.16}$$

The matrix elements of $\hat{H}'$ and $\hat{H}''$ are given by the expressions:

$$\begin{aligned}&\langle l',k'_{\rm B},j,\sigma|\hat{H}'|l,k_{\rm B},j',\sigma'\rangle = \varepsilon'_{l,j,\sigma}(k_{\rm B})\delta_{l',l}\delta_{k'_{\rm B},k_{\rm B}}\delta_{j,j'}\delta_{\sigma,\sigma'}, \\ &\langle l',k'_{\rm B},j,\sigma|\hat{H}''|l,k_{\rm B},j',\sigma'\rangle = -\frac{\hbar^2 k_{\rm so}}{m}\langle\sigma|\hat{\sigma}_x|\sigma'\rangle\langle j|\hat{k}_z|j'\rangle\delta_{l',l}\delta_{k'_{\rm B},k_{\rm B}},\end{aligned} \tag{3.17}$$

where $\langle\sigma|\hat{\sigma}_x|\sigma'\rangle = 1-\delta_{\sigma,\sigma'}$. The final equation for the eigenenergies $\varepsilon_{l,\eta}(k_{\rm B})$ and eigenspinors $\theta_{l,k_{\rm B},\eta}(j,\sigma)$ is obtained using Eq. (3.16) together with Eq. (3.17) by equating the band indices $l'=l$ and Bloch's quasi-momenta $k'_{\rm B}=k_{\rm B}$:

$$\begin{aligned}&\sum_{j',\sigma'}\Bigg\{\delta_{j,j'}\delta_{\sigma,\sigma'}\left[\varepsilon_l^{(0)}(k_{\rm B}+\sigma k_{\rm so}) + \varepsilon_j^z - \frac{\hbar^2 k_{\rm so}^2}{2m}\right] - \\ &- \frac{\hbar^2 k_{\rm so}}{m}(1-\delta_{\sigma,\sigma'})\langle j|\hat{k}_z|j'\rangle\Bigg\}\theta_{l,k_{\rm B},\eta}(j',\sigma') = \\ &= \varepsilon_{l,\eta}(k_{\rm B})\theta_{l,k_{\rm B},\eta}(j,\sigma).\end{aligned} \tag{3.18}$$

We want to emphasize that Eq. (3.18) can be applied to calculate the band structure for an arbitrary potential $V(z)$ and periodic potential $U(x)$ of a general form. Note the specific influence of the spin-orbit coupling: a) j-states are mixed by RSOI; b) the Bloch bands of the corresponding truly 1D problem with different l are split into subbands independently, that is, the splitting of band l *does not depend* on the splitting of bands with $l'\neq l$. Therefore as soon as the truly 1D band structure has been obtained, one can take any of its Bloch bands, let us say l, apply (3.18) to it and find the Bloch bands labeled with index l in the presence of $V(z)$ and RSOI. The same inference remains valid if LDSOI is additionally included into the model.

3.3 Harmonic confinement

Here we consider a particular case where the operator $V(\hat{z})$ represents a harmonic confinement of strength ω_0. In this case the matrix elements of $\hat{k}_z$ are

$$\langle j|\hat{k}_z|j'\rangle = \pm{\rm i}\,\delta_{j,j'\pm1}\sqrt{\frac{(j+\frac{1}{2}\mp\frac{1}{2})m\omega_0}{2\hbar}}. \tag{3.19}$$

3.3.1 Eigenenergies

If in (3.18) one keeps only the first two transverse modes, the problem reduces to the diagonalization of a 4×4 matrix and becomes solvable analytically. The validity of this approximation is discussed in Ref. [91]. After the diagonalization of (3.18), where now $j = 0, 1$, we obtain the following eigenenergies:

$$\begin{aligned} \varepsilon_{l,\eta=1,2}(k_{\mathrm{B}}) &= \varepsilon_l^+(k_{\mathrm{B}}) - \Xi_{l_{1,2}}(k_{\mathrm{B}}), \\ \varepsilon_{l,\eta=3,4}(k_{\mathrm{B}}) &= \varepsilon_l^+(k_{\mathrm{B}}) + \Xi_{l_{2,1}}(k_{\mathrm{B}}), \end{aligned} \tag{3.20}$$

where

$$\begin{aligned} \varepsilon_l^+(k_{\mathrm{B}}) &\equiv \frac{\varepsilon_l^{(0)}(k_{\mathrm{B}} + k_{\mathrm{so}}) + \varepsilon_l^{(0)}(k_{\mathrm{B}} - k_{\mathrm{so}})}{2} + \hbar\omega_0 - \frac{\hbar^2 k_{\mathrm{so}}^2}{2m}, \\ \Xi_{l_{1,2}}(k_{\mathrm{B}}) &\equiv \sqrt{\Xi^2 + \left(\varepsilon_l^-(k_{\mathrm{B}}) \mp \frac{\hbar\omega_0}{2}\right)^2}, \\ \varepsilon_l^-(k_{\mathrm{B}}) &\equiv \frac{\varepsilon_l^{(0)}(k_{\mathrm{B}} + k_{\mathrm{so}}) - \varepsilon_l^{(0)}(k_{\mathrm{B}} - k_{\mathrm{so}})}{2}, \\ \Xi &\equiv \frac{\hbar^2 k_{\mathrm{so}}}{m}\sqrt{\frac{m\omega_0}{2\hbar}}. \end{aligned} \tag{3.21}$$

Since $\varepsilon_l^{(0)}(k_{\mathrm{B}}) = \varepsilon_l^{(0)}(-k_{\mathrm{B}})$, the relations between the eigenenergies (3.20) follow:

$$\begin{aligned} \varepsilon_{l,\eta=1}(k_{\mathrm{B}}) &= \varepsilon_{l,\eta=2}(-k_{\mathrm{B}}), \\ \varepsilon_{l,\eta=3}(k_{\mathrm{B}}) &= \varepsilon_{l,\eta=4}(-k_{\mathrm{B}}), \end{aligned} \tag{3.22}$$

as expected due to the existence of both the time reversal symmetry and band overlap [97]. In fig. 3.1 we show the first Bloch band of the corresponding truly 1D problem and the four Bloch sub-bands growing out of it under the influence of RSOI and the transverse confinement. The spin-orbit coupling strength is chosen such that $Lk_{\mathrm{so}} = \pi/2$. The periodic potential has the form:

$$U(x) = V_0\left[1 - \cos\left(\frac{2\pi}{L}x\right)\right]. \tag{3.23}$$

The second Bloch band and its four sub-bands are plotted in fig. 3.2. It can be seen that for $l = 1$ the Bloch band of the truly 1D problem without RSOI and its four sub-bands for the quasi-1D system with RSOI are all under the potential barrier while for $l = 2$ they are above it. As usual RSOI does not remove the spin degeneracy at $k_{\mathrm{B}} = 0$. It follows from (3.20) that the bands split when $\varepsilon_l^-(k_{\mathrm{B}}) \neq 0$. The derivative of the function $\varepsilon_l^-(k_{\mathrm{B}})$ at $k_{\mathrm{B}} = 0$ is easily found from (3.21):

$$\left.\frac{d\varepsilon_l^-(k_{\mathrm{B}})}{dk_{\mathrm{B}}}\right|_{k_{\mathrm{B}}=0} = v_l^{(0)}(k_{\mathrm{so}}), \tag{3.24}$$

where $v_l^{(0)}(k_{\mathrm{B}})$ is the group velocity of the corresponding truly 1D problem. Since for the chosen parameters the group velocity in (3.24) is not equal to zero (see figs. 3.1 and

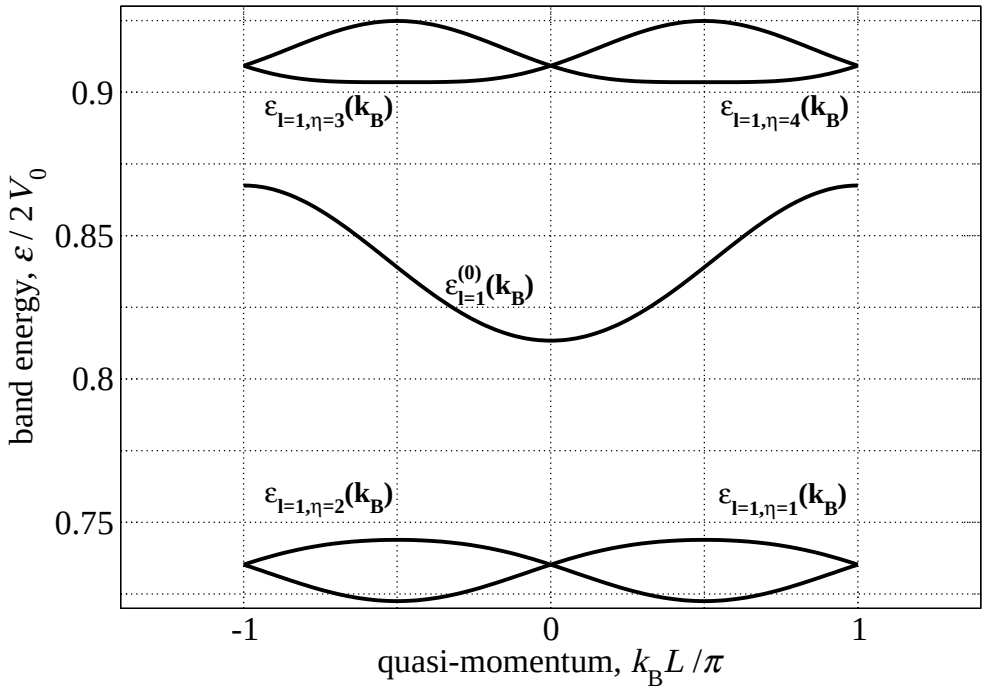

Figure 3.1: The first Bloch band of the corresponding truly 1D system $\varepsilon^{(0)}_{l=1}(k_{\rm B})$ together with the four Bloch sub-bands $\varepsilon_{l=1,\eta}(k_{\rm B})$ of the quasi-1D system in the presence of RSOI and the transverse confinement.

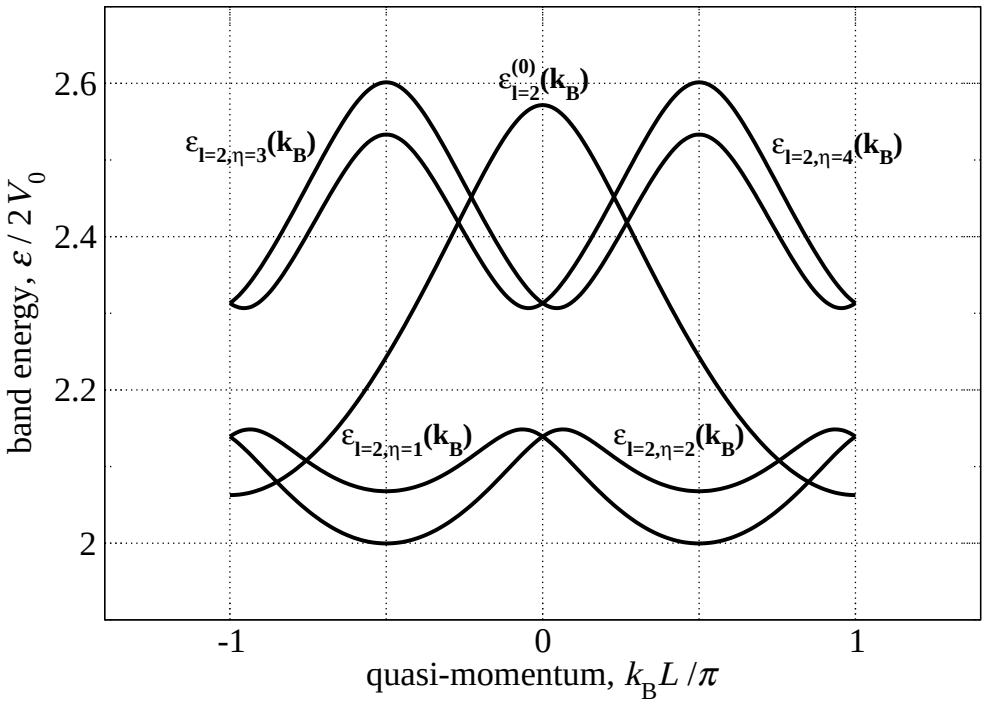

Figure 3.2: The second Bloch band of the corresponding truly 1D system $\varepsilon^{(0)}_{l=2}(k_{\rm B})$ together with the four Bloch sub-bands $\varepsilon_{l=2,\eta}(k_{\rm B})$ of the quasi-1D system in the presence of RSOI and the transverse confinement.

3.2), it follows from (3.20) and (3.21) that the band splitting near the point $k_{\rm B} = 0$ is *linear* in $k_{\rm B}$. This is also the case for a 2DEG where the linear momentum-dependence of the splitting is observed experimentally [98].

3.3.2 Eigenstates

The corresponding normalized eigenspinors $\theta_{l,k_{\rm B},\eta}(j,\sigma)$ are expressed in terms of non-normalized ones, denoted through $\tilde{\theta}_{l,k_{\rm B},\eta}(j,\sigma)$, as:

$$\begin{aligned} \theta_{l,k_{\rm B},\eta=1,4} &= N_{l,k_{\rm B},\eta=1,4}^{-\frac{1}{2}} \tilde{\theta}_{l,k_{\rm B},\eta=1,4}\,, \\ \theta_{l,k_{\rm B},\eta=2,3} &= N_{l,k_{\rm B},\eta=2,3}^{-\frac{1}{2}} \tilde{\theta}_{l,k_{\rm B},\eta=2,3}\,, \end{aligned} \tag{3.25}$$

where

$$\begin{aligned} \tilde{\theta}_{l,k_{\rm B},\eta=1,4} &\equiv \begin{bmatrix} \frac{\mathrm{i}}{\Xi}\left[\varepsilon_l^-(k_{\rm B}) - \frac{\hbar\omega_0}{2} \mp \Xi_{l_1}(k_{\rm B})\right] \\ 0 \\ 0 \\ 1 \end{bmatrix}, \\ \tilde{\theta}_{l,k_{\rm B},\eta=2,3} &\equiv \begin{bmatrix} 0 \\ -\frac{\mathrm{i}}{\Xi}\left[\varepsilon_l^-(k_{\rm B}) + \frac{\hbar\omega_0}{2} \pm \Xi_{l_2}(k_{\rm B})\right] \\ 1 \\ 0 \end{bmatrix}. \end{aligned} \tag{3.26}$$

We have introduced the notation

$$\theta_{l,k_{\rm B},\eta} \equiv \begin{bmatrix} \theta_{l,k_{\rm B},\eta}(j=0,\sigma=+1) \\ \theta_{l,k_{\rm B},\eta}(j=0,\sigma=-1) \\ \theta_{l,k_{\rm B},\eta}(j=1,\sigma=+1) \\ \theta_{l,k_{\rm B},\eta}(j=1,\sigma=-1) \end{bmatrix}, \tag{3.27}$$

and an analogous one for the non-normalized spinor $\tilde{\theta}_{l,k_{\rm B},\eta}$. In (3.25) $N_{l,k_{\rm B},\eta}$ are the normalization constants:

$$N_{l,k_{\rm B},\eta} = \sum_{j=0}^{1} \sum_{\sigma=-1}^{+1} |\tilde{\theta}_{l,k_{\rm B},\eta}(j,\sigma)|^2. \tag{3.28}$$

Note that using (3.21) and (3.25) one gets the relations

$$N_{l,k_{\rm B},\eta=1,4} = N_{l,-k_{\rm B},\eta=2,3}. \tag{3.29}$$

For $k_{\rm so} \to 0$ the spinors in (3.25) take the form:

$$\theta_{l,k_{\rm B},\eta=1,2,3,4} = \begin{bmatrix} -\mathrm{i} \\ 0 \\ 0 \\ 0 \end{bmatrix}, \begin{bmatrix} 0 \\ -\mathrm{i} \\ 0 \\ 0 \end{bmatrix}, \begin{bmatrix} 0 \\ 0 \\ 1 \\ 0 \end{bmatrix}, \begin{bmatrix} 0 \\ 0 \\ 0 \\ 1 \end{bmatrix}. \tag{3.30}$$

In the limit $U(x) \to 0$ we have $\varepsilon_l^{(0)}(k_{\rm B}) \to \hbar^2 k_B^2/2m$, $u_{l,k_{\rm B}}(x) \to 1$ and from (3.20) and (3.21) we get:

$$\begin{aligned} \varepsilon_{l,\eta=1,2}(k_x) &\to \frac{\hbar^2 k_x^2}{2m} + \hbar\omega_0 - \Xi_{1,2}^{(0)}(k_x), \\ \varepsilon_{l,\eta=3,4}(k_x) &\to \frac{\hbar^2 k_x^2}{2m} + \hbar\omega_0 + \Xi_{2,1}^{(0)}(k_x), \end{aligned} \tag{3.31}$$

where

$$\Xi_{1,2}^{(0)}(k_x) \equiv \sqrt{\Xi^2 + \left(\frac{\hbar^2 k_x k_{\rm so}}{m} \mp \frac{\hbar\omega_0}{2}\right)^2}. \tag{3.32}$$

Further, in this limit from (3.26) we find:

$$\begin{aligned} \tilde{\theta}_{l,k_x,\eta=1,4} &\to \begin{bmatrix} \frac{\mathrm{i}}{\Xi}\left[\frac{\hbar^2 k_x k_{\rm so}}{m} - \frac{\hbar\omega_0}{2} \mp \Xi_1^{(0)}(k_x)\right] \\ 0 \\ 0 \\ 1 \end{bmatrix}, \\ \tilde{\theta}_{l,k_x,\eta=2,3} &\to \begin{bmatrix} 0 \\ -\frac{\mathrm{i}}{\Xi}\left[\frac{\hbar^2 k_x k_{\rm so}}{m} + \frac{\hbar\omega_0}{2} \pm \Xi_2^{(0)}(k_x)\right] \\ 1 \\ 0 \end{bmatrix}. \end{aligned} \tag{3.33}$$

As a consequence the spinorial Bloch amplitude transforms into a pure spinor without any real space dependence as it can be seen from (3.15). Expressions (3.31) and (3.32) recover the results obtained in Ref. [91].

3.3.3 Polarizations

Finally, let us discuss the polarizations

$$P_{l,\eta}^{(i)}(k_{\rm B}) \equiv \langle l, k_{\rm B}, \eta | \hat{\sigma}_i | l, k_{\rm B}, \eta \rangle, \tag{3.34}$$

where $\hat{\sigma}_i$, $i = x, y, z$ are the Pauli spin operators. Writing the identity operator in the $\{|l, k_{\rm B}, j, \sigma\rangle\}$ basis, and taking into account the structure of the Bloch spinors (3.25) and (3.26) we obtain

$$\begin{aligned} P_{l,\eta}^{(x)}(k_{\rm B}) = \sum_{j=0}^{1} \sum_{\sigma',\sigma''=-1}^{+1} &\big[\theta_{l,k_{\rm B},\eta}^*(j,\sigma') \times \\ &\times (1 - \delta_{\sigma',\sigma''})\theta_{l,k_{\rm B},\eta}(j,\sigma'')\big] = 0, \quad \forall\, l, k_{\rm B} \in \text{B.Z.}, \end{aligned} \tag{3.35}$$

$$\begin{aligned} P_{l,\eta}^{(y)}(k_{\rm B}) = \sum_{j=0}^{1} \sum_{\sigma',\sigma''=-1}^{+1} &\big[\theta_{l,k_{\rm B},\eta}^*(j,\sigma')\, \mathrm{i}^{\sigma''} \times \\ &\times (1 - \delta_{\sigma',\sigma''})\theta_{l,k_{\rm B},\eta}(j,\sigma'')\big] = 0, \quad \forall\, l, k_{\rm B} \in \text{B.Z.}, \end{aligned} \tag{3.36}$$

where $\eta = 1, 2, 3, 4$. The last two equations show that the longitudinal, that is along the wire, and the perpendicular to the 2DEG plane components of the polarization identically vanish. However, the polarization along the in-plane confinement direction has a finite value:

$$P^{(z)}_{l,\eta}(k_{\rm B}) = \sum_{j=0}^{1}\sum_{\sigma=-1}^{+1} \theta^{*}_{l,k_{\rm B},\eta}(j,\sigma)\,\sigma\,\theta_{l,k_{\rm B},\eta}(j,\sigma), \qquad \forall\, l, k_{\rm B} \in \text{B.Z.}, \eta = 1,2,3,4. \tag{3.37}$$

From Eqs. (3.37) and (3.25) we derive the polarizations in the four Bloch sub-bands formed out of the truly 1D Bloch band with index l:

$$P^{(z)}_{l,\eta=1,4}(k_{\rm B}) = N^{-1}_{l,k_{\rm B},\eta=1,4} \times \left\{ \frac{1}{\Xi^2}\left[\varepsilon^{-}_{l}(k_{\rm B}) - \frac{\hbar\omega_0}{2} \mp \Xi_{l_1}(k_{\rm B})\right]^2 - 1 \right\}, \tag{3.38}$$

$$P^{(z)}_{l,\eta=2,3}(k_{\rm B}) = N^{-1}_{l,k_{\rm B},\eta=2,3} \times \left\{ 1 - \frac{1}{\Xi^2}\left[\varepsilon^{-}_{l}(k_{\rm B}) + \frac{\hbar\omega_0}{2} \pm \Xi_{l_2}(k_{\rm B})\right]^2 \right\}. \tag{3.39}$$

Using (3.29) and equalities $\varepsilon^{-}_{l}(k_{\rm B}) = -\varepsilon^{-}_{l}(-k_{\rm B})$, $\Xi_{l_{1,2}}(k_{\rm B}) = \Xi_{l_{2,1}}(-k_{\rm B})$, the symmetry relation for the polarizations

$$P^{(z)}_{l,\eta=1,4}(k_{\rm B}) = -P^{(z)}_{l,\eta=2,3}(-k_{\rm B}), \tag{3.40}$$

is derived $\forall\, l, k_{\rm B} \in$ B.Z. This symmetry is clearly seen in figs. 3.3 and 3.4, where the four polarizations (3.38) and (3.39) are plotted for $l = 1$ and $l = 2$, respectively. Fig. 3.3 also shows that the polarizations do not change sign and never approach unity in the first Bloch band. This picture changes for the polarizations in the second Bloch band (see fig. 3.4). In this band the polarizations change sign. Also there exist nearly fully spin-polarized domains in the first Brillouin zone. As one can see those domains are the ones where the group velocity takes its largest absolute values. The same happens in the limiting case $U(x) \to 0$ where the group velocity has infinite values for infinite momentum. Indeed, when $U(x) \to 0$, from (3.38) one finds for example that $\lim_{k_x \to \pm\infty} P^{(z)}_{\eta=1}(k_x) = \mp 1$ in agreement with Ref. [91]. Thus in the absence of the periodic potential the states can again be characterized by the spin quantum number for large absolute values of the longitudinal momentum.

3.4 A periodic structure with $V(z) = 0$

In this section we briefly present the resulting energy spectrum when the potential $V(z)$ vanishes and the periodic potential $U(x)$ is arbitrary. Here the solutions of (3.10) are plane waves, $|j\rangle \equiv |k_z\rangle$, $\varepsilon^{z}_{j} \equiv \varepsilon^{z}_{k_z} = \hbar^2 k_z^2/2m$ and $\langle k_z|\hat{k}_z|k'_z\rangle = \delta_{k_z,k'_z} k_z$. The diagonalization of Eq. (3.18) leads to the dispersion relations:

$$\varepsilon^{\rm 2D}_{l,\eta=1,2}(k_{\rm B}, k_z) = \frac{\varepsilon^{(0)}_{l}(k_{\rm B}+k_{\rm so}) + \varepsilon^{(0)}_{l}(k_{\rm B}-k_{\rm so})}{2} + \\ + \frac{\hbar^2 k_z^2}{2m} - \frac{\hbar^2 k_{\rm so}^2}{2m} \pm \sqrt{\left(\varepsilon^{-}_{l}(k_{\rm B})\right)^2 + \left(\frac{\hbar^2 k_{\rm so} k_z}{m}\right)^2}, \tag{3.41}$$

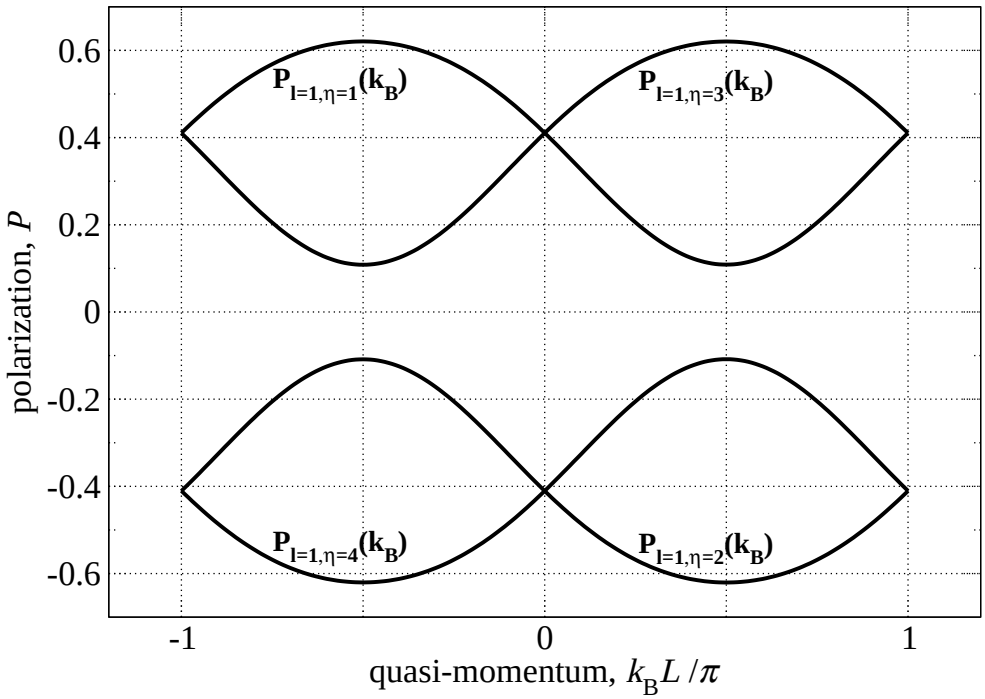

Figure 3.3: Spin polarizations along the z-axis in the four Bloch sub-bands with $l = 1$.

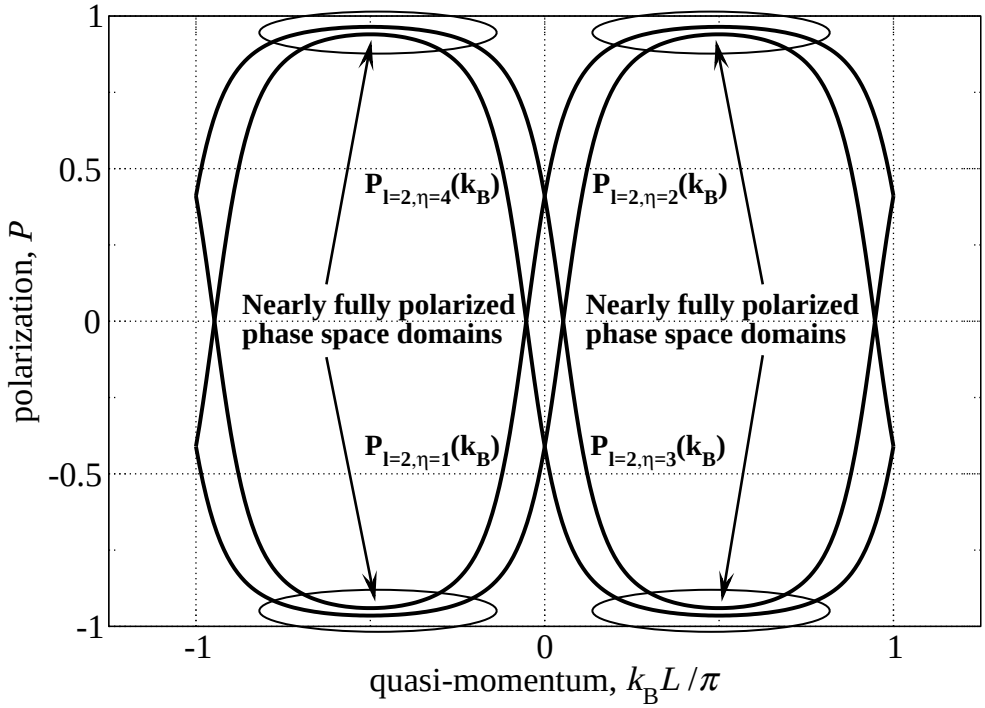

Figure 3.4: Spin polarizations along the z-axis in the four Bloch sub-bands with $l = 2$.

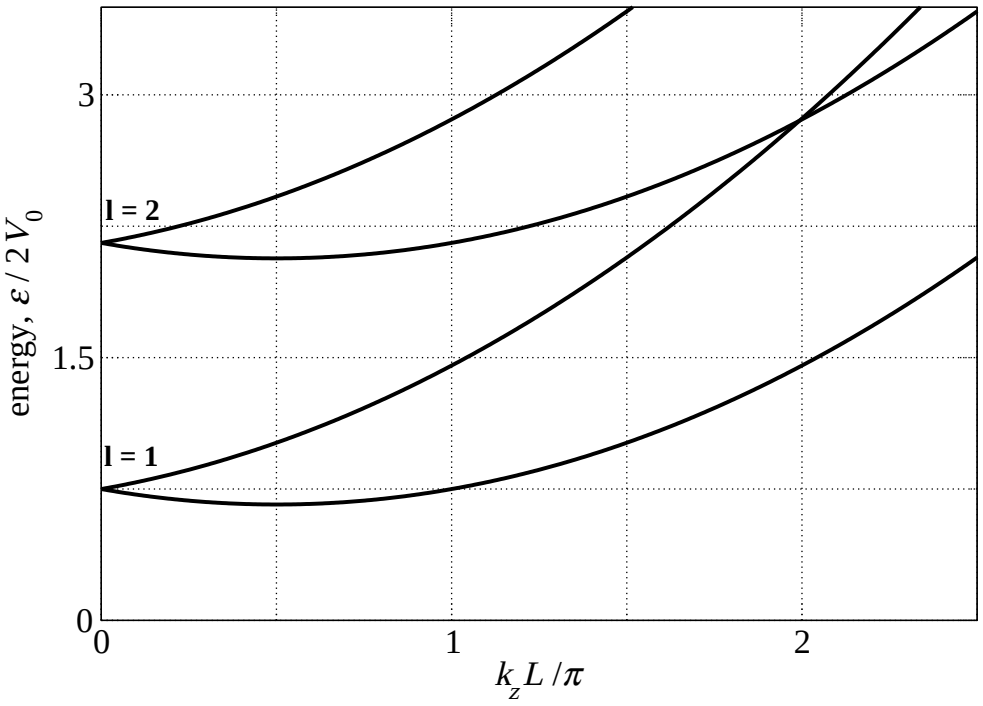

Figure 3.5: $k_{\mathrm{B}} = 0$ cut of the energy spectrum for a periodic structure with $V(z) = 0$. Energy branches with $l = 1, 2$ are depicted.

where we have added the upper index 2D to stress that in this system the energy spectrum is two-dimensional. It can be easily checked that at $k_z = 0$ Eq. (3.41) gives the same dispersion relation as the one derived from Eqs. (3.20) and (3.21) in the limiting case $\omega_0 = 0$. For $k_{\mathrm{B}} = 0$ and $k_z > 0$ it follows from (3.41):

$$\varepsilon^{\mathrm{2D}}_{l,\eta=1,2}(k_{\mathrm{B}} = 0, k_z) = \varepsilon^{(0)}_l(k_{\mathrm{so}}) - \frac{\hbar^2 k^2_{\mathrm{so}}}{2m} + \frac{\hbar^2 k_z^2}{2m} \pm \frac{\hbar^2 k_{\mathrm{so}} k_z}{m}. \tag{3.42}$$

From Eq. (3.42) one can clearly see that the energy branch with $\eta = 2$ has its minimum at $k_z = k_{\mathrm{so}}$ for all bands l. The splitting of the two branches is linear in k_z. The last expression also shows that for different band indices l the corresponding energy branches are parallel and there are not anti-crossings. This is also shown in fig. 3.5

Finally, in the limiting case $U(x) \to 0$, we have $\varepsilon^{(0)}_l(k_{\mathrm{B}}) \to \hbar^2 k_x^2/2m$ and from Eq. (3.41) it follows:

$$\varepsilon^{\mathrm{2D}}_{1,2}(k_x, k_z) = \frac{\hbar^2 k^2}{2m} \pm \frac{\hbar^2 k_{\mathrm{so}} k}{m}, \tag{3.43}$$

where $k \equiv |\vec{k}| = \sqrt{k_x^2 + k_z^2}$. One sees that Eq. (3.43) is nothing but the Rashba dispersion relation (2.14), that is the energy spectrum of the Hamiltonian (3.1) has been recovered.

3.5 Magnetic field and orbit-orbit coupling

Above we have considered periodic structures formed in a 2DEG with RSOI. However the influence of an external homogeneous stationary magnetic field on the energy spectrum has not been studied. Here we generalize the results of Ref. [66] to the case of a uniform stationary magnetic field applied along the z-axis and orbit-orbit coupling. More precisely we investigate the energy spectrum of the following Hamiltonian,

$$\hat{H} = \frac{\hbar^2\hat{\vec{k}}^2}{2m} + V(\hat{z}) - \frac{\hbar^2 k_{\rm so}}{m}\left(\hat{\sigma}_x\hat{k}_z - \hat{\sigma}_z\hat{k}_x\right) + U(\hat{x})\left(1+\gamma\frac{\hat{z}^2}{L^2}\right) - g\mu_{\rm B}\hat{\sigma}_z H_0, \tag{3.44}$$

where H_0 is the z-component of the magnetic field $\vec{H}_0 = (0,0,H_0)$, and we have used the gauge in which the components of the vector potential are $A_x = -H_0 y$, $A_y = A_z = 0$ (Landau gauge). Additionally, we have taken into account the fact that in a 2DEG $y = 0$. In Eq. (3.44) γ is the strength of the coupling between the orbital degrees of freedom x and z, g the electron spin g-factor and $\mu_{\rm B}$ the Bohr magneton.

3.5.1 An in-plane transverse static magnetic field

Let us first consider this problem without the orbit-orbit coupling,

$$\hat{H} = \frac{\hbar^2\hat{\vec{k}}^2}{2m} + V(\hat{z}) - \frac{\hbar^2 k_{\rm so}}{m}\left(\hat{\sigma}_x\hat{k}_z - \hat{\sigma}_z\hat{k}_x\right) - g\mu_{\rm B}\hat{\sigma}_z H_0. \tag{3.45}$$

The eigenstates of Hamiltonian (3.45) are Bloch spinors with the spinorial amplitude given by Eq. (3.15),

$$u_{l,k_{\rm B},\eta}(x;j,\sigma) = u_{l,k_{\rm B}+\sigma k_{\rm so}}(x)\theta_{l,k_{\rm B},\eta}(j,\sigma),$$

where $u_{l,k_{\rm B}}(x)$ is the Bloch amplitude of the corresponding truly 1D problem without the magnetic field and without RSOI, and $\theta_{l,k_{\rm B},\eta}(j,\sigma)$ is the eigenspinor. This eigenspinor is obtained from the solution of the eigenvalue equation for the Hamiltonian (3.45):

$$\begin{aligned}
&\sum_{j',\sigma'}\Bigg\{\delta_{j,j'}\delta_{\sigma,\sigma'}\Bigg[\varepsilon_l^{(0)}(k_{\rm B}+\sigma k_{\rm so}) - g\mu_{\rm B}\sigma H_0 + \varepsilon_j^z - \\
&-\frac{\hbar^2 k_{\rm so}^2}{2m}\Bigg] - \frac{\hbar^2 k_{\rm so}}{m}(1-\delta_{\sigma,\sigma'})\langle j|\hat{k}_z|j'\rangle\Bigg\}\theta_{l,k_{\rm B},\eta}(j',\sigma') = \\
&= \varepsilon_{l,\eta}(k_{\rm B})\theta_{l,k_{\rm B},\eta}(j,\sigma).
\end{aligned} \tag{3.46}$$

Therefore the only change in comparison with the case without a magnetic field is in the diagonal matrix elements of the Hamiltonian.

Harmonic confinement

Reproducing the same calculations as before, that is, taking into account only the first two transverse modes ($j = 0, 1$, $\sigma = \pm 1$, $\eta = 1, 2, 3, 4$), one finds that the only change in the final results for the eigenenergies and eigenspinors consists in replacing the function $\varepsilon_l^-(k_\mathrm{B})$, Eq. (3.21), with

$$\varepsilon_l^-(k_\mathrm{B}; H_0) = \frac{\varepsilon_l^{(0)}(k_\mathrm{B} + k_\mathrm{so}) - \varepsilon_l^{(0)}(k_\mathrm{B} - k_\mathrm{so})}{2} - g\mu_\mathrm{B} H_0, \tag{3.47}$$

where we have explicitly shown the dependence on the z-component H_0 of the magnetic field. The expressions for the eigenenergies, Eq. (3.20) with the auxiliary Eq. (3.21), and eigenspinors, Eq. (3.26), written through the function $\varepsilon_l^-(k_\mathrm{B})$ are unchanged. Also the structure (that is the zero and non-zero components) of the four dimensional eigenspinors is the same.

The time reversal symmetry is now broken and as a result the symmetry relations between the eigenenergies and eigenspinors hold only if one simultaneously changes the direction of the magnetic field. For the eigenenergies we have:

$$\begin{aligned} \varepsilon_{l,\eta=1}(k_\mathrm{B}; H_0) &= \varepsilon_{l,\eta=2}(-k_\mathrm{B}; -H_0), \\ \varepsilon_{l,\eta=3}(k_\mathrm{B}; H_0) &= \varepsilon_{l,\eta=4}(-k_\mathrm{B}; -H_0). \end{aligned} \tag{3.48}$$

For the eigenspinors the symmetry relations are written as:

$$\begin{aligned} &\theta_{l,k_\mathrm{B},\eta=1}(j = \{0,1\}, \sigma = \{+1,-1\}; H_0) = \\ &= \theta_{l,k_\mathrm{B},\eta=2}(j = \{0,1\}, \sigma = \{-1,+1\}; -H_0), \\ &\theta_{l,k_\mathrm{B},\eta=3}(j = \{0,1\}, \sigma = \{-1,+1\}; H_0) = \\ &= \theta_{l,k_\mathrm{B},\eta=4}(j = \{0,1\}, \sigma = \{+1,-1\}; -H_0), \end{aligned} \tag{3.49}$$

where it is also taken into account that the z-projection of the spin operator (and as a result its eigenvalues) changes its sign under the time reversal. The only non-vanishing polarization is again the one along the confinement (and also magnetic field) direction. The symmetry relations for its components are:

$$P^{(z)}_{l,\eta=1,4}(k_\mathrm{B}; H_0) = -P^{(z)}_{l,\eta=2,3}(-k_\mathrm{B}; -H_0). \tag{3.50}$$

3.5.2 Effects of orbit-orbit coupling for the case of a harmonic confinement

Finally, we would like to note that since for the harmonic confinement model, $V(z) = m\omega_0^2 z^2/2$, with the first two transverse modes an operator even with respect to $\hat{z}$ is effectively diagonal, the results obtained above remain valid in the presence of the orbit-orbit coupling, Eq. (3.44), with the following change. The corresponding truly 1D problem without RSOI, transverse confinement and magnetic field has to be solved now not for the periodic potential $U(x)$ but for the periodic potential $U_{\gamma,j}(x) \equiv U(x)[1 +$

$\gamma\hbar(j+1/2)/m\omega_0 L^2]$. Thus the solution of this truly 1D problem acquires a dependence on the transverse mode quantum number j through the periodic potential dependence on that quantum number: $\varepsilon_l^{(0)}(k_\mathrm{B}) \to \varepsilon_{\gamma,j;l}^{(0)}(k_\mathrm{B})$, $|l,k_\mathrm{B}\rangle \to |l,k_\mathrm{B}\rangle_{\gamma,j}$. As a result the eigenenergies and eigenstates in Eq. (3.12), also acquire an additional dependence on the transverse mode quantum number j: $\varepsilon'_{l,j,\sigma}(k_\mathrm{B}) \to \varepsilon_{l,j,\sigma}^{\prime(\gamma,j)}(k_\mathrm{B})$, $|l,k_\mathrm{B},j,\sigma\rangle \to |l,k_\mathrm{B},j,\sigma\rangle_{\gamma,j}$. The eigenenergies $\varepsilon_{l,j,\sigma}^{\prime(\gamma,j)}(k_\mathrm{B})$ and eigenstates $|l,k_\mathrm{B},j,\sigma\rangle_{\gamma,j}$ are a solution of the eigenvalue problem for the Hamiltonian

$$\hat{H}'_{\gamma,j} \equiv \frac{\hbar^2}{2m}\left(\hat{k}_x + \hat{\sigma}_z k_\mathrm{so}\right)^2 + U_{\gamma,j}(\hat{x}) + \frac{\hbar^2\hat{k}_z^2}{2m} + \frac{m\omega_0^2\hat{z}^2}{2} - \frac{\hbar^2 k_\mathrm{so}^2}{2m}. \tag{3.51}$$

This solution is the one for which the transverse mode index j' related to the Hamiltonian $\hbar^2\hat{k}_z^2/2m + m\omega_0^2\hat{z}^2/2$ is equal to j. The states $|l,k_\mathrm{B},j,\sigma\rangle_{\gamma,j}$ represent an alternative basis of the Hilbert space. This basis is now used to construct the corresponding matrix representation of the Hamiltonian (3.44). This approach is completely analogous to the one used to derive Eqs. (3.18) and (3.46). It is easy to see that within this matrix representation of the Hamiltonian (3.44) the structure (location of zero and non-zero entries) of the resulting 4×4 matrix is the same as in the case without orbit-orbit coupling, *i.e.*, as in the case of Eq. (3.46) where $j = 0, 1$. Thus this 4×4 matrix is diagonalized in the same manner as Eq. (3.46) where $j = 0, 1$. We label the eigenenergies and eigenspinors obtained from this diagonalization as $\varepsilon_{\gamma;l,\eta}(k_\mathrm{B}; H_0)$ and $\theta_{\gamma;l,k_\mathrm{B},\eta}(j,\sigma; H_0)$ to stress their dependence on the orbit-orbit coupling strength γ. The symmetry relations (3.48)-(3.50) are, of course, unchanged.

3.6 Materials of interest

Here we would like to mention that although our theory is general, the concrete results presented in the figures of this chapter are relevant for III-V compounds. For example in InAs the spin-orbit coupling strength α is enhanced up to $4 \cdot 10^{-11}\,\mathrm{eV}\cdot\mathrm{m}$ as it is demonstrated in Ref. [80]. The effective mass is $m = 0.036m_0$. Then for L in the range between 70 nm and 100 nm the dimensionless parameter $k_\mathrm{so}L = g\pi/2$ with g being in the range between 0.84 and 1.2.

3.7 Conclusion

We have considered a 2DEG with RSOI in the presence of two 1D in-plane potentials along mutually orthogonal directions, assuming the first of those potentials to be periodic while making no assumption about the second one. It has been found that in such a system the coordinate part of the Bloch amplitude is the same as the one of the corresponding truly one-dimensional problem without RSOI. However, its Bloch's quasi-momentum has a spin-dependent shift proportional to the spin-orbit coupling strength. A general eigenvalue problem for the band structure has been presented in terms of the spinorial part of Bloch's amplitude. The cases where the second potential

represents either a harmonic confinement or where it vanishes have been studied as applications of the general formalism. For the case of a harmonic confinement with only the first two transverse modes retained analytical relations have been obtained and general symmetry properties of the resulting band structure have been determined. Analytical expressions for the polarizations have been derived as well. Regions of high polarization corresponding to regions of large absolute values of the group velocity have been found. Since in the case of a vanishing transverse potential there are not transverse modes, the restriction to a few first transverse modes is not necessary. In this sense the analytical relations we have established between the energy spectrum of this 2D system and its corresponding truly 1D problem without RSOI are exact.

Chapter 4

Tight-binding model: discrete variable basis

In collaboration with D. Bercioux, M. Grifoni, and K. Richter, Refs. [67, 69].

4.1 Introduction

This chapter is devoted to a discrete variable representation which will be used in the next chapter to calculate the charge and spin ratchet currents in the spin-orbit dissipative medium described in Chapter 1 in Subsection 1.2.4. A discrete variable representation was used in Chapter 1 in Subsection 1.1.3 to show how to solve a dissipative problem with the model of Caldeira and Leggett. There we demonstrated how to calculate the particle ratchet current using the DVR basis. The DVR basis was introduced there as the basis composed of the eigenstates of the coordinate operator $\hat{x}$ which was defined on a subspace of the Hilbert space. This subspace was obtained by the truncation of the basis of the Hilbert space using a few Bloch bands of the Hamiltonian of the isolated system, $\hat{H}_0^{1D}$, Eq. (1.6). In the present chapter we perform the truncation of the Hilbert space basis using a few Bloch bands of the Hamiltonian (3.51) and find a common eigenbasis $\{|\alpha\rangle\}$ of the operators $\hat{x}$ and $\hat{\sigma}_z$ on the corresponding subspace. This basis, called σ-DVR basis, is a convenient tool to calculate the charge and spin ratchet currents.

4.2 Diagonalization of the $\hat{\sigma}_z$ operator

Among possible eigenstates of the operator $\hat{\sigma}_z$ the eigenstates of the Hamiltonian $\hat{H}'_{\gamma,j}$, Eq. (3.51), represent a good starting point in deriving the σ-DVR basis. We have,

$$\hat{\sigma}_z|l, k_{\rm B}, j, \sigma\rangle_{\gamma,j} = \sigma|l, k_{\rm B}, j, \sigma\rangle_{\gamma,j}. \tag{4.1}$$

Let us remind that in Eq. (4.1) l, $k_{\rm B}$, j, σ stand for the Bloch band index, quasi-momentum, transverse mode index and z-projection of the spin, respectively. Since

in the presence of the orbit-orbit coupling the periodic potential $U_{\gamma,j}(x)$ depends on γ and j (see Chapter 3, Subsection 3.5.2), we have labeled the ket-symbol with the subscript γ, j. In the ensuing analysis we follow the same rule and label all the bra- and ket-symbols with the subscript γ, j, that is ${}_{\gamma,j}\langle\cdots|$ and $|\cdots\rangle_{\gamma,j}$.

4.3 Diagonalization of the $\hat{x}$ operator

In this section we diagonalize the coordinate operator using the eigenstates of $\hat{\sigma}_z$ from the previous section. We first look at the corresponding matrix structure of the $\hat{x}$ operator and then find the structure of its eigenvalues.

4.3.1 Matrix structure

It is convenient to begin the diagonalization of the coordinate operator writing its matrix in the $\{|l, k_{\rm B}, j, \sigma\rangle_{\gamma,j}\}$ representation:

$$ {}_{\gamma,j'}\langle l', k'_{\rm B}, j', \sigma'|\hat{x}|l, k_{\rm B}, j, \sigma\rangle_{\gamma,j} = \delta_{j',j}\delta_{\sigma',\sigma}\ {}_{\gamma,j}\langle l', k'_{\rm B} + \sigma k_{\rm so}|\hat{x}|l, k_{\rm B} + \sigma k_{\rm so}\rangle_{\gamma,j}. \tag{4.2}$$

The diagonal blocks,

$$\begin{aligned} &{}_{\gamma,j}\langle l', k'_{\rm B}, j, \sigma = 1|\hat{x}|l, k_{\rm B}, j, \sigma = 1\rangle_{\gamma,j} = {}_{\gamma,j}\langle l', k'_{\rm B} + k_{\rm so}|\hat{x}|l, k_{\rm B} + k_{\rm so}\rangle_{\gamma,j}, \quad \forall\, j, \\ &{}_{\gamma,j}\langle l', k'_{\rm B}, j, \sigma = -1|\hat{x}|l, k_{\rm B}, j, \sigma = -1\rangle_{\gamma,j} = {}_{\gamma,j}\langle l', k'_{\rm B} - k_{\rm so}|\hat{x}|l, k_{\rm B} - k_{\rm so}\rangle_{\gamma,j}, \quad \forall\, j, \end{aligned} \tag{4.3}$$

are unitary equivalent for a given value of the index j and thus the eigenvalues of $\hat{x}$ do not depend on σ.

4.3.2 Eigenvalue structure

The matrices ${}_{\gamma,j}\langle l', k'_{\rm B} \pm k_{\rm so}|\hat{x}|l, k_{\rm B} \pm k_{\rm so}\rangle_{\gamma,j}$ and ${}_{\gamma,j}\langle l', k'_{\rm B}|\hat{x}|l, k_{\rm B}\rangle_{\gamma,j}$ are unitary equivalent. Therefore, one may employ the eigenbasis $\{|l, k_{\rm B}\rangle\}$ of the Hamiltonian (1.6) in order to restrict the Hilbert space to a subspace retaining only a few Bloch bands of the Hamiltonian (1.6). Afterwards one has to find the eigenvalues of the matrix $\langle l', k'_{\rm B}|\hat{x}|l, k_{\rm B}\rangle$ constructed using the retained Bloch bands. Since the periodic potential in Eq. (1.6) is arbitrary, the results obtained in this way will be also valid when $U(x)$ is replaced with $U_{\gamma,j}(x)$ from the Hamiltonian (3.51). This will give us the eigenvalues of ${}_{\gamma,j}\langle l', k'_{\rm B}|\hat{x}|l, k_{\rm B}\rangle_{\gamma,j}$ and hence the eigenvalues of ${}_{\gamma,j}\langle l', k'_{\rm B} \pm k_{\rm so}|\hat{x}|l, k_{\rm B} \pm k_{\rm so}\rangle_{\gamma,j}$. Below we implement this route.

Let $\mathcal{H}$ be the Hilbert space of all possible states and let us choose in this space the basis of the Bloch states $\{|l, k_{\rm B}\rangle\}$ which are the eigenstates of the Hamiltonian (1.6):

$$\begin{aligned} &\langle x|l, k_{\rm B}\rangle = e^{{\rm i}k_{\rm B}x}u_{l,k_{\rm B}}(x), \\ &u_{l,k_{\rm B}}(x + L) = u_{l,k_{\rm B}}(x), \quad \forall\ k_{\rm B} \in \text{B.Z.},\ l = 1, 2, \dots, \end{aligned} \tag{4.4}$$

where L is the period of the Bloch amplitude $u_{l,k_{\rm B}}(x)$ and B.Z. stands for the first Brillouin zone.

Any vector $|\psi\rangle \in \mathcal{H}$ represents a linear combination

$$|\psi\rangle = \sum_{l=1}^{\infty} \sum_{k_\mathrm{B} \in \mathrm{B.Z.}} c_{l,k_\mathrm{B}} |l, k_\mathrm{B}\rangle. \tag{4.5}$$

Another basis $|\alpha\rangle$ is obtained using a transformation

$$|\alpha\rangle = \hat{U}^{-1} |l, k_\mathrm{B}\rangle, \quad \forall\ k_\mathrm{B} \in \mathrm{B.Z.},\ l = 1, 2, \dots\ , \tag{4.6}$$

where $\hat{U}$ is an arbitrary unitary operator.

Let us consider an operator $\hat{\mathcal{O}}$ corresponding to an observable $\mathcal{O}$. Its matrix representations in the two bases (4.4) and (4.6) are

$$\begin{aligned} &\mathcal{O}_\mathrm{B} = \langle l', k'_\mathrm{B} | \hat{\mathcal{O}} | l, k_\mathrm{B} \rangle, \quad \forall\ k_\mathrm{B}, k'_\mathrm{B} \in \mathrm{B.Z.},\ l, l' = 1, 2, \dots\ , \\ &\mathcal{O}_\alpha = \langle \alpha' | \hat{\mathcal{O}} | \alpha \rangle, \quad \forall\ \alpha, \alpha'. \end{aligned} \tag{4.7}$$

The eigenvalues $\{\lambda_i\}$ of the two matrices (4.7) are the same and represent all possible values of the observable $\mathcal{O}$.

Now let us consider a subspace $\mathcal{S} \subset \mathcal{H}$ generated by Bloch's states corresponding to a finite number, N_B, of bands. A vector $|\psi^\mathcal{S}\rangle \in \mathcal{S}$ has the form:

$$|\psi\rangle = \sum_{i=1}^{N_\mathrm{B}} \sum_{k_\mathrm{B} \in \mathrm{B.Z.}} c_{l_i,k_\mathrm{B}} |l_i, k_\mathrm{B}\rangle. \tag{4.8}$$

In this subspace the operator $\hat{\mathcal{O}}$ has the matrix representation:

$$\mathcal{O}^\mathcal{S}_\mathrm{B} = \langle l_{i'}, k'_\mathrm{B} | \hat{\mathcal{O}} | l_i, k_\mathrm{B} \rangle, \quad \forall\ k_\mathrm{B}, k'_\mathrm{B} \in \mathrm{B.Z.},\ i, i' = 1, 2, \dots N_\mathrm{B}. \tag{4.9}$$

Now the eigenvalues $\{\lambda^\mathcal{S}_n\}$ of (4.9) do not represent all possible values of the observable $\mathcal{O}$ but they only give approximate values of some of them. If the operator $\hat{\mathcal{O}}$ corresponds to a continuous observable with the spectrum from $-\infty$ to ∞, the eigenvalues $\{\lambda^\mathcal{S}_n\}$ are some of the eigenvalues $\{\lambda_i\}$, that is in this case $\{\lambda^\mathcal{S}_n\} \subset \{\lambda_i\}$.

A new basis $\{\alpha^\mathcal{S}\}$ of the subspace $\mathcal{S}$ is related to the Bloch one as:

$$|\alpha^\mathcal{S}\rangle = \hat{U}^{-1}_\mathcal{S} |l_i, k_\mathrm{B}\rangle, \quad \forall\ k_\mathrm{B} \in \mathrm{B.Z.},\ i = 1, 2, \dots, N_\mathrm{B}, \tag{4.10}$$

where now $\hat{U}^{-1}_\mathcal{S}$ is not an arbitrary unitary operator, but a unitary operator with the following property:

$$\hat{U}_\mathcal{S}: \quad |v\rangle \in \mathcal{S} \ \Rightarrow\ \hat{U}_\mathcal{S} |v\rangle \in \mathcal{S}, \quad \forall\ |v\rangle \in \mathcal{S}. \tag{4.11}$$

In this case the matrix

$$\mathcal{O}^\mathcal{S}_\alpha = \langle \alpha'^\mathcal{S} | \hat{\mathcal{O}} | \alpha^\mathcal{S} \rangle, \quad \forall\ \alpha'^\mathcal{S}, \alpha^\mathcal{S} \tag{4.12}$$

has the same set of eigenvalues $\{\lambda^\mathcal{S}_n\}$ as the matrix $\mathcal{O}^\mathcal{S}_\mathrm{B}$ in (4.9).

Let us specify the observable $\mathcal{O}$ to be particle's coordinate x with the corresponding operator denoted as $\hat{x}$. We consider the operator $\hat{x}$ in the subspace $\mathcal{S}$. Its matrix with respect to the Bloch basis is

$$x_{\mathrm{B}}^{\mathcal{S}} = \langle l_{i'}, k'_{\mathrm{B}} | \hat{x} | l_i, k_{\mathrm{B}} \rangle, \quad \forall\ k_{\mathrm{B}}, k'_{\mathrm{B}} \in \text{B.Z.}, \ i, i' = 1, 2, \ldots, N_{\mathrm{B}}. \tag{4.13}$$

Let us choose the translational operator as the unitary operator $\hat{U}_{\mathcal{S}}$, that is

$$\hat{U}_{\mathcal{S}}(a) = e^{\frac{i}{\hbar} a \hat{p}}. \tag{4.14}$$

It is obvious that for an arbitrary value of a the operator $\hat{U}_{\mathcal{S}}(a)$ does not satisfy the property (4.11). However, in the case $a = L$ a Bloch state $|l, k_{\mathrm{B}}\rangle$ is translated into a Bloch state with the same l, k_{B} and thus (4.11) is fulfilled. Hence, the matrix

$$\tilde{x}_{\mathrm{B}}^{\mathcal{S}} = \langle l_{i'}, k'_{\mathrm{B}} | \hat{U}_{\mathcal{S}}(L) \hat{x} \hat{U}_{\mathcal{S}}^{-1}(L) | l_i, k_{\mathrm{B}} \rangle, \quad \forall\ k_{\mathrm{B}}, k'_{\mathrm{B}} \in \text{B.Z.}, \ i, i' = 1, 2, \ldots, N_{\mathrm{B}} \tag{4.15}$$

has the same eigenvalues as the matrix $x_{\mathrm{B}}^{\mathcal{S}}$ in (4.13). But due to the equality

$$\hat{U}_{\mathcal{S}}(L) \hat{x} \hat{U}_{\mathcal{S}}^{-1}(L) = \hat{x} + L \tag{4.16}$$

the two matrices $x_{\mathrm{B}}^{\mathcal{S}}$ and $\tilde{x}_{\mathrm{B}}^{\mathcal{S}}$ are related as follows:

$$\begin{aligned} &\langle l_{i'}, k'_{\mathrm{B}} | \hat{U}_{\mathcal{S}}(L) \hat{x} \hat{U}_{\mathcal{S}}^{-1}(L) | l_i, k_{\mathrm{B}} \rangle = \langle l_{i'}, k'_{\mathrm{B}} | \hat{x} | l_i, k_{\mathrm{B}} \rangle + L \delta_{i',i} \delta_{k'_{\mathrm{B}}, k_{\mathrm{B}}}, \\ &\forall\ k_{\mathrm{B}}, k'_{\mathrm{B}} \in \text{B.Z.}, \ i, i' = 1, 2, \ldots, N_{\mathrm{B}}. \end{aligned} \tag{4.17}$$

From (4.17) it follows that the eigenvalues of the matrix $x_{\mathrm{B}}^{\mathcal{S}}$ are invariant under a shift equal to jL with j being an integer. That is for any $\lambda_k^{\mathcal{S}} \in \{\lambda_n^{\mathcal{S}}\}$ there exists $\lambda_m^{\mathcal{S}} \in \{\lambda_n^{\mathcal{S}}\}$ such that

$$\lambda_k^{\mathcal{S}} = jL + \lambda_m^{\mathcal{S}}. \tag{4.18}$$

Let us denote through $\{d_k^{\mathcal{S}}\}$ those eigenvalues of $q_{\mathrm{B}}^{\mathcal{S}}$ the distance between which is less than L,

$$|d_r^{\mathcal{S}} - d_{r'}^{\mathcal{S}}| < L, \quad \forall\ d_r^{\mathcal{S}}, d_{r'}^{\mathcal{S}} \in \{d_k^{\mathcal{S}}\}, \tag{4.19}$$

and which are in the zeroth elementary cell. Then each of the eigenvalues $\{\lambda_n^{\mathcal{S}}\}$ of the matrix $x_{\mathrm{B}}^{\mathcal{S}}$ is obtained from its corresponding eigenvalue $d_m \in \{d_k^{\mathcal{S}}\}$ by a shift jL with a proper integer j. It means that each elementary cell contains the same number of eigenvalues of the coordinate operator. Since the total number of the eigenvalues $\{\lambda_n^{\mathcal{S}}\}$ is equal to $N_{\mathrm{B}}N$ where N is the number of the elementary cells, we conclude that there are N_{B} eigenvalues in each elementary cell. This gives us the final expression for the eigenvalues of the matrix $x_{\mathrm{B}}^{\mathcal{S}}$ (N is even to be definite):

$$\begin{aligned} &\lambda_{m,j}^{\mathcal{S}} = jL + d_m^{\mathcal{S}}, m = 1, 2, \ldots, N_{\mathrm{B}}, \\ &j = -\frac{N}{2} + 1, -\frac{N}{2} + 2, \ldots, -1, 0, 1, \ldots, \frac{N}{2} - 1, \frac{N}{2} \end{aligned} \tag{4.20}$$

and $N \to \infty$ afterwards.

As it was mentioned above, in the Hamiltonian (1.6) the periodic potential $U(x)$ was arbitrary. The results are thus also valid if we replace $U(x)$ with the periodic potential $U_{\gamma,j}(x)$ from the Hamiltonian (3.51). Therefore, we conclude that the eigenvalues of the matrix ${}_{\gamma,j}\langle l', k'_{\rm B} \pm k_{\rm so}|\hat{x}|l, k_{\rm B} \pm k_{\rm so}\rangle_{\gamma,j}$ are

$$x_{\gamma;\zeta,m,j} = mL + d_{\gamma;\zeta,j}, \tag{4.21}$$

where $m = 0, \pm 1, \pm 2 \ldots$, $\zeta = 1, 2, \ldots, N_{\rm B}$ and the eigenvalues $d_{\gamma;\zeta,j}$ are distributed within one elementary cell. If, for example, the system is divided into the elementary cells in such a way that the origin of coordinates is at the center of an elementary cell, then $-L/2 < d_{\gamma;\zeta,j} \leqslant L/2$. In Eq. (4.21) we have taken into account that the periodic potential $U_{\gamma,j}(x)$ depends on γ and j and thus the eigenvalues distributed within one elementary cell also acquire a dependence on γ and j.

4.4 σ-DVR basis

From (4.2) and (4.21) it follows that one can label the eigenstates of $\hat{x}$ with the quantum numbers ζ, m, j, σ, that is as $|\zeta, m, j, \sigma\rangle_{\gamma,j}$, and in the $\{|l, k_{\rm B}, j, \sigma\rangle_{\gamma,j}\}$ representation these eigenstates have the form:

$${}_{\gamma,j'}\langle l, k_{\rm B}, j', \sigma'|\zeta, m, j, \sigma\rangle_{\gamma,j} = \delta_{j',j}\delta_{\sigma',\sigma}\ {}_{\gamma,j}\langle l, k_{\rm B}, j, \sigma|\zeta, m, j, \sigma\rangle_{\gamma,j}. \tag{4.22}$$

The corresponding eigenvalues are $x_{\gamma;\zeta,m,j,\sigma} = x_{\gamma;\zeta,m,j}$. From the eigenvalue equation

$$\hat{x}|\zeta, m, j, \sigma\rangle_{\gamma,j} = x_{\gamma;\zeta,m,j}|\zeta, m, j, \sigma\rangle_{\gamma,j} \tag{4.23}$$

written in the $\{|l, k_{\rm B}, j, \sigma\rangle_{\gamma,j}\}$ representation through the use of (4.2),

$$\begin{aligned} &\sum_{l',k'_{\rm B}} {}_{\gamma,j}\langle l, k_{\rm B} + \sigma k_{\rm so}|\hat{x}|l', k'_{\rm B} + \sigma k_{\rm so}\rangle_{\gamma,j}\ {}_{\gamma,j}\langle l', k'_{\rm B}, j, \sigma|\zeta, m, j, \sigma\rangle_{\gamma,j} = \\ &= x_{\gamma;\zeta,m,j}\ {}_{\gamma,j}\langle l, k_{\rm B}, j, \sigma|\zeta, m, j, \sigma\rangle_{\gamma.j}, \end{aligned} \tag{4.24}$$

it follows that

$$\begin{aligned} {}_{\gamma,j}\langle l, k_{\rm B}, j, \sigma = 1|\zeta, m, j, \sigma = 1\rangle_{\gamma,j} &= {}_{\gamma,j}\langle l, k_{\rm B} + k_{\rm so}|\zeta, m\rangle_{\gamma,j}, \\ {}_{\gamma,j}\langle l, k_{\rm B}, j, \sigma = -1|\zeta, m, j, \sigma = -1\rangle_{\gamma,j} &= {}_{\gamma,j}\langle l, k_{\rm B} - k_{\rm so}|\zeta, m\rangle_{\gamma,j}. \end{aligned} \tag{4.25}$$

Since $|\zeta, m, j, \sigma\rangle_{\gamma,j}$ is also the eigenstate of $\hat{\sigma}_z$ corresponding to the eigenvalue $\sigma_{\zeta,m,j,\sigma} = \sigma$, we infer that the σ-DVR basis states $|\alpha\rangle$, mentioned in the introduction of this chapter, are just the $|\zeta, m, j, \sigma\rangle_{\gamma,j}$ states, that is $\{|\alpha\rangle\} \equiv \{|\zeta, m, j, \sigma\rangle_{\gamma,j}\}$.

4.5 Tight-binding model of a spin-orbit superlattice in the σ-DVR basis

In this section we will develop a tight-binding model for the Hamiltonian (3.44) using the σ-DVR basis $\{|\zeta, m, j, \sigma\rangle_{\gamma,j}\}$ obtained in Subsection 4.3.2, Eqs. (4.22) and (4.25).

4.5.1 Hamiltonian in the σ-DVR basis

Let us represent the Hamiltonian $\hat{H}$, Eq. (3.44), in the σ-DVR basis obtained in the previous section, *i.e.*, using the $|\zeta, m, j, \sigma\rangle_{\gamma,j}$ states,

$$\hat{H} = \sum_{\substack{\zeta,m,j,\sigma \\ \zeta',m',j',\sigma'}} {}_{\gamma,j'}\langle\zeta', m', j', \sigma'|\hat{H}|\zeta, m, j, \sigma\rangle_{\gamma,j}|\zeta', m', j', \sigma'\rangle_{\gamma,j'} \ {}_{\gamma,j}\langle\zeta, m, j, \sigma|. \tag{4.26}$$

In the rest of this chapter and in the following one we assume that in Eq. (3.44) $V(z) = m\omega_0^2 z^2/2$. Using Eqs. (4.22) and (4.25) as well as Eq. (3.13) with the modifications mentioned in Subsection 3.5.2, we may write

$$\begin{aligned} {}_{\gamma,j'}\langle\zeta', m', j', \sigma'|\hat{H}|\zeta, m, j, \sigma\rangle_{\gamma,j} &= \sum_{l,k_{\mathrm{B}},\eta} \varepsilon_{\gamma;l,\eta}(k_{\mathrm{B}}) \, {}_{\gamma,j'}\langle\zeta', m'|l, k_{\mathrm{B}} + \sigma' k_{\mathrm{so}}\rangle_{\gamma,j'} \times \\ \times \ {}_{\gamma,j}\langle l, k_{\mathrm{B}} + \sigma k_{\mathrm{so}}|\zeta, m\rangle_{\gamma,j} \, &\theta_{\gamma;l,k_{\mathrm{B}},\eta}(j', \sigma'; H_0)\theta^*_{\gamma;l,k_{\mathrm{B}},\eta}(j, \sigma; H_0). \end{aligned} \tag{4.27}$$

4.5.2 Approximations and the effective tight-binding model

The tight-binding approximation of (4.26) is obtained if one assumes that the matrix elements in Eq. (4.27) with $|m' - m| > 1$ are negligibly small.

We consider temperatures low enough and assume that electrons populate only the lowest Bloch sub-bands with $l = 1$ (*i.e.*, $N_{\mathrm{B}} = 1$). Under this condition the periodic potential can be of arbitrary shape and the only limitation on it is the validity of the tight-binding approximation.

In this thesis we thoroughly study the case where the four lowest Bloch sub-bands are the ones with $l = 1$, $\eta = 1, 2, 3, 4$ and the only ones which are populated with electrons. For simplicity we consider weak orbit-orbit coupling and calculate the corresponding eigenenergies $\varepsilon_{\gamma;l,\eta}(k_{\mathrm{B}})$ and eigenspinors $\theta_{\gamma;l,k_{\mathrm{B}},\eta}(j, \sigma; H_0)$ retaining only the first two transverse modes, that is $j = 0, 1$. In this case $\hat{H}$ has the form

$$\begin{aligned} \hat{H} = \sum_m \Bigg[&\sum_{j,\sigma} \varepsilon_{\gamma;j,\sigma}|m, j, \sigma\rangle_{\gamma,j} \ {}_{\gamma,j}\langle m, j, \sigma| + \\ &+ \sum_{j,\sigma'\neq\sigma} \Delta^{\mathrm{intra}}_{\gamma;j,\sigma';j,\sigma}(m)|m, j, \sigma'\rangle_{\gamma,j} \ {}_{\gamma,j}\langle m, j, \sigma| + \\ &+ \sum_{j'\neq j,\sigma',\sigma} \Delta^{\mathrm{intra}}_{\gamma;j',\sigma';j,\sigma}(m)|m, j', \sigma'\rangle_{\gamma,j'} \ {}_{\gamma,j}\langle m, j, \sigma| + \\ &+ \sum_{j',j,\sigma',\sigma} \Big(\Delta^{\mathrm{inter,b}}_{\gamma;j',\sigma';j,\sigma}(m)|m, j', \sigma'\rangle_{\gamma,j'} \ {}_{\gamma,j}\langle m + 1, j, \sigma| + \\ &+ \Delta^{\mathrm{inter,f}}_{\gamma;j',\sigma';j,\sigma}(m)|m + 1, j', \sigma'\rangle_{\gamma,j'} \ {}_{\gamma,j}\langle m, j, \sigma| \Big) \Bigg], \end{aligned} \tag{4.28}$$

where

$$|m, j, \sigma\rangle_{\gamma,j} \equiv |\zeta = 1, m, j, \sigma\rangle_{\gamma,j}, \tag{4.29}$$

and we have defined the on-site energies $\varepsilon_{\gamma;j,\sigma}$ and hopping matrix elements $\Delta^{\text{intra}}_{\gamma;j',\sigma';j,\sigma}(m)$, $\Delta^{\text{inter,b}}_{\gamma;j',\sigma';j,\sigma}(m)$ and $\Delta^{\text{inter,f}}_{\gamma;j',\sigma';j,\sigma}(m)$ as follows

$$\begin{aligned}
&\varepsilon_{\gamma;j,\sigma} \equiv {}_{\gamma,j}\langle m,j,\sigma|\hat{H}|m,j,\sigma\rangle_{\gamma,j},\\
&\Delta^{\text{intra}}_{\gamma;j',\sigma';j,\sigma}(m) \underset{(j',\sigma')\neq(j,\sigma)}{\equiv} {}_{\gamma,j'}\langle m,j',\sigma'|\hat{H}|m,j,\sigma\rangle_{\gamma,j},\\
&\Delta^{\text{inter,b}}_{\gamma;j',\sigma';j,\sigma}(m) \equiv {}_{\gamma,j'}\langle m,j',\sigma'|\hat{H}|m+1,j,\sigma\rangle_{\gamma,j},\\
&\Delta^{\text{inter,f}}_{\gamma;j',\sigma';j,\sigma}(m) \equiv {}_{\gamma,j'}\langle m+1,j',\sigma'|\hat{H}|m,j,\sigma\rangle_{\gamma,j}.
\end{aligned} \tag{4.30}$$

Note that

$$[\Delta^{\text{intra}}_{\gamma;j',\sigma';j,\sigma}(m)]^* = \Delta^{\text{intra}}_{\gamma;j,\sigma;j',\sigma'}(m), \tag{4.31}$$

$$[\Delta^{\text{inter,b}}_{\gamma;j',\sigma';j,\sigma}(m)]^* = \Delta^{\text{inter,f}}_{\gamma;j,\sigma;j',\sigma'}(m). \tag{4.32}$$

Introducing the notations

$$\begin{aligned}
&\{\xi\} \equiv \{(j,\sigma)\},\\
&\xi = 1 \Leftrightarrow (0,1),\ \xi = 2 \Leftrightarrow (0,-1),\\
&\xi = 3 \Leftrightarrow (1,1),\ \xi = 4 \Leftrightarrow (1,-1),
\end{aligned} \tag{4.33}$$

we finally have

$$\begin{aligned}
\hat{H} = \sum_m \Bigg[&\sum_{\xi=1}^{4} \varepsilon_{\gamma;\xi}|m,\xi\rangle_{\gamma,\xi}\ {}_{\gamma,\xi}\langle m,\xi| +\\
&+ \sum_{\xi\neq\xi'=1}^{4} \Delta^{\text{intra}}_{\gamma;\xi',\xi}(m)|m,\xi'\rangle_{\gamma,\xi'}\ {}_{\gamma,\xi}\langle m,\xi| +\\
&+ \sum_{\xi,\xi'=1}^{4} \Big(\Delta^{\text{inter,b}}_{\gamma;\xi',\xi}(m)|m,\xi'\rangle_{\gamma,\xi'}\ {}_{\gamma,\xi}\langle m+1,\xi| +\\
&+ \Delta^{\text{inter,f}}_{\gamma;\xi',\xi}(m)|m+1,\xi'\rangle_{\gamma,\xi'}\ {}_{\gamma,\xi}\langle m,\xi| \Big) \Bigg].
\end{aligned} \tag{4.34}$$

Equation (4.34) represents a tight-binding model which can now be used to perform actual calculations of quantum transport in a dissipative system. This tight-binding model is graphically depicted in Fig. 4.1.

To conclude this subsection, we would like to note that because of the simultaneous presence of the harmonic confinement and RSOI the system splits into two subsystems. The first subsystem is characterized by $\xi = 1, 4$ and the second one by $\xi = 2, 3$. These subsystems are totally decoupled: there is no electron exchange between them. Such a state of affairs persists if one considers more than two transverse modes. In this work, for simplicity, we only consider one subsystem, namely the one with $\xi = 1, 4$. Such uncoupled subsystems also appear within the hard wall model of the transverse confinement [92].

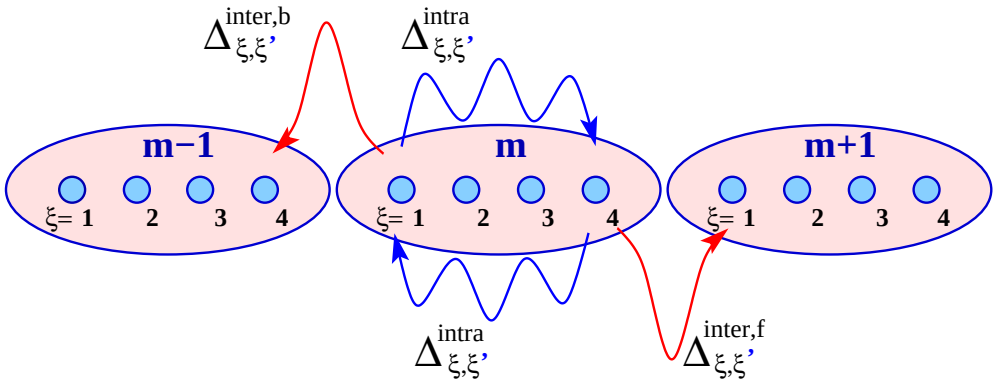

Figure 4.1: A graphical view on the effective tight-binding model given by Eq. (4.34). The system represents an infinite set of pseudo-cells. The pseudo-cell index is denoted as m. Inside each pseudo-cell there are four pseudo-band states denoted through ξ. The matrix elements $\Delta^{\mathrm{inter,b}}_{\gamma;\xi,\xi'}$ and $\Delta^{\mathrm{inter,f}}_{\gamma;\xi,\xi'}$ describe inter-pseudo-cell tunneling events while the matrix elements $\Delta^{\mathrm{intra}}_{\gamma;\xi,\xi'}$ describe an intra-pseudo-cell dynamics.

4.5.3 An additional relation between some hopping matrix elements

In the context of the present chapter it is also relevant to invest additional effort to employ the structure of the DVR states in order to find a useful relation between the hopping matrix elements $\Delta^{\mathrm{inter,f}}_{\gamma;1,4}(m)$ and $\Delta^{\mathrm{inter,f}}_{\gamma;4,1}(m)$ of the tight-binding model developed in the previous subsection. This relation will be extremely useful in the analysis of the charge and spin ratchet mechanisms studied in the next chapter.

The scalar products ${}_{\gamma,j}\langle\zeta,m|l,k_{\mathrm{B}}\rangle_{\gamma,j}$ are nothing else than the Bloch states of the corresponding truly 1D problem without the magnetic field and without RSOI in the representation of the coordinate operator $\hat{x}$ operating on the subspace $\mathcal{S}\subset\mathcal{H}$ (see Subsection 4.3.2). Thus using the eigenvalues of this coordinate operator, Eq. (4.21), we have:

$$ {}_{\gamma,j}\langle\zeta,m|l,k_{\mathrm{B}}\rangle_{\gamma,j} = \mathrm{e}^{\mathrm{i}k_{\mathrm{B}}(mL+d_{\gamma;\zeta,j})}u^{\mathrm{DVR}}_{\gamma,j;l,k_{\mathrm{B}}}(d_{\gamma;\zeta,j}), \tag{4.35}$$

where we denoted the Bloch amplitude with the abbreviation DVR in order to stress that it originates from the discrete variable representation and differs from the one which originates from the continuum variable representation.

The difference of the squares of the absolute values of the hopping matrix elements, $|\Delta^{\mathrm{inter,f}}_{\gamma;1,4}(m)|^2$ and $|\Delta^{\mathrm{inter,f}}_{\gamma;4,1}(m)|^2$, can be expressed in terms of the DVR Bloch amplitudes as

$$ |\Delta^{\mathrm{inter,f}}_{\gamma;1,4}(m)|^2 - |\Delta^{\mathrm{inter,f}}_{\gamma;4,1}(m)|^2 = -\frac{\hbar^3 k_{\mathrm{so}}^2\omega_0}{m}\sum_{k_{\mathrm{B}},k'_{\mathrm{B}}}\sin[(k_{\mathrm{B}}-k'_{\mathrm{B}})L]\mathrm{Im}[F_{\gamma;k_{\mathrm{B}},k'_{\mathrm{B}}}], \tag{4.36}$$

where we have introduced a function $F_{\gamma;k_{\mathrm{B}},k'_{\mathrm{B}}}$ defined as

$$ \begin{aligned} F_{\gamma;k_{\mathrm{B}},k'_{\mathrm{B}}} &= u^{\mathrm{DVR}}_{\gamma,0;1,k_{\mathrm{B}}+k_{\mathrm{so}}}(d_{\gamma;1,0})u^{\mathrm{DVR}}_{\gamma,1;1,k'_{\mathrm{B}}-k_{\mathrm{so}}}(d_{\gamma;1,1})\times \\ &\times\left[u^{\mathrm{DVR}}_{\gamma,1;1,k_{\mathrm{B}}-k_{\mathrm{so}}}(d_{\gamma;1,1})u^{\mathrm{DVR}}_{\gamma,0;1,k'_{\mathrm{B}}+k_{\mathrm{so}}}(d_{\gamma;1,0})\right]^*. \end{aligned} \tag{4.37}$$

The function $F_{\gamma;k_\mathrm{B},k'_\mathrm{B}}$ has two useful properties which directly follow from its definition (4.37). The first property comes from the fact that $F_{\gamma;k_\mathrm{B},k'_\mathrm{B}}$ is real if the Bloch amplitudes are real:

$$\mathrm{Im}[u^{\mathrm{DVR}}_{\gamma,j;1,k_\mathrm{B}}(d_{\gamma;1,j})] = 0 \;\Rightarrow\; \mathrm{Im}[F_{\gamma;k_\mathrm{B},k'_\mathrm{B}}] = 0. \tag{4.38}$$

The second property is that $F_{\gamma=0;k_\mathrm{B},k'_\mathrm{B}}$ is an even function in both of its arguments. Indeed, when $\gamma = 0$, we have $u_{\gamma,j;l,k_\mathrm{B}}(x) = u_{l,k_\mathrm{B}}(x)$, $d_{\gamma;\zeta,j} = d_\zeta$, that is

$$F_{\gamma=0;k_\mathrm{B},k'_\mathrm{B}} = u^{\mathrm{DVR}}_{1,k_\mathrm{B}+k_\mathrm{so}}(d_1)u^{\mathrm{DVR}}_{1,k'_\mathrm{B}-k_\mathrm{so}}(d_1)\big[u^{\mathrm{DVR}}_{1,k_\mathrm{B}-k_\mathrm{so}}(d_1)u^{\mathrm{DVR}}_{1,k'_\mathrm{B}+k_\mathrm{so}}(d_1)\big]^*. \tag{4.39}$$

One then finds from Eq. (4.39) that $F_{\gamma=0;-k_\mathrm{B},k'_\mathrm{B}} = F_{\gamma=0;k_\mathrm{B},k'_\mathrm{B}}$ and $F_{\gamma=0;k_\mathrm{B},-k'_\mathrm{B}} = F_{\gamma=0;k_\mathrm{B},k'_\mathrm{B}}$. As a consequence, from this property one gets

$$\begin{aligned} \mathrm{Im}[F_{\gamma=0;-k_\mathrm{B},k'_\mathrm{B}}] &= \mathrm{Im}[F_{\gamma=0;k_\mathrm{B},k'_\mathrm{B}}], \\ \mathrm{Im}[F_{\gamma=0;k_\mathrm{B},-k'_\mathrm{B}}] &= \mathrm{Im}[F_{\gamma=0;k_\mathrm{B},k'_\mathrm{B}}], \end{aligned} \tag{4.40}$$

which means that $\mathrm{Im}[F_{\gamma=0;k_\mathrm{B},k'_\mathrm{B}}]$ is even in k_B and k'_B. The same is also valid for $\mathrm{Re}[F_{\gamma=0;k_\mathrm{B},k'_\mathrm{B}}]$.

4.6 Conclusion

In this chapter we have found a common basis of the coordinate, $\hat{x}$, and spin, $\hat{\sigma}_z$, operators, the σ-DVR basis. To obtain this basis we have used the eigenstates of the Hamiltonian (3.51) and truncated the Hilbert space basis using a few Bloch bands of the Hamiltonian (1.6) in which $U(x)$ was replaced with $U_{\gamma,j}(x)$ from the Hamiltonian (3.51). Afterwards we have employed the obtained σ-DVR basis to develop an effective tight-binding model of the Hamiltonian (3.44) with $V(z) = m\omega_0^2 z^2/2$. To simplify the model and at the same time make it applicable to study low temperature transport, only the four lowest Bloch sub-bands corresponding to the first Bloch band have been taken into account. Finally, we have used an explicit structure of the Bloch states in the DVR representation and found an additional relation between some of the hopping matrix elements of the previously obtained effective tight-binding model.

Chapter 5

Quantum dissipative spin-orbit ratchet effects

In collaboration with D. Bercioux, M. Grifoni, and K. Richter, Refs. [67, 69, 70].

5.1 Introduction

In this chapter we investigate the charge and spin ratchet mechanisms implemented as Brownian charge and spin motors, respectively. Specifically, we consider non-interacting electrons in a quantum wire formed by a harmonic transverse confinement in a 2DEG with RSOI. The electrons are also subject to a 1D periodic potential along the wire direction. The amplitude of this periodic potential is assumed to vary across the quantum wire due to a coupling between the in-plane orbital degrees of freedom. Additionally, an in-plane magnetic field perpendicular to the wire is also taken into consideration. This system is described by the Hamiltonian (3.44) with $V(z) = m\omega_0^2 z^2/2$. To obtain expressions for the charge and spin ratchet currents the effective tight-binding form (4.34) of this Hamiltonian will be used. An orbital coupling between this originally isolated system and an external environment is described within the model of Caldeira and Leggett (1.7). This coupling causes dissipative processes affecting indirectly the spin dynamics through RSOI. An external ac driving originates in our work from an ac electric and/or ac magnetic fields.

5.2 Electrically driven quantum dissipative spin ratchet

In this section we consider a pure electric driving and show that the net stationary charge current is strongly suppressed if the transport is governed only by electrons of the Bloch sub-bands related to the same Bloch band which would result from the corresponding truly 1D problem without RSOI. However, at the same time and under the same conditions a net stationary spin current turns out to be activated in a spatially

asymmetric situation and for finite values of the spin-orbit coupling strength and the coupling strength between the orbital degrees of freedom. The magnetic field does not destroy this picture, but it can partly reduce or on the contrary enhance the ratchet effect.

A general formulation of the problem we are going to solve in this chapter was already given in Chapter 1 in Subsection 1.2.4. For the sake of convenience we first recapitulate this general formulation in a precise mathematical fashion and afterwards solve the problem.

The full Hamiltonian of our problem is

$$\hat{H}_{\text{full}}(t) = \hat{H} + \hat{H}_{\text{ext}}(t) + \hat{H}_{\text{bath}}, \tag{5.1}$$

where $\hat{H}$ is the Hamiltonian of the isolated periodic system, $\hat{H}_{\text{ext}}(t)$ describes an external driving and $\hat{H}_{\text{bath}}$ represents the term responsible for dissipative processes.

5.2.1 Isolated system

The isolated quasi-1D periodic system is formed in a 2DEG ($x-z$ plane) with RSOI using a periodic potential along the x-axis and a harmonic confinement along the z-axis. The whole system is in a uniform stationary magnetic field along the z-axis (Hamiltonian (3.44) with $V(z) = m\omega_0^2 z^2/2$):

$$\hat{H} = \frac{\hbar^2 \hat{\vec{k}}^2}{2m} + \frac{m\omega_0^2 \hat{z}^2}{2} - \frac{\hbar^2 k_{\text{so}}}{m}\left(\hat{\sigma}_x \hat{k}_z - \hat{\sigma}_z \hat{k}_x\right) + U(\hat{x})\left(1 + \gamma \frac{\hat{z}^2}{L^2}\right) - g\mu_{\text{B}} \hat{\sigma}_z H_0, \tag{5.2}$$

where H_0 is the z-component of the magnetic field $\vec{H}_0 = (0, 0, H_0)$, and we have used the gauge in which the components of the vector potential are $A_x = -H_0 y$, $A_y = A_z = 0$ (Landau gauge, see Ref. [56]). Additionally, we have taken into account the fact that in a 2DEG $y = 0$. In Eq. (5.2) the operator $\hat{\vec{k}}$ is related to the momentum operator $\hat{\vec{p}}$ as $\hat{\vec{p}} = \hbar\hat{\vec{k}}$, ω_0 is the harmonic confinement strength, k_{so} the spin-orbit interaction strength, γ the strength of the coupling between the orbital degrees of freedom x and z, g the electron spin g-factor, μ_{B} the Bohr magneton, and $U(\hat{x})$ denotes the periodic potential with period L,

$$U(x + L) = U(x). \tag{5.3}$$

5.2.2 Interaction with an external environment

The system is also coupled to an external bath. In this thesis we assume the transverse confinement to be strong enough so that the probabilities of direct bath-excited transitions between the transverse modes are negligibly small. In other words, the wire is truly 1D from the point of view of the bath which directly changes only the dynamics along the wire. Thus in our model the external environment couples to the electronic

degrees of freedom only through $\hat{x}$. The bath itself as well as its interaction with the quantum wire are described within the Caldeira-Leggett model (see Eq. (1.7)),

$$\hat{H}_{\text{bath}} = \frac{1}{2}\sum_{\alpha=1}^{N_O}\left[\frac{\hat{p}_\alpha^2}{m_\alpha} + m_\alpha\omega_\alpha^2\left(\hat{x}_\alpha - \frac{c_\alpha}{m_\alpha\omega_\alpha^2}\hat{x}\right)^2\right]. \tag{5.4}$$

The bath is fully characterized by its spectral density defined as (see Eq. (1.8))

$$J(\omega) \equiv \frac{\pi}{2}\sum_{\alpha=1}^{N_O}\frac{c_\alpha^2}{m_\alpha\omega_\alpha}\delta(\omega-\omega_\alpha). \tag{5.5}$$

It is important to emphasize that, due to the spin-orbit interaction and orbit-orbit coupling, the direct dissipative interaction between the longitudinal dynamics in the wire and the external environment has an indirect impact on the transition rates between different transverse modes. The transverse dynamics in the wire indirectly feels the presence of the external bath through the spin-orbit interaction and orbit-orbit coupling.

5.2.3 External driving

In the following we assume that the periodic structure is subject to an external homogeneous time-dependent electric field. Only the x-component of the electric field vector is non-zero, that is, the electric field is parallel or anti-parallel to the x-axis. Experimentally this can be implemented using for example linearly polarized light. The external force thus couples only to the x-component of the electron coordinate operator and has the form of Eq. (1.10),

$$\hat{H}_{\text{ext}} = eE(t)\hat{x}, \tag{5.6}$$

where $-e$ is the elementary electronic charge and the electric field $E(t)$ is unbiased. In this work we use the time-dependence (1.11),

$$-eE(t) = F\cos(\Omega(t)). \tag{5.7}$$

The term "unbiased electric field" (see also Subsection 1.1.1 about a general definition of unbiased forces) should not be confused with voltage bias. An external periodic force is called unbiased if its mean value, that is its average over one period, is equal to zero. It is obviously our case as one can see from Eq. (5.7).

5.2.4 Charge and spin currents

The dynamical quantities of interest are the charge and spin currents. Specifically, the longitudinal charge current $J_{\text{C}}(t)$ is given (see for example [28]) as a statistical average of the longitudinal charge current operator $\hat{J}_{\text{C}}(t)$, *i.e.*, the product of the velocity operator $\hat{v}(t)$ and the elementary electronic charge $-e$,

$$\hat{J}_{\text{C}}(t) = -e\hat{v}(t), \tag{5.8}$$

$$J_{\mathrm{C}}(t) = -e\frac{d}{dt}\mathrm{Tr}[\hat{x}\hat{\rho}(t)], \tag{5.9}$$

where, as in Eq. (1.27), $\hat{\rho}(t) = \mathrm{Tr}_{\mathrm{B}}\hat{W}(t)$ is the reduced statistical operator of the system, that is the full one $\hat{W}(t)$ with the bath degrees of freedom traced out.

Using the definition (1.55) of the spin current operator we obtain for the longitudinal spin current operator the following expression,

$$\hat{J}^i_{\mathrm{S}}(t) = \frac{d}{dt}\big(\hat{\sigma}_i\hat{x}\big), \tag{5.10}$$

where $i = x, y, z$ and we have omitted the factor $\hbar/2$. As it was discussed in Subsection 1.2.2, one of the advantages of the definition (1.55) over the conventional one, Eq. (1.47), was that the spin current based on Eq. (1.55) could be conserved even in systems with RSOI. In the context of quasi-1D systems it means that using the longitudinal spin current based on Eq. (5.10),

$$J^i_{\mathrm{S}}(t) = \frac{d}{dt}\mathrm{Tr}\big(\hat{\sigma}_i\hat{x}\hat{\rho}(t)\big), \tag{5.11}$$

the continuity equation for the spin density can often be written without a source term, which means that the spin current defined in this way is conserved. This conserved spin current can be uniquely related to the spin accumulation at a sample boundary. The out-of-plane polarized spin accumulation can experimentally be measured with Kerr rotation microscopy [99] or the Faraday rotation technique [100]. The in-plane spin polarization is not directly measured by Kerr rotation microscopy, but it can still be scanned by a magneto-optic Kerr microscope using, *e.g.*, the cleaved edge technology as discussed by Kotissek *et al.* in Ref. [101]. From the discussion of Subsection 1.2.2 we know that even when the continuity equation contains a source term, there is still one advantage of the spin current operator definition (1.55). This definition leads to a very reasonable physical result: the corresponding spin current vanishes in insulators. Since in our case the longitudinal spin current operator (5.10) is based on the definition (1.55), it must also vanish in insulators. In Subsection 5.2.7 we will return to this point and analytically prove that when the periodic potential gets stronger and as a result the energy bands get narrower, that is when the system turns into an insulator, the spin current given by Eq. (5.11) goes to zero. A further discussion of the difference between the conventional definition of the spin current and the alternative spin current definition used in our work is given in Subsection 5.2.8.

Below we will calculate only the spin current polarized along the z-axis and denote this current as J_{S}, *i.e.*, $J_{\mathrm{S}}(t) \equiv J^z_{\mathrm{S}}(t)$. The components of the spin current polarized along the x and y axes are zero as it demonstrated at the end of this subsection.

It is convenient to calculate the traces in (5.9) and (5.11) using the basis which diagonalizes both $\hat{x}$ and $\hat{\sigma}_z$, because this requires to determine only the diagonal elements of the reduced density matrix. This basis is the σ-DVR basis $\{|\alpha\rangle\}$ from Chapter 4. It was defined in Section 4.1 and obtained in Section 4.4. Since $\hat{x}|\alpha\rangle = x_\alpha|\alpha\rangle$ and

$\hat{\sigma}_z|\alpha\rangle = \sigma_\alpha|\alpha\rangle$, the charge and spin currents (5.9) and (5.11) are rewritten as

$$\begin{aligned} J_{\mathrm{C}}(t) &= -e\sum_\alpha x_\alpha \frac{d}{dt}P_\alpha(t), \\ J_{\mathrm{S}}(t) &= \sum_\alpha \sigma_\alpha x_\alpha \frac{d}{dt}P_\alpha(t), \end{aligned} \tag{5.12}$$

where $P_\alpha(t) \equiv \langle\alpha|\hat{\rho}(t)|\alpha\rangle$ is the population of the σ-DVR state $|\alpha\rangle$ at time t.

Let us now show that the longitudinal spin current components $J_{\mathrm{S}}^{x,y}(t)$ polarized along the x and y axes vanish.

The expressions for the spin currents

$$J_{\mathrm{S}}^{x,y}(t) = \frac{d}{dt}\mathrm{Tr}\big(\hat{\sigma}_{x,y}\hat{x}\hat{\rho}(t)\big) \tag{5.13}$$

can easily be found using the σ-DVR basis $\{|\alpha\rangle\} \equiv \{|\zeta, m, j, \sigma\rangle_{\gamma,j}\}$ from Chapter 4:

$$\begin{aligned} J_{\mathrm{S}}^{x}(t) = 2\frac{d}{dt}\mathrm{Tr}_{\mathrm{B}}\sum_{\zeta,m,j}(mL + d_{\gamma;\zeta,j})\times \\ \times \mathrm{Re}\big({}_{\gamma,j}\langle\zeta, m, j, \sigma' = +1|\hat{W}(t)|\zeta, m, j, \sigma = -1\rangle_{\gamma,j}\big), \end{aligned} \tag{5.14}$$

$$\begin{aligned} J_{\mathrm{S}}^{y}(t) = -2\frac{d}{dt}\mathrm{Tr}_{\mathrm{B}}\sum_{\zeta,m,j}(mL + d_{\gamma;\zeta,j})\times \\ \times \mathrm{Im}\big({}_{\gamma,j}\langle\zeta, m, j, \sigma' = +1|\hat{W}(t)|\zeta, m, j, \sigma = -1\rangle_{\gamma,j}\big), \end{aligned} \tag{5.15}$$

where we have explicitly written the trace over the bath degrees of freedom in order to work further with the σ-DVR matrix elements of the full statistical operator $\hat{W}(t)$.

It turns out that the case of a harmonic confinement allows one to formulate selection rules for the σ-DVR matrix elements of the full statistical operator. These selection rules are very useful for understanding some of the properties of the spin transport.

To find the selection rules mentioned above let us decompose the Hamiltonian $\hat{H}$ in (5.2) into

$$\hat{H} = \hat{H}_0 + \hat{H}_{\mathrm{R-Z}}, \tag{5.16}$$

where

$$\hat{H}_0 = \frac{\hbar^2\hat{\vec{k}}^2}{2m} + \frac{m\omega_0^2\hat{z}^2}{2} + U(\hat{x})\left(1 + \gamma\frac{\hat{z}^2}{L^2}\right), \tag{5.17}$$

$$\hat{H}_{\mathrm{R-Z}} = -\frac{\hbar^2 k_{\mathrm{so}}}{m}\big(\hat{\sigma}_x\hat{k}_z - \hat{\sigma}_z\hat{k}_x\big) - g\mu_{\mathrm{B}}\hat{\sigma}_z H_0 = -\frac{\hbar^2 k_{\mathrm{so}}}{m}\big(\hat{\sigma}_x\hat{k}_z - \hat{\sigma}_z\hat{k}'_x\big), \tag{5.18}$$

and $\hat{k}'_x = \hat{k}_x - g\mu_{\mathrm{B}}H_0 m/\hbar^2 k_{\mathrm{so}}$. The full statistical operator has the form $\hat{W}(t) = \hat{U}(t, t_0)\hat{W}(t_0)\hat{U}^\dagger(t, t_0)$, where the evolution operator $\hat{U}(t, t_0)$ is given as the time-ordered

exponent

$$\begin{aligned}\hat{U}(t,t_0) &= \mathrm{T}\exp\left[-\frac{\mathrm{i}}{\hbar}\int_{t_0}^{t} dt'\hat{H}_{\mathrm{full}}(t')\right]= \\ &= \sum_{n=0}^{\infty}\left(-\frac{\mathrm{i}}{\hbar}\right)^n\int_{t_0}^{t}dt_n\cdots\int_{t_0}^{t_2}dt_1\hat{H}_{\mathrm{full}}(t_n)\cdots\hat{H}_{\mathrm{full}}(t_1).\end{aligned} \tag{5.19}$$

Only the terms of $\hat{H}_{\mathrm{R-Z}}$ with odd powers contain the spin operators. These terms are linear in $\hat{\sigma}_x$ and $\hat{\sigma}_z$ or bilinear in these spin operators which is equivalent to being linear in $\hat{\sigma}_y$. Contributions to the matrix elements ${}_{\gamma,j}\langle\zeta,m,j,\sigma'=+1|\hat{W}(t)|\zeta,m,j,\sigma=-1\rangle_{\gamma,j}$ come from the first order terms in $\hat{\sigma}_x$. It is easy to see that these terms represent products of the factors $(\hat{H}_0+\hat{H}_{\mathrm{ext}}(t_k)+\hat{H}_{\mathrm{bath}})$ ordered chronologically (we mean the chronological ordering on the Keldysh contour [102] and thus operators from $\hat{U}^{\dagger}(t,t_0)$ are also included under this terminology), an odd number of factors $\hat{k}_z$ distributed in between $(\hat{H}_0+\hat{H}_{\mathrm{ext}}(t_k)+\hat{H}_{\mathrm{bath}})$ in all possible ways and a number (even or odd) of factors $\hat{k}'_x$ also distributed in between $(\hat{H}_0+\hat{H}_{\mathrm{ext}}(t_k)+\hat{H}_{\mathrm{bath}})$ in all possible ways. Such a structure is related to the fact that the Rashba-Zeeman Hamiltonian, $\hat{H}_{\mathrm{R-Z}}$, is bilinear in the operators $\hat{\sigma}_x$ and $\hat{k}_z$. To clarify our above statement we write down the third order term coming for example from $\hat{U}(t,t_0)$ (a similar result is obtained for products which are composed from different, $\hat{U}(t,t_0)$, $\hat{U}^{\dagger}(t,t_0)$ or $\hat{W}(t_0)$, parts of the full statistical operator):

$$\begin{aligned}&\hat{H}_{\mathrm{full}}(t_3)\hat{H}_{\mathrm{full}}(t_2)\hat{H}_{\mathrm{full}}(t_1)=\hat{H}^3_{\mathrm{R-Z}}+\hat{H}^2_{\mathrm{R-Z}}\big(\hat{H}_0+\\ &+\hat{H}_{\mathrm{ext}}(t_1)+\hat{H}_{\mathrm{bath}}\big)+\hat{H}_{\mathrm{R-Z}}\big(\hat{H}_0+\hat{H}_{\mathrm{ext}}(t_2)+\\ &+\hat{H}_{\mathrm{bath}}\big)\hat{H}_{\mathrm{R-Z}}+\hat{H}_{\mathrm{R-Z}}(\hat{H}_0+\hat{H}_{\mathrm{ext}}(t_2)+\hat{H}_{\mathrm{bath}}\big)\times\\ &\times(\hat{H}_0+\hat{H}_{\mathrm{ext}}(t_1)+\hat{H}_{\mathrm{bath}}\big)+(\hat{H}_0+\hat{H}_{\mathrm{ext}}(t_3)+\\ &+\hat{H}_{\mathrm{bath}}\big)\hat{H}^2_{\mathrm{R-Z}}+(\hat{H}_0+\hat{H}_{\mathrm{ext}}(t_3)+\hat{H}_{\mathrm{bath}}\big)\hat{H}_{\mathrm{R-Z}}\times\\ &\times(\hat{H}_0+\hat{H}_{\mathrm{ext}}(t_1)+\hat{H}_{\mathrm{bath}}\big)+(\hat{H}_0+\hat{H}_{\mathrm{ext}}(t_3)+\\ &+\hat{H}_{\mathrm{bath}}\big)(\hat{H}_0+\hat{H}_{\mathrm{ext}}(t_2)+\hat{H}_{\mathrm{bath}}\big)\hat{H}_{\mathrm{R-Z}}+(\hat{H}_0+\\ &+\hat{H}_{\mathrm{ext}}(t_3)+\hat{H}_{\mathrm{bath}}\big)(\hat{H}_0+\hat{H}_{\mathrm{ext}}(t_2)+\hat{H}_{\mathrm{bath}}\big)(\hat{H}_0+\\ &+\hat{H}_{\mathrm{ext}}(t_1)+\hat{H}_{\mathrm{bath}}\big).\end{aligned} \tag{5.20}$$

Since for a harmonic confinement all the factors $(\hat{H}_0+\hat{H}_{\mathrm{ext}}(t_k)+\hat{H}_{\mathrm{bath}})$ and $\hat{k}'_x$ couple states with indices j and j' only of identical parity and the factors $\hat{k}_z^{2m+1}$ couple states with indices j and j' only of opposite parity, we conclude that the matrix elements ${}_{\gamma,j}\langle\zeta,m,j,\sigma'=+1|\hat{W}(t)|\zeta,m,j,\sigma=-1\rangle_{\gamma,j}$, being diagonal in j, are equal to zero:

$${}_{\gamma,j}\langle\zeta,m,j,\sigma'=+1|\hat{W}(t)|\zeta,m,j,\sigma=-1\rangle_{\gamma,j}=0. \tag{5.21}$$

The selection rules (5.21) represent a specific property of systems with a harmonic confinement. From (5.14), (5.15) and (5.21) one gets

$$J_{\mathrm{S}}^{x,y}(t)=0. \tag{5.22}$$

In spite of the fact that this result is only valid for the case of a harmonic confinement it is still general in two respects: 1) it is valid not only for the stationary state but for all times $t \geqslant t_0$; 2) the external force $F(t)$ is arbitrary.

5.2.5 Ratchet transport: averaged charge and spin currents

We are interested in the long-time limit of the currents $\bar{J}_{\rm C}(t)$ and $\bar{J}_{\rm S}(t)$ averaged over the driving period $T = 2\pi/\Omega$ with the time average of a time dependent function $f(t)$ defined as $\bar{f}(t) \equiv (1/T)\int_t^{t+T} dt' f(t')$. From (5.12) it follows

$$\begin{aligned} \bar{J}_{\rm C}(t) &= -e\sum_{\alpha} x_\alpha \frac{d}{dt}\bar{P}_\alpha(t), \\ \bar{J}_{\rm S}(t) &= \sum_{\alpha} \sigma_\alpha x_\alpha \frac{d}{dt}\bar{P}_\alpha(t). \end{aligned} \tag{5.23}$$

The advantage of working in the σ-DVR basis is that real-time path integral techniques can be used to exactly trace out the bath degrees of freedom [31,38]. Moreover, at driving frequencies larger than the ones characterizing the internal dynamics of the quasi-1D system coupled to the bath, the averaged populations $\bar{P}_\alpha(t)$ can be found from the master equation having the form (1.37),

$$\frac{d}{dt}\bar{P}_\alpha(t) = \sum_{\substack{\beta \\ (\beta\neq\alpha)}} \bar{\Gamma}_{\alpha\beta}\bar{P}_\beta(t) - \sum_{\substack{\beta \\ (\beta\neq\alpha)}} \bar{\Gamma}_{\beta\alpha}\bar{P}_\alpha(t), \tag{5.24}$$

valid at long times. In Eq. (5.24) $\bar{\Gamma}_{\alpha\beta}$ is an averaged transition rate from the state $|\beta\rangle$ to the state $|\alpha\rangle$. In order to obtain concrete expressions for the averaged currents one needs explicit expressions for these σ-DVR transition rates. This is the subject of the next subsection.

5.2.6 Transition Rates

The tight-binding model introduced in Section 4.5 relies upon the fact that the hopping matrix elements (4.30) are small. In this case the second-order approximation, Eq. (1.38), for the averaged transition rates in Eq. (5.24) can be used. In the present context Eq. (1.38) takes the form,

$$\begin{aligned} \bar{\Gamma}^{m',m}_{\gamma;\xi',\xi} = \frac{|\Delta^{m',m}_{\gamma;\xi',\xi}|^2}{\hbar^2}\int_{-\infty}^{\infty} d\tau \mathrm{e}^{-[(x_{\gamma;m,\xi}-x_{\gamma;m',\xi'})^2/\hbar]Q(\tau)+\mathrm{i}[(\varepsilon_{\gamma;\xi}-\varepsilon_{\gamma;\xi'})/\hbar]\tau}\times \\ \times J_0\left[\frac{2F(x_{\gamma;m,\xi}-x_{\gamma;m',\xi'})}{\hbar\Omega}\sin\left(\frac{\Omega\tau}{2}\right)\right], \end{aligned} \tag{5.25}$$

where $x_{\gamma;m,\xi} \equiv x_{\gamma;\zeta=1,m,\xi} = mL + d_{\gamma;\xi}$ with $d_{\gamma;\xi} \equiv d_{\gamma;1,j}$, $\Delta^{m',m}_{\gamma;\xi',\xi} \equiv {}_{\gamma,\xi'}\langle m',\xi'|\hat{H}|m,\xi\rangle_{\gamma,\xi}$ the hopping matrix element between the states $|m',\xi'\rangle_{\gamma,\xi'}$ and $|m,\xi\rangle_{\gamma,\xi}$.

The transition rates are functions of the orbit-orbit coupling strength γ because the Bloch amplitudes as well as the difference $\Delta d_\gamma \equiv d_{\gamma;1,0} - d_{\gamma;1,1}$ depend on γ. Within the context of the tight-binding model the eigenvalues $d_{\gamma;1,0}$ and $d_{\gamma;1,1}$ tend to zero and fulfil $\Delta d_\gamma / l_\mathrm{r} \ll 1$, where $l_\mathrm{r} = \min[L, \sqrt{\hbar/m\omega_0}, \hbar\Omega/F, \ldots]$. Consequently, the transition rates depend on γ predominantly through the Bloch amplitudes, and in this work we pay no regard to terms of order $\mathcal{O}(\Delta d_\gamma / l_\mathrm{r})$. This is also consistent with our model taking into account only the first two transverse modes. Keeping terms of order $\mathcal{O}(\Delta d_\gamma / l_\mathrm{r})$ would mean that the strength γ of the orbit-orbit coupling is large enough so that one would need to consider more than just the first two transverse modes because in this case the non-diagonal elements would be comparable with the diagonal ones.

Using the notations,

$$\begin{aligned} \bar{\Gamma}^{m,m}_{\gamma;\xi',\xi} &\equiv \bar{\Gamma}^{\mathrm{intra}}_{\gamma;\xi',\xi}, \quad \xi' \neq \xi, \\ \bar{\Gamma}^{m,m+1}_{\gamma;\xi',\xi} &\equiv \bar{\Gamma}^{\mathrm{inter,b}}_{\gamma;\xi',\xi}, \\ \bar{\Gamma}^{m+1,m}_{\gamma;\xi',\xi} &\equiv \bar{\Gamma}^{\mathrm{inter,f}}_{\gamma;\xi',\xi}, \end{aligned} \tag{5.26}$$

from (5.25) one obtains

$$\bar{\Gamma}^{\mathrm{intra}}_{\gamma;\xi',\xi} = 0, \tag{5.27}$$

and

$$\begin{aligned} \bar{\Gamma}^{\mathrm{inter,b}}_{\gamma;\xi',\xi} &= |\Delta^{\mathrm{inter,b}}_{\gamma;\xi',\xi}(m)|^2 J_{\gamma;\xi',\xi}, \\ \bar{\Gamma}^{\mathrm{inter,f}}_{\gamma;\xi',\xi} &= |\Delta^{\mathrm{inter,f}}_{\gamma;\xi',\xi}(m)|^2 J_{\gamma;\xi',\xi}, \end{aligned} \tag{5.28}$$

where

$$J_{\gamma;\xi',\xi} = \frac{1}{\hbar^2} \int_{-\infty}^{\infty} d\tau \mathrm{e}^{-\frac{L^2}{\hbar} Q(\tau) + \mathrm{i}[(\varepsilon_{\gamma;\xi} - \varepsilon_{\gamma;\xi'})/\hbar]\tau} J_0 \left[\frac{2FL}{\hbar\Omega} \sin\left(\frac{\Omega\tau}{2} \right) \right]. \tag{5.29}$$

Note that $\bar{\Gamma}^{\mathrm{inter,b}}_{\gamma;\xi',\xi}$ and $\bar{\Gamma}^{\mathrm{inter,f}}_{\gamma;\xi',\xi}$ do not depend on m due to the Bloch theorem which leads to an m-dependence of $\Delta^{\mathrm{inter,b}}_{\gamma;\xi',\xi}(m)$ and $\Delta^{\mathrm{inter,f}}_{\gamma;\xi',\xi}(m)$ only through a phase factor as it is shown in Subsection 4.5.3. From (4.32) and (5.28) it follows that

$$\bar{\Gamma}^{\mathrm{inter,b}}_{\gamma;\xi,\xi} = \bar{\Gamma}^{\mathrm{inter,f}}_{\gamma;\xi,\xi}, \tag{5.30}$$

$$\bar{\Gamma}^{\mathrm{inter,b}}_{\gamma;\xi',\xi} \bar{\Gamma}^{\mathrm{inter,b}}_{\gamma;\xi,\xi'} = \bar{\Gamma}^{\mathrm{inter,f}}_{\gamma;\xi',\xi} \bar{\Gamma}^{\mathrm{inter,f}}_{\gamma;\xi,\xi'}. \tag{5.31}$$

To calculate the charge and spin currents we additionally need the transition rates

$$\bar{\Gamma}_{\gamma;\xi,\xi'} \equiv \bar{\Gamma}^{\mathrm{inter,f}}_{\gamma;\xi,\xi'} + \bar{\Gamma}^{\mathrm{intra}}_{\gamma;\xi,\xi'} + \bar{\Gamma}^{\mathrm{inter,b}}_{\gamma;\xi,\xi'}. \tag{5.32}$$

As pointed out at the end of Subsection 4.5.2, the system is split into two subsystems isolated from each other. Since electron exchange between the subsystems is absent one can write

$$\bar{\Gamma}_{\gamma;1,2} = \bar{\Gamma}_{\gamma;1,3} = \bar{\Gamma}_{\gamma;2,1} = \bar{\Gamma}_{\gamma;2,4} = \bar{\Gamma}_{\gamma;3,1} = \bar{\Gamma}_{\gamma;3,4} = \bar{\Gamma}_{\gamma;4,2} = \bar{\Gamma}_{\gamma;4,3} = 0. \tag{5.33}$$

The last equalities are very useful because they allow us to significantly simplify the expressions for the charge and spin currents which are derived in the next section.

5.2.7 Calculation of the charge and spin ratchet currents

The expressions for the stationary averaged charge and spin currents,

$$\bar{J}_{\mathrm{C}}^{\infty} \equiv \lim_{t\to\infty} \bar{J}_{\mathrm{C}}(t), \quad \bar{J}_{\mathrm{S}}^{\infty} \equiv \lim_{t\to\infty} \bar{J}_{\mathrm{S}}(t), \tag{5.34}$$

can be found from the averaged master equation (5.24) which we rewrite here using the explicit form of the σ-DVR indices and tight-binding approximation derived in Subsection 4.5.2 and utilizing the notations of Subsection 5.2.6 for the transition rates:

$$\begin{aligned}
\frac{d}{dt}\bar{P}^{m}_{\gamma;\xi}(t) = &\sum_{\substack{\xi'=1\\(\xi'\neq\xi)}}^{4} \left[\bar{\Gamma}^{\mathrm{inter,f}}_{\gamma;\xi,\xi'}\bar{P}^{m-1}_{\gamma;\xi'}(t) + \bar{\Gamma}^{\mathrm{intra}}_{\gamma;\xi,\xi'}\bar{P}^{m}_{\gamma;\xi'}(t) + \bar{\Gamma}^{\mathrm{inter,b}}_{\gamma;\xi,\xi'}\bar{P}^{m+1}_{\gamma;\xi'}(t)\right] - \\
- &\sum_{\substack{\xi'=1\\(\xi'\neq\xi)}}^{4} \left[\bar{\Gamma}^{\mathrm{inter,b}}_{\gamma;\xi',\xi} + \bar{\Gamma}^{\mathrm{intra}}_{\gamma;\xi',\xi} + \bar{\Gamma}^{\mathrm{inter,f}}_{\gamma;\xi',\xi}\right]\bar{P}^{m}_{\gamma;\xi}(t) + \left[\bar{\Gamma}^{\mathrm{inter,f}}_{\gamma;\xi,\xi}\bar{P}^{m-1}_{\gamma;\xi}(t) + \bar{\Gamma}^{\mathrm{inter,b}}_{\gamma;\xi,\xi}\bar{P}^{m+1}_{\gamma;\xi}(t)\right] - \\
- &\left[\bar{\Gamma}^{\mathrm{inter,b}}_{\gamma;\xi,\xi} + \bar{\Gamma}^{\mathrm{inter,f}}_{\gamma;\xi,\xi}\right]\bar{P}^{m}_{\gamma;\xi}(t).
\end{aligned} \tag{5.35}$$

From (5.12) and (5.35) one finds

$$\bar{J}_{\mathrm{C}}^{\infty} = -eL\sum_{\xi,\xi'=1}^{4}\left[\bar{\Gamma}^{\mathrm{inter,f}}_{\gamma;\xi,\xi'} - \bar{\Gamma}^{\mathrm{inter,b}}_{\gamma;\xi,\xi'}\right]p^{\infty}_{\gamma;\xi'}, \tag{5.36}$$

$$\bar{J}_{\mathrm{S}}^{\infty} = \sum_{\xi,\xi'=1}^{4}\left[\left(d_{\gamma;\xi}\sigma_{\xi} - d_{\gamma;\xi'}\sigma_{\xi'}\right)\left(\bar{\Gamma}^{\mathrm{inter,f}}_{\gamma;\xi,\xi'} + \bar{\Gamma}^{\mathrm{inter,b}}_{\gamma;\xi,\xi'}\right) + L\sigma_{\xi}\left(\bar{\Gamma}^{\mathrm{inter,f}}_{\gamma;\xi,\xi'} - \bar{\Gamma}^{\mathrm{inter,b}}_{\gamma;\xi,\xi'}\right)\right]p^{\infty}_{\gamma;\xi'}, \tag{5.37}$$

where we have used Eq. (4.21). To derive Eq. (5.37) we have additionally made use of Eq. (5.27). In Eq. (5.37) $\sigma_{\xi} \equiv \sigma_{\zeta=1,m,\xi}$ and $\sigma_1 = \sigma_3 = 1,\ \sigma_2 = \sigma_4 = -1$ as it follows from Eq. (4.33). The quantities $p^{\infty}_{\gamma;\xi}$ are defined as

$$p_{\gamma;\xi}(t) \equiv \sum_{m}\bar{P}^{m}_{\gamma;\xi}(t), \quad p^{\infty}_{\gamma;\xi} \equiv \lim_{t\to\infty} p_{\gamma;\xi}(t), \tag{5.38}$$

and they satisfy the constraint

$$p_{\gamma;1}(t) + p_{\gamma;2}(t) + p_{\gamma;3}(t) + p_{\gamma;4}(t) = 1, \quad \forall\ t. \tag{5.39}$$

As already mentioned at the end of Subsection 4.5.2, we only consider the subsystem with $\xi = 1, 4$. The properties of the stationary averaged transport do not depend on initial conditions. We choose the following ones:

$$p_{\gamma;1}(t=0) = 1, \quad p_{\gamma;4}(t=0) = 0. \tag{5.40}$$

Because of the constraint (5.39) $p_{\gamma;2}(t=0) = p_{\gamma;3}(t=0) = 0$ and since there is no electron exchange between the subsystems, the states of the subsystem with $\xi = 2, 3$

remain empty at any time, $p_{\gamma;2}(t) = p_{\gamma;3}(t) = 0,\ \forall t$. This leads to $p^{\infty}_{\gamma;2} = p^{\infty}_{\gamma;3} = 0$. Then from the master equation (5.35) with the initial conditions (5.40) and using (5.32), (5.33) one obtains

$$p^{\infty}_{\gamma;1} = \frac{\bar{\Gamma}_{\gamma;1,4}}{\bar{\Gamma}_{\gamma;1,4} + \bar{\Gamma}_{\gamma;4,1}}, \quad p^{\infty}_{\gamma;4} = \frac{\bar{\Gamma}_{\gamma;4,1}}{\bar{\Gamma}_{\gamma;1,4} + \bar{\Gamma}_{\gamma;4,1}}. \tag{5.41}$$

Using Eqs. (5.27), (5.30)-(5.32) and (5.41) it follows from (5.36)

$$\bar{J}^{\infty}_{\mathrm{C}} = 0, \tag{5.42}$$

that is the absence of the stationary averaged charge transport. Note, however, that we cannot assert that upon taking into account terms of higher order in $\Delta d_{\gamma}/l_{\mathrm{r}}$ the charge ratchet current remains zero. Using Eqs. (5.27), (5.30), (5.32) and (5.41) we get from Eq. (5.37)

$$\bar{J}^{\infty}_{\mathrm{S}} = \frac{2L}{\bar{\Gamma}_{\gamma;1,4} + \bar{\Gamma}_{\gamma;4,1}} \big(\bar{\Gamma}^{\mathrm{inter,f}}_{\gamma;1,4}\bar{\Gamma}^{\mathrm{inter,b}}_{\gamma;4,1} - \bar{\Gamma}^{\mathrm{inter,b}}_{\gamma;1,4}\bar{\Gamma}^{\mathrm{inter,f}}_{\gamma;4,1}\big). \tag{5.43}$$

The last expression can be rewritten in terms of the hopping matrix elements $\Delta^{\mathrm{inter,f}}_{\gamma;\xi',\xi}(m)$. Making use of Eqs. (4.32), (5.27), (5.28) and (5.32) we derive the stationary averaged spin current:

$$\bar{J}^{\infty}_{\mathrm{S}} = 2L \frac{J_{\gamma;1,4}J_{\gamma;4,1}}{J_{\gamma;1,4} + J_{\gamma;4,1}} \big(|\Delta^{\mathrm{inter,f}}_{\gamma;1,4}(m)|^2 - |\Delta^{\mathrm{inter,f}}_{\gamma;4,1}(m)|^2\big). \tag{5.44}$$

Using Eqs. (5.44) and (4.36) the non-equilibrium stationary averaged spin current can be written as

$$\begin{aligned} \bar{J}^{\infty}_{\mathrm{n-e,S}} = -2\bigg(\frac{J_{\gamma;1,4}J_{\gamma;4,1}}{J_{\gamma;1,4} + J_{\gamma;4,1}} - \frac{J^{(0)}_{\gamma;1,4}J^{(0)}_{\gamma;4,1}}{J^{(0)}_{\gamma;1,4} + J^{(0)}_{\gamma;4,1}}\bigg) \times \\ \times \frac{L\hbar^3 k^2_{\mathrm{so}}\omega_0}{m} \sum_{k_{\mathrm{B}},k'_{\mathrm{B}}} \sin[(k_{\mathrm{B}} - k'_{\mathrm{B}})L]\,\mathrm{Im}[F_{\gamma;k_{\mathrm{B}},k'_{\mathrm{B}}}], \end{aligned} \tag{5.45}$$

where $J^{(0)}_{\gamma;\xi',\xi}$ is given by Eq. (5.29) with $F = 0$ and the function $F_{\gamma;k_{\mathrm{B}},k'_{\mathrm{B}}}$ is defined by Eq. (4.37). Note the structure of Eq. (5.45). It is the product of two factors of different physical origin. The factor in the second line describes the isolated system and the one in the first line is purely due to the dissipative coupling to an external environment. To get Eq. (5.45) we have eliminated from $\bar{J}^{\infty}_{\mathrm{S}}$ the equilibrium spin current arising due to the non-compensation [57] of the spin currents from different bands of the Rashba-Bloch spectrum of the isolated system. It turns out that this effect is strong enough to indenture in a dissipative system. Below we only consider the non-equilibrium spin current, $\bar{J}^{\infty}_{\mathrm{n-e,S}}$, and not the full one, $\bar{J}^{\infty}_{\mathrm{S}}$.

Let us at this point also mention the dependence of the spin current $\bar{J}^{\infty}_{\mathrm{n-e,S}}$ on the magnetic field H_0. Since the magnetic field is applied along the z-axis, it couples to the

system through the $\hat{\sigma}_z$ operator and thus the hopping matrix elements $\Delta^{\mathrm{inter,f}}_{\gamma;1(4),4(1)}(m)$ do not depend on H_0. It then follows that the spin current depends on the magnetic field only through its dissipative prefactor. The dependence on H_0 comes into play through the on-site energies $\varepsilon_{\gamma;1(4)}$. The difference $\varepsilon_{\gamma;4} - \varepsilon_{\gamma;1}$ which enters the integrals $J_{\gamma;1(4),4(1)}$ and $J^{(0)}_{\gamma;1(4),4(1))}$ can be written as:

$$\varepsilon_{\gamma;4} - \varepsilon_{\gamma;1} = \frac{1}{N}\sum_{k_{\mathrm{B}}}\left[\varepsilon^{(0)}_{\gamma,1;1}(k_{\mathrm{B}}) - \varepsilon^{(0)}_{\gamma,0;1}(k_{\mathrm{B}})\right] + \hbar\omega_0 + 2g\mu_{\mathrm{B}}H_0, \tag{5.46}$$

where N is the number of the elementary cells and $\varepsilon^{(0)}_{\gamma,j;l}(k_{\mathrm{B}})$ are the eigenvalues of the truly 1D Hamiltonian

$$\hat{H}^{\mathrm{1D}}_{0;\gamma,j} \equiv \frac{\hbar^2\hat{k}_x^2}{2m} + U(\hat{x})\left[1 + \gamma\frac{\hbar}{m\omega_0 L^2}\left(j + \frac{1}{2}\right)\right]. \tag{5.47}$$

Since the existence of the spin ratchet mechanism is dictated by the difference $|\Delta^{\mathrm{inter,f}}_{\gamma;1,4}(m)|^2 - |\Delta^{\mathrm{inter,f}}_{\gamma;4,1}(m)|^2$, in the presence of a transverse in-plane uniform stationary magnetic field the existence of the spin current is possible under the same conditions as without this field. For completeness we list these conditions below.

From (5.45) one finds, as mentioned in Subsection 5.2.4, that when the electronic states become localized, the stationary averaged spin current vanishes. Indeed, in this insulating limit the function $F_{\gamma;k_{\mathrm{B}},k'_{\mathrm{B}}}$ does not depend on the quasi-momenta k_{B} and k'_{B} and Eq. (5.45) gives zero.

5.2.8 Role of the spin current definition

Here we would like to discuss the difference between the conventional spin current definition based on the spin current operator (1.47) and the definition of the spin current used in our work, that is the definition based on the spin current operator (1.55). We will consider the z-polarized components of the spin currents obtained from the two definitions. The conventional spin current operator and the conventional spin current will be denoted as $\hat{J}^{\mathrm{conv}}_{\mathrm{S}}(t)$ and $J^{\mathrm{conv}}_{\mathrm{S}}(t)$, respectively. The spin current operator and the spin current which are used in our work will be denoted as $\hat{J}_{\mathrm{S}}(t)$ and $J_{\mathrm{S}}(t)$, respectively.

The two definitions and the difference between them are

$$\begin{aligned} J_{\mathrm{S}}(t) &= \frac{d}{dt}(\hat{\sigma}_z\hat{x}), \quad J^{\mathrm{conv}}_{\mathrm{S}}(t) = \hat{\sigma}_z\frac{d\hat{x}}{dt}, \\ J_{\mathrm{S}}(t) - J^{\mathrm{conv}}_{\mathrm{S}}(t) &= \frac{d\hat{\sigma}_z}{dt}\hat{x}. \end{aligned} \tag{5.48}$$

One easily finds that

$$\frac{d\hat{\sigma}_z}{dt} = -\frac{2\hbar k_{\mathrm{so}}}{m}\hat{\sigma}_y\hat{k}_z. \tag{5.49}$$

Thus the relation between the spin currents is

$$\begin{aligned} J_{\mathrm{S}}^{\mathrm{conv}}(t) &= J_{\mathrm{S}}(t) + \mathrm{i}\frac{2\hbar k_{\mathrm{so}}}{m}\mathrm{Tr}_{\mathrm{B}}\sum_{\zeta,m,j}(mL + d_{\gamma;\zeta,j})\times \\ &\times \big({}_{\gamma,j}\langle\zeta,m,j,\sigma'=+1|\hat{k}_z\hat{W}(t)|\zeta,m,j,\sigma=-1\rangle_{\gamma,j} - \\ &- {}_{\gamma,j}\langle\zeta,m,j,\sigma'=-1|\hat{k}_z\hat{W}(t)|\zeta,m,j,\sigma=+1\rangle_{\gamma,j}\big). \end{aligned} \tag{5.50}$$

The second term in Eq. (5.50) can be finite for our system. To show this we consider the product $\hat{H}_{\mathrm{full}}(t_3)\hat{H}_{\mathrm{full}}(t_2)\hat{H}_{\mathrm{full}}(t_1)$ in Eq. (5.20). This product contains for example the term $\hat{H}^3$ where $\hat{H}$ is given by Eq. (5.16). We can write this term as

$$\begin{aligned} \hat{H}^3 &= \hat{H}_0^3 + \left(\frac{\hbar^2 k_{\mathrm{so}}}{m}\right)^2 \hat{H}_0\hat{\vec{k}}^2 - \frac{\hbar^2 k_{\mathrm{so}}}{m}\big[\hat{H}_0^2(\hat{\sigma}_x\hat{k}_z - \\ &- \hat{\sigma}_z\hat{k}'_x) + \hat{H}_0(\hat{\sigma}_x\hat{k}_z - \hat{\sigma}_z\hat{k}'_x)\hat{H}_0\big] - \frac{\hbar^2 k_{\mathrm{so}}}{m}(\hat{\sigma}_x\hat{k}_z - \\ &- \hat{\sigma}_z\hat{k}'_x)\hat{H}_0^2 - \left(\frac{\hbar^2 k_{\mathrm{so}}}{m}\right)^3(\hat{\sigma}_x\hat{k}_z - \hat{\sigma}_z\hat{k}'_x)\hat{\vec{k}}^2 + \\ &+ \left(\frac{\hbar^2 k_{\mathrm{so}}}{m}\right)^2\big[\hat{k}_z\hat{H}_0\hat{k}_z + \hat{k}'_x\hat{H}_0\hat{k}'_x + \mathrm{i}\hat{\sigma}_y(\hat{k}_z\hat{H}_0\hat{k}'_x - \\ &- \hat{k}'_x\hat{H}_0\hat{k}_z) + \hat{\vec{k}}^2\hat{H}_0^2\big]. \end{aligned} \tag{5.51}$$

From Eq. (5.51) we see that the operator $\hat{k}_z\hat{W}(t)$ has terms like

$$\mathrm{i}\left(\frac{\hbar^2 k_{\mathrm{so}}}{m}\right)^2\hat{k}_z\hat{\sigma}_y(\hat{k}_z\hat{H}_0\hat{k}'_x - \hat{k}'_x\hat{H}_0\hat{k}_z), \tag{5.52}$$

which are even with respect to $\hat{k}_z$ and odd with respect to $\hat{\sigma}_y$. Therefore, in general we have

$$\begin{aligned} &{}_{\gamma,j}\langle\zeta,m,j,\sigma'=+1|\hat{k}_z\hat{W}(t)|\zeta,m,j,\sigma=-1\rangle_{\gamma,j} - \\ &- {}_{\gamma,j}\langle\zeta,m,j,\sigma'=-1|\hat{k}_z\hat{W}(t)|\zeta,m,j,\sigma=+1\rangle_{\gamma,j} \neq 0, \end{aligned} \tag{5.53}$$

which means that the two spin current definitions are different in our problem. The physical reason for this can be understood from Eq. (5.52). The term given by Eq. (5.52) is finite since $\hat{k}'_x$ and $\hat{k}_z$ do not commute with $\hat{H}_0$. It happens because of the presence of both the periodic potential and the confinement as it is obvious from Eq. (5.17). Thus we conclude that unlike free Rashba electrons the two definitions of the spin current are not equivalent for Rashba-Bloch electrons with a transverse confinement.

As one can see from Eqs. (5.23), (5.25) and (5.35) in the insulating limit $\bar{J}_{\mathrm{S}}(t) \to 0$. This is just a consequence of the fact that the spin current definition which we use represents a full derivative. It is quite reasonable from the physical point of view that the spin ratchet effect being a transport phenomenon is absent in insulators. However,

the conventional definition of the spin current is not a full derivative. The spin current $J_{\mathrm{S}}^{\mathrm{conv}}(t)$ differs from the spin current $J_{\mathrm{S}}(t)$ by the second term in Eq. (5.50). There is not any general physical reason for this term, averaged over one driving period, to vanish in the insulating limit at long times because it is not proportional to the time derivative of the averaged populations of the states but it is proportional to the averaged non-diagonal (in the spin and transverse mode subspaces) elements of the reduced statistical operator. These averaged non-diagonal elements can in general be finite in insulators. The spin ratchet effect obtained from the conventional definition of the spin current could then take place in insulators which would be unphysical.

5.2.9 Spin ratchet effect: analytical analysis

Let us analyze the existence of the spin ratchet mechanism.

When the spin-orbit interaction is absent, that is $k_{\mathrm{so}} = 0$, we get from (5.45)

$$\bar{J}^{\infty}_{\mathrm{n-e,S}}\big|_{k_{\mathrm{so}}=0} = 0. \tag{5.54}$$

Further, if the orbital degrees of freedom x and z are not coupled, that is $\gamma = 0$, it follows from Eqs. (5.45) and (4.40) that

$$\bar{J}^{\infty}_{\mathrm{n-e,S}}\big|_{\gamma=0} = 0. \tag{5.55}$$

Finally, if the periodic potential is symmetric, the Bloch amplitudes are real and we find from Eqs. (5.45) and (4.38)

$$\bar{J}^{\infty}_{\mathrm{n-e,S}} = 0, \quad \textit{for symmetric periodic potentials.} \tag{5.56}$$

Summarizing the above results we conclude that in order to generate a finite stationary averaged spin current three conditions must simultaneously be fulfilled: 1) presence of the spin-orbit interaction in the isolated system; 2) finite coupling between the orbital degrees of freedom x and z; 3) absence of the real space inversion center in the isolated system.

Among these three conditions the second condition is perhaps less transparent and a simplified physical interpretation is necessary. We propose the following physical explanation. The orbit-orbit coupling leads to the situation in which the strength of the periodic potential varies across the quasi-1D wire. The periodic potential is equal to $U(x)$ in the center of the wire and gets stronger closer to its edges. Thus the electron group velocity is larger in the central region of the wire and decreases closer to the edges. At the same time the electron distribution across the channel depends on the transverse mode j. It is given by the Hermite polynomials. For $j = 0$ the electrons populate the center of the wire while for $j = 1$ they are distributed in regions closer to the edges. Hence, the electrons with $j = 0$ are faster than those with $j = 1$. Because of the mixing between the confinement and RSOI different transverse modes carry different spin states. Therefore, we conclude that different spin states have different group velocities along the wire. This difference results in a finite longitudinal spin current.

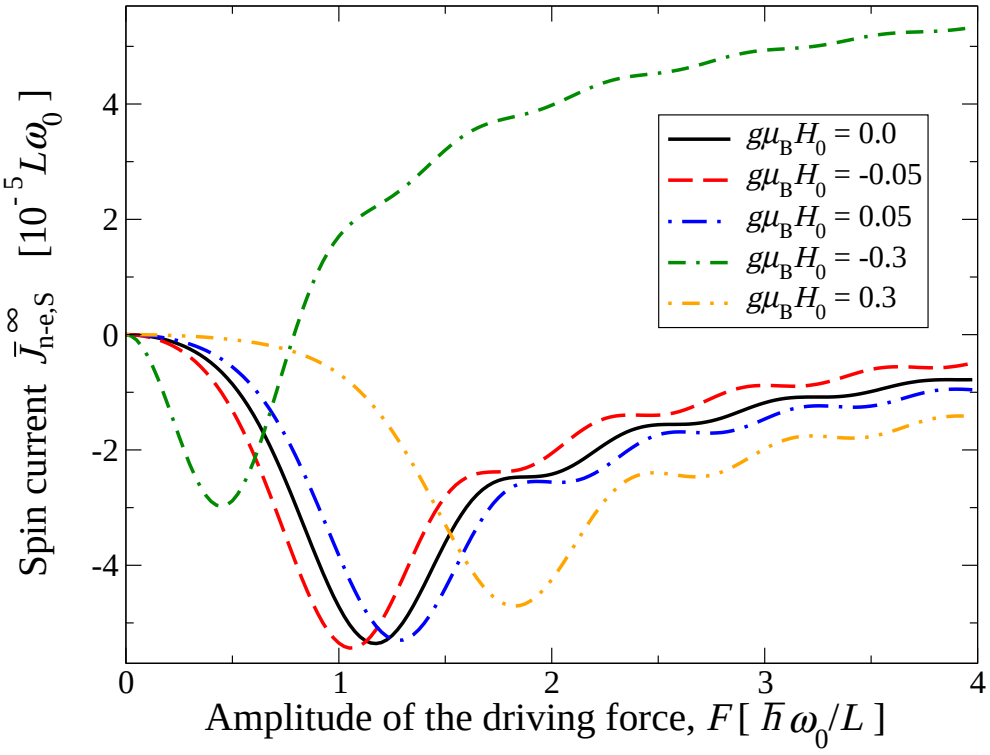

Figure 5.1: Non-equilibrium spin current, $\bar{J}^{\infty}_{\text{n-e,S}}$, as a function of the amplitude, F, of the driving force for different values of the z-projection of the magnetic field H_0. Further parameters: temperature $k_{\text{Boltz.}}T = 0.5$, spin-orbit coupling strength k_{so} with $k_{\text{so}}L = \pi/2$, orbit-orbit coupling strength $\gamma = 0.08$, driving frequency $\Omega = 0.2$, viscosity coefficient $\eta = 0.08$.

Finally, one observes that a transverse in-plane uniform stationary magnetic field alone is not enough to produce the spin current in a driven dissipative system. The magnetic field can only affect the magnitude of the spin current when the properties of the isolated system meet the three conditions derived above.

5.2.10 Spin ratchet effect: numerical analysis

In this section we show some results obtained numerically for the theoretical model developed in the previous sections. As an example we consider an InGaAs/InP quantum wire structure. The values of the corresponding parameters used to get the results are similar to the ones from Ref. [103]. In particular, $\hbar\omega_0 = 0.225$ meV, $\alpha \equiv \hbar^2 k_{\text{so}}/m = 9.94 \times 10^{-12}$ eV·m (which gives $k_{\text{so}} = 4.82 \times 10^6$ m^{-1}), $m = 0.037 m_0$ (m_0 is the free-electron mass). The value, $g = 7.5$, of the electron spin g-factor (in our notations $g \equiv -g^*/2$, where g^* is the effective gyroscopic factor measured experimentally) is taken from Ref. [104]. From these parameters and for example for the period of the super-lattice $L = 2.5\sqrt{\hbar/m\omega_0} \approx 0.24$ μm, which is easily achievable technologically at present [105], it follows that $k_{\text{so}}L \approx 0.368\pi$.

The asymmetric periodic potential is

$$U(x) = \hbar\omega_0 \left\{ 2.6 \left[1 - \cos\left(\frac{2\pi x}{L} - 1.9 \right) \right] + 1.9 \cos\left(\frac{4\pi x}{L} \right) \right\}. \tag{5.57}$$

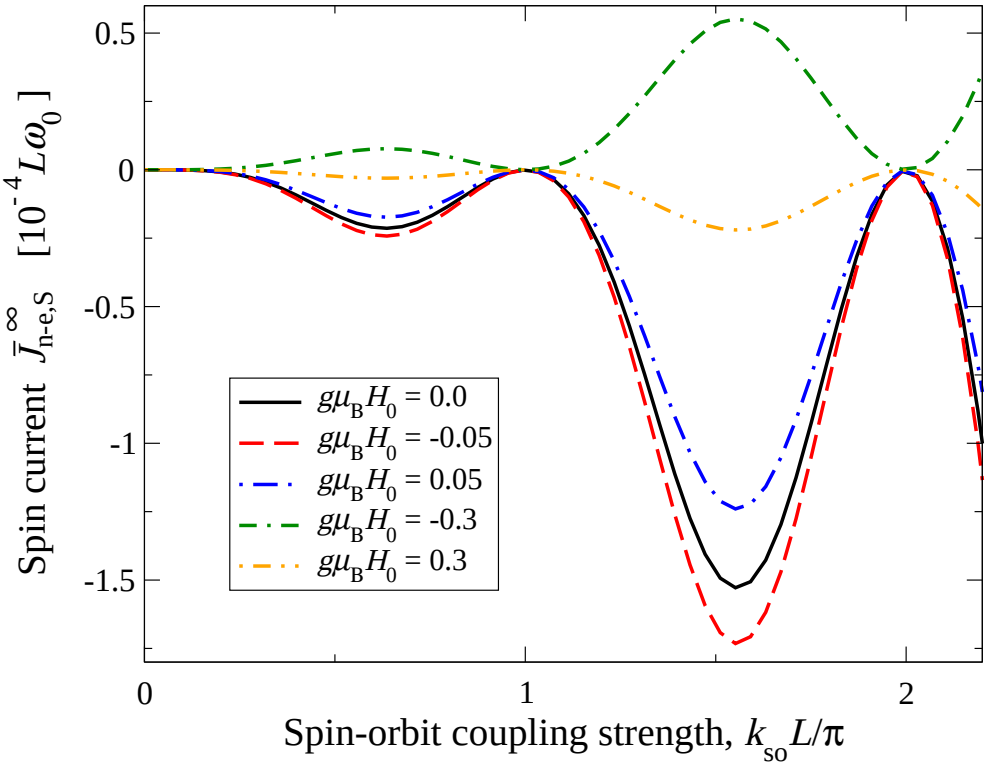

Figure 5.2: Non-equilibrium spin current, $\bar{J}^{\infty}_{\text{n-e,S}}$, as a function of the spin-orbit coupling strength, k_{so}, for different values of the z-projection of the magnetic field H_0. The driving amplitude is $F = 1.0\,\hbar\omega_0/L$. The other parameters are as in Fig. 5.1.

The bath is assumed to be Ohmic with exponential cutoff, *i.e.*, we use the spectral density (1.9),

$$J(\omega) = \eta\omega \exp\left(-\frac{\omega}{\omega_c}\right),$$

We remind (see Subsection 1.1.3) that η is the viscosity coefficient and ω_c is the cutoff frequency. For the the numerical analysis $\omega_c = 10\,\omega_0$ is used throughout this subsection.

To present the results we use in all the figures the units of $\hbar\omega_0$ and ω_0 for energies and frequencies, respectively. The viscosity coefficient is taken in units of $m\omega_0$.

Let us discuss possible values of the driving parameters. In a dissipationless system (or in a system with weak dissipation) of size L one should restrict possible values of the driving amplitude and frequency, $0 < FL < \hbar\omega_0$ and $0 < \Omega < \omega_0$, in order to stay within the validity of the model with the first two transverse modes opened. In a strongly dissipative system, as in our case, it is not necessary to fulfil the last inequalities because an electron loses a huge amount of its energy due to intensive dissipative processes. In general, our model of a driven strongly dissipative system taking into account the first four Bloch sub-bands remains valid if at long times the electron energy averaged over one period of the driving force, $\epsilon_{av}(F, \Omega, \eta)$ (which is a function of the driving and dissipation parameters), is smaller than $\hbar\omega_0$, $\epsilon_{av}(F, \Omega, \eta) < \hbar\omega_0$. This can take place even if $FL > \hbar\omega_0$ and $\Omega > \omega_0$ because even at such driving the strong dissipation (large values of η) will consume major amount of the electron

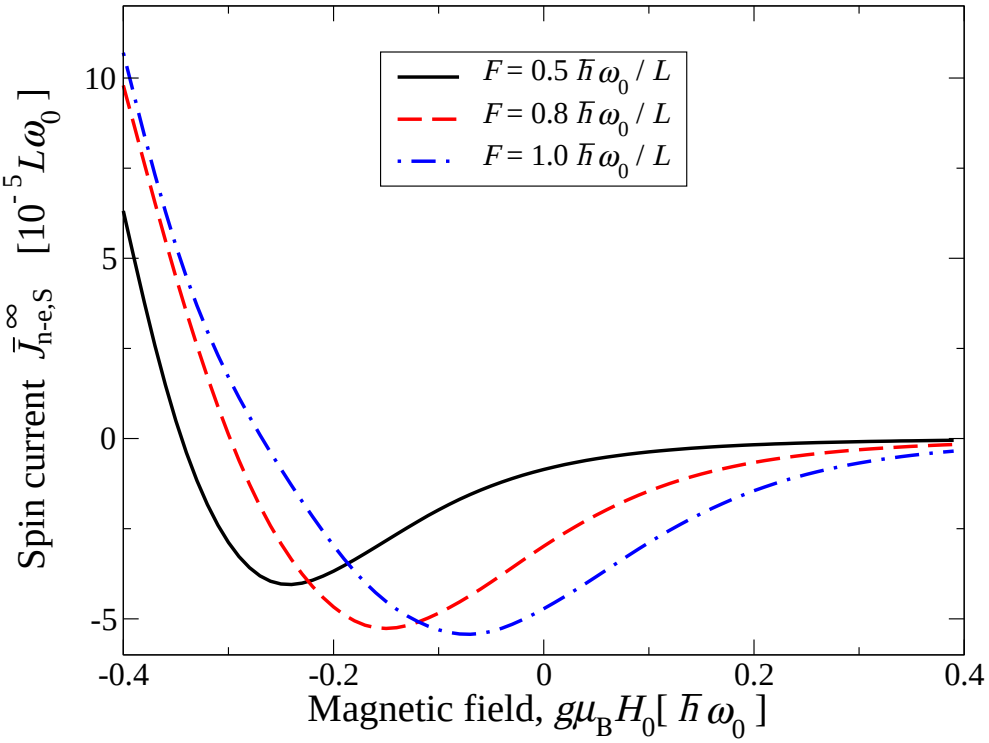

Figure 5.3: Non-equilibrium spin current, $\bar{J}^{\infty}_{\mathrm{n-e,S}}$, as a function of the magnetic field, $g\mu_{\mathrm{B}}H_0$, for different values of the amplitude of the driving force, F. The other parameters are as in Fig. 5.1.

energy.

In Fig. 5.1 the non-equilibrium spin current as a function of the amplitude of the external driving is shown for different values of the z-projection of the magnetic field. For small values of the driving amplitude and small magnetic fields it is seen that if the magnetic field has the same direction as the z-axis, the spin current decreases, while the opposite direction of the magnetic field amplifies the spin current. This behavior can be physically understood from Eq. (5.46). Positive values of H_0 can be equivalently considered as larger values of $\hbar\omega_0$, that is of the distance between the transverse modes. This in turn leads to a decrease of the transition probabilities which suppresses the spin current. On the contrary, negative values of H_0 correspond to smaller values of $\hbar\omega_0$ leading to an increase of the transition rates and thus the spin current is enhanced. Another physical explanation is that the magnetic field aligns the spins along its direction. Therefore, when H_0 is positive or negative the spins are forced to point in the direction of the z-axis or in the opposite direction, respectively. The spin current gets more polarized in the direction of the z-axis for $H_0 > 0$ or in the opposite direction for $H_0 < 0$. As a consequence its magnitude decreases for $H_0 > 0$ or increases for $H_0 < 0$ since it was polarized in the direction opposite to the one of the z-axis in the absence of the magnetic field.

The same dependence of the spin current on the magnetic field with small values of its magnitude (as well as for a small value of the driving amplitude $FL = 1.0\,\hbar\omega_0$) is found in Fig. 5.2 in view of its dependence on the spin-orbit interaction strength

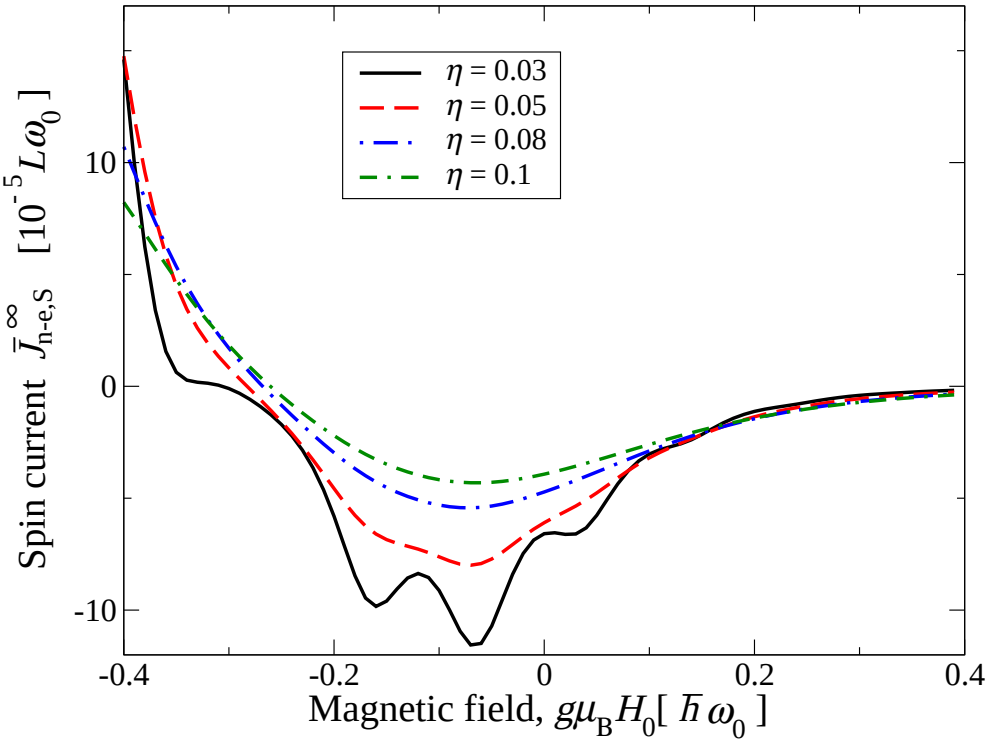

Figure 5.4: Non-equilibrium spin current, $\bar{J}^{\infty}_{\text{n-e,S}}$, as a function of the magnetic field, $g\mu_B H_0$, for different values of the viscosity coefficient, η. The driving amplitude is $F = 1.0\hbar\omega_0/L$. The other parameters are as in Fig. 5.1.

k_{so}. As before, for $H_0 > 0$ the magnitude of the spin-current gets smaller and for $H_0 < 0$ it gets larger. The minima and maxima of the spin current magnitude in Fig. 5.2 are related to the periodicity of the energy spectrum in the $\vec{k}$-space. The minima of the spin current magnitude are located at $nG/2$ where $n = 0, 1, 2, \ldots$, and G is the reciprocal lattice vector. Physically this reflects the fact that for those values of k_{so} the Rashba split of the energy bands becomes minimal. From Eqs. (3.20) and (3.21) as well as from Figs. 3.1 and 3.2 it is clear that for $k_{so} = nG/2$ the band minima meet each other and the band structure looks almost like a band structure without RSOI. In this case the only trace of RSOI is in the hybridization effects (Ξ term in Eq. (3.21)) which are very weak in the tight-binding case. As a result at $k_{so} = nG/2$ the values of the spin current are very close to zero but, because of the hybridization, the spin current is not exactly zero at these points. The oscillatory behavior of the spin current is thus a specific feature of the Rashba-Bloch energy spectrum: it results from both the periodicity of the energy spectrum in the $\vec{k}$-space and Rashba split of the energy bands. These oscillations cannot appear within the usual Rashba spectrum, discussed in Chapter 2, because in this case the band minima never meet each other when k_{so} increases. Instead, the distance between them gets larger for larger values of k_{so} as it is obvious from Eq. (2.14) as well as from Fig. 2.6e.

One can see that the presence of the magnetic field does not change the locations of minima and maxima of the spin current as a function of k_{so}. This has the following physical explanation. In terms of the band energy versus the quasi-momentum

$\vec{k}$ dependence RSOI produces a horizontal (that is the energy of the bands does not change) split of the energy bands as well as their hybridization (see Figs. 3.1 and 3.2). As discussed above, due to the periodicity of the energy spectrum in the $\vec{k}$-space this split can be minimal or maximal for some values of $k_{\rm so}$ leading to the corresponding minima and maxima in Fig. 5.2. The magnetic field also produces hybridization but, in contrast to the horizontal split of RSOI, it produces a vertical (that is along the energy axis) split similar to the one shown in Fig. 2.6d for a 2DEG in a magnetic field and without RSOI. This vertical split is not correlated with the periodicity of the energy bands in the $\vec{k}$-space. Thus the locations of the minima and maxima in Fig. 5.2 remain untouched by the magnetic field.

However, the picture explained above is only valid for small values of the driving amplitude F and magnitude of the magnetic field $|H_0|$ where the spin current has a linear response to the magnetic field. When $|H_0|$ increases further, the spin current depends non-linearly on H_0 and a complicated interplay between the magnetic field, driving and dissipative processes develops. This dependence of the spin current on the magnetic field is depicted in Fig. 5.3 for different values of the amplitude of the driving force. In order to stay within the validity of our model, where only the first two transverse modes are opened, the magnitude of the magnetic field must satisfy the condition:

$$g\mu_{\rm B}|H_0| \leqslant 0.5(\hbar\omega_0 + \Delta\varepsilon_{\gamma;4,1}), \tag{5.58}$$

where $\Delta\varepsilon_{\gamma;4,1} \equiv \sum_{k_{\rm B}} \left[\varepsilon^{(0)}_{\gamma,1;1}(k_{\rm B}) - \varepsilon^{(0)}_{\gamma,0;1}(k_{\rm B})\right]/N$. For the values of the parameters used to obtain the numerical results we have $\Delta\varepsilon_{\gamma;4,1} = -0.07\hbar\omega_0$. Thus $g\mu_{\rm B}|H_0| \leqslant 0.465\hbar\omega_0$. As it can be seen from Fig. 5.3 the magnitude of the spin current decays for large positive values of H_0. This happens because the distance between the Bloch sub-bands becomes large and thus the transition processes are less probable. For a certain negative value of H_0 the magnitude of the spin current has a maximum after which it starts to decrease and vanishes at some point $H_0^{(0)} < 0$. After this point and for $H_0 < H_0^{(0)}$ the spin current reverses its sign and its magnitude increases again. This behavior clearly demonstrates that the magnetic field can, without changing its direction, act in phase (*i.e.* destroy the spin transport) with the dissipative processes as well as out-of-phase (*i.e.* intensify the spin kinetics) with them. Mathematically it comes from the fact that in Eq. (5.25) for the transition rates the magnetic field H_0 and the imaginary part of the twice integrated bath correlation function $\mathrm{Im}[Q(\tau)]$ enter the arguments of the same trigonometric functions. This is clarified by Eq. (5.29) appropriately rewritten below for the case $\xi' = 1$, $\xi = 4$:

$$J_{\gamma;1,4} = \frac{2}{\hbar^2}\int_0^\infty d\tau \mathrm{e}^{-\frac{L^2}{\hbar}Q_{\rm R}(\tau)} \cos\left[\left(\frac{\Delta\varepsilon_{\gamma;4,1}}{\hbar} + \omega_0 + \frac{2g\mu_{\rm B}H_0}{\hbar}\right)\tau - \frac{L^2}{\hbar}Q_{\rm I}(\tau)\right] \times \\ \times J_0\left[\frac{2FL}{\hbar\Omega}\sin\left(\frac{\Omega\tau}{2}\right)\right], \tag{5.59}$$

where $Q_{\rm R}(\tau) \equiv \mathrm{Re}[Q(\tau)]$, $Q_{\rm I}(\tau) \equiv \mathrm{Im}[Q(\tau)]$. The physical explanation of why in our system the magnetic field interacts only with the friction part of the dissipation and not with its noise part is rooted in the roles which the magnetic field and dissipation play

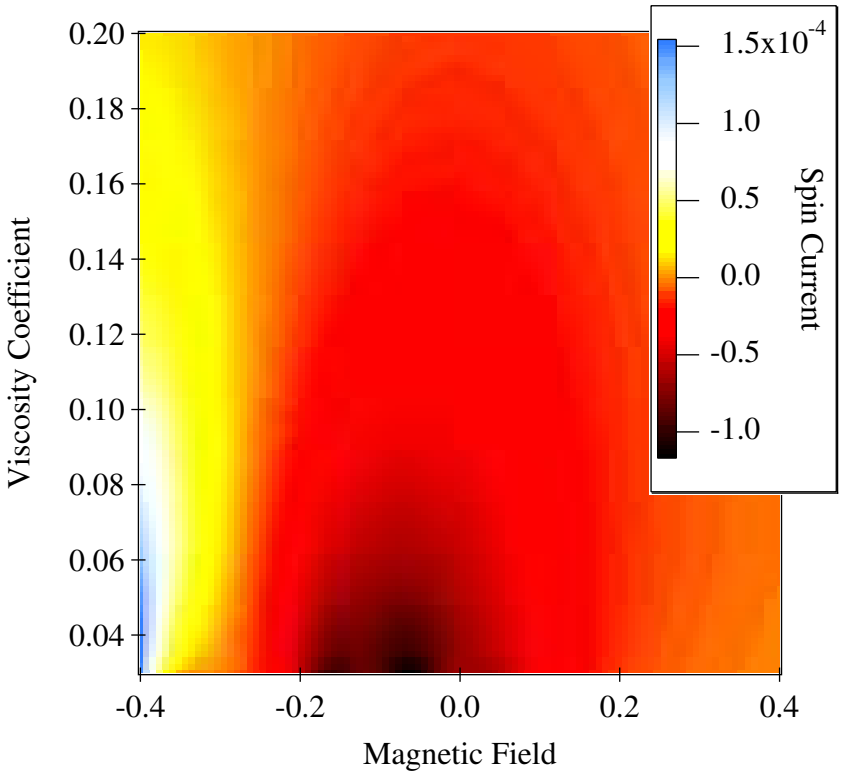

Figure 5.5: Contour plot of the non-equilibrium spin current, $\bar{J}^{\infty}_{\mathrm{n-e,S}}$ $[L\omega_0]$, as a function of the magnetic field, $g\mu_{\mathrm{B}}H_0$ $[\hbar\omega_0]$, and viscosity coefficient, η. The other parameters are as in Fig. 5.1.

for quantum coherence. On the one side quantum coherence in a dissipative system dies out due to the noise part of the Feynman-Vernon influence weight functional. On the other side, within the Feynman path integral formalism, we see that in our system a transverse in-plane uniform stationary magnetic field cannot produce the additional phase due to the integral of the vector potential along the Feynman paths (see Subsection 5.2.1). Thus in our system quantum coherence is totally insensitive to the magnetic field and as a result cannot interact with the noise part of the Feynman-Vernon influence weight functional.

The mutual impact of the magnetic field and quantum dissipative processes on the spin current in the system is shown in Fig. 5.4 where the spin current is plotted versus the magnetic field, H_0, and the viscosity coefficient, η, plays a role of a parameter. Again for large positive values of H_0 the spin current vanishes. As expected, the spin current gets smaller if the dissipation in the system gets stronger. When the dissipation gets weaker ($\eta = 0.05$ and $\eta = 0.03$ curves) the oscillations of the spin current become observable. These oscillations are related to the interaction between the magnetic field and driving and can be described in terms of the photon emission/absorption processes [38] since changing H_0 is equivalent to changing the distance between the corresponding Bloch sub-bands.

The minima in Figs. 5.3 and 5.4 at negative values of H_0 appear as a result of a cooperative action of the orbit-orbit coupling, confinement, magnetic field, driving and dissipation. Its location changes when the strength of the driving and dissipation

varies.

For completeness in Fig. 5.5 we also show the spin current as a contour plot using the variables H_0 and η. The main effect of the interaction between the electrons and external environment is the electron dressing. The dressed electrons are heavier and as a result less mobile. Since the spin degree of freedom is carried by these dressed electrons, the spin current decreases when the viscosity coefficient grows.

5.3 Quantum dissipative charge-spin ratchet: role of magnetic driving

For semiconductor heterostructures with spin-orbit interactions, described for example by Rashba, Eq. (2.1), or Dresselhaus, Eq. (2.3), spin-orbit Hamiltonians, the spin ratchet effect is rooted in an asymmetric excitation of spin dynamics by the orbital dynamics induced by an electric field. For electrically driven coherent and dissipative systems with Rashba spin-orbit interaction (RSOI) the spin ratchet mechanism has been confirmed [62, 67, 69]. Even for symmetric periodic potentials and symmetric driving the spin ratchet effect exists [62]. However, the charge ratchet effect is absent in both the coherent and dissipative cases when both the periodic potential and driving force are symmetric. This could deepen the impression that a system with symmetric periodic potentials will never respond to time-symmetric external fields via the charge ratchet mechanism and systems with spin-orbit interactions like all other systems obey this habitual rule. The present section reveals that this is a delusion and in reality systems with spin-orbit interactions provide a unique opportunity to answer the fundamental questions related to the role of symmetries in the charge ratchet phenomena in general.

Here we show that the space asymmetry of the periodic potentials and the time asymmetry of the driving fields, usually required as key properties of charge ratchets, are not necessary as the Rashba spin flip processes alone are sufficient even if a dissipative system is time-symmetrically driven. Specifically, it is found that the charge ratchet effect in this case exists for space-symmetric periodic potentials and time-symmetric driving by electric and magnetic fields. It stems just from the simultaneous presence of quantum dissipation and the spin flip processes of Rashba electrons. The ratchet charge current in the system is unusual. Its queerness consists in the fact that this current, in contrast to early predictions for systems without spin-orbit interactions [28, 34], appears even when only one energy band provides electrons for transport and no harmonic mixing is present in the driving fields. This charge current is of pure spin-orbit nature and, as a result, it disappears when the spin-orbit coupling strength vanishes. Therefore such spin-orbit charge currents can be controlled by the same gate voltage which controls the strength of the spin-orbit coupling in the system. It is evident that this peculiarity of the charge ratchet current is very attractive from the experimental point of view.

5.3.1 Driving Hamiltonian and the σ-DVR basis: transition rates

The full Hamiltonian of the problem is given by Eq. (5.1). The terms $\hat{H}$ and $\hat{H}_{\rm bath}$ are unchanged. They are given by Eqs. (5.2) and (5.4). The driving term now differs from Eq. (5.6) because now we also include an ac magnetic field. This ac magnetic field has only the z-component, *i.e.*, it is parallel or anti-parallel to the z-axis. Therefore the driving Hamiltonian is

$$\hat{H}_{\rm ext} = eE(t)\hat{x} - g\mu_{\rm B}H(t)\hat{\sigma}_z. \tag{5.60}$$

The vector potential is chosen using the Landau gauge $\vec{A}(t) = (-H(t)y, 0, 0)$. Since $y = 0$ in the 2DEG, the vector potential is not explicitly present in the model. In Eq. (5.60) the time dependence $E(t)$ of the electric field is given by Eq. (5.7). For the magnetic field we use the same time dependence,

$$H(t) = H\cos(\Omega t), \tag{5.61}$$

where H is the amplitude of the magnetic driving.

It is clear that the σ-DVR basis allows the path integral formalism to handle the magnetic driving on an equal footing with the standard electric driving since in this basis the whole driving Hamiltonian $\hat{H}_{\rm ext}(t)$ in Eq. (5.60) is diagonal. We note that this is an exceptional situation arising due to the chosen mutual orientation of the electric and magnetic driving fields.

Since the whole driving Hamiltonian is diagonal in the σ-DVR basis, the argument of the Bessel function in Eq. (5.25) changes,

$$2F(x_{\gamma;m,\xi} - x_{\gamma;m',\xi'}) \to 2F(x_{\gamma;m,\xi} - x_{\gamma;m',\xi'}) + 2g\mu_{\rm B}H(\sigma_\xi - \sigma_{\xi'}). \tag{5.62}$$

As a result, instead of Eq. (5.28), we now have,

$$\begin{aligned} \bar{\Gamma}^{\rm inter,b}_{\gamma;\xi',\xi} &= |\Delta^{\rm inter,b}_{\gamma;\xi',\xi}(m)|^2 J^{\rm inter,b}_{\gamma;\xi',\xi}, \\ \bar{\Gamma}^{\rm inter,f}_{\gamma;\xi',\xi} &= |\Delta^{\rm inter,f}_{\gamma;\xi',\xi}(m)|^2 J^{\rm inter,f}_{\gamma;\xi',\xi}, \end{aligned} \tag{5.63}$$

where

$$\begin{aligned} J^{\rm inter,b}_{\gamma;\xi',\xi} &= \frac{1}{\hbar^2}\int_{-\infty}^{\infty} d\tau \mathrm{e}^{-\frac{L^2}{\hbar}Q(\tau) + \mathrm{i}[(\varepsilon_{\gamma;\xi} - \varepsilon_{\gamma;\xi'})/\hbar]\tau} \times \\ &\times J_0\left[\frac{2FL + 2g\mu_{\rm B}H(\sigma_\xi - \sigma_{\xi'})}{\hbar\Omega}\sin\left(\frac{\Omega\tau}{2}\right)\right], \\ J^{\rm inter,f}_{\gamma;\xi',\xi} &= \frac{1}{\hbar^2}\int_{-\infty}^{\infty} d\tau \mathrm{e}^{-\frac{L^2}{\hbar}Q(\tau) + \mathrm{i}[(\varepsilon_{\gamma;\xi} - \varepsilon_{\gamma;\xi'})/\hbar]\tau} \times \\ &\times J_0\left[\frac{-2FL + 2g\mu_{\rm B}H(\sigma_\xi - \sigma_{\xi'})}{\hbar\Omega}\sin\left(\frac{\Omega\tau}{2}\right)\right]. \end{aligned} \tag{5.64}$$

Before starting a rigorous exploration one can already anticipate that the magnetic field driving brings a whiff of fresh physics because the spin dynamics can be controlled, as can be seen from Eq. (5.64), directly and not only through the spin-orbit interaction mediating between the electric field and electron spins.

5.3.2 Derivation of the charge and spin ratchet currents

To obtain the charge and spin ratchet currents we note that the relation given by Eq. (5.30) is still valid. Further we assume that

$$\varepsilon_{\gamma;\xi} - \varepsilon_{\gamma;\xi'} \neq n\hbar\Omega, \quad n = 0, \pm 1, \dots \ . \tag{5.65}$$

Then Eq. (5.27) takes place also in the presence of an ac magnetic field. However, as one can see from Eqs. (5.63) and (5.64), the relation given by Eq. (5.31) is no longer valid,

$$\bar{\Gamma}^{\mathrm{inter,b}}_{\gamma;\xi',\xi}\bar{\Gamma}^{\mathrm{inter,b}}_{\gamma;\xi,\xi'} \neq \bar{\Gamma}^{\mathrm{inter,f}}_{\gamma;\xi',\xi}\bar{\Gamma}^{\mathrm{inter,f}}_{\gamma;\xi,\xi'}. \tag{5.66}$$

Because of the inequality (5.66) the charge ratchet current is not zero anymore. Indeed, using Eqs. (5.27), (5.30), (5.32) and (5.41) it follows from (5.36) that

$$\bar{J}^{\infty}_{\mathrm{C}} = -eL\frac{2}{\bar{\Gamma}_{\gamma;1,4} + \bar{\Gamma}_{\gamma;4,1}}\big(\bar{\Gamma}^{\mathrm{inter,f}}_{\gamma;1,4}\bar{\Gamma}^{\mathrm{inter,f}}_{\gamma;4,1} - \bar{\Gamma}^{\mathrm{inter,b}}_{\gamma;1,4}\bar{\Gamma}^{\mathrm{inter,b}}_{\gamma;4,1}\big). \tag{5.67}$$

Using (4.32), (5.27), (5.63) and (5.32) we get from (5.67)

$$\bar{J}^{\infty}_{\mathrm{C}} = eL\frac{2|\Delta^{\mathrm{inter,f}}_{\gamma;1,4}(m)|^2|\Delta^{\mathrm{inter,f}}_{\gamma;4,1}(m)|^2\big(J^{\mathrm{inter,b}}_{\gamma;1,4}J^{\mathrm{inter,b}}_{\gamma;4,1} - J^{\mathrm{inter,f}}_{\gamma;1,4}J^{\mathrm{inter,f}}_{\gamma;4,1}\big)}{|\Delta^{\mathrm{inter,f}}_{\gamma;1,4}(m)|^2\big(J^{\mathrm{inter,f}}_{\gamma;1,4} + J^{\mathrm{inter,b}}_{\gamma;4,1}\big) + |\Delta^{\mathrm{inter,f}}_{\gamma;4,1}(m)|^2\big(J^{\mathrm{inter,f}}_{\gamma;4,1} + J^{\mathrm{inter,b}}_{\gamma;1,4}\big)}. \tag{5.68}$$

The expression for the spin ratchet current (5.43) written through the transition rates does not change, but Eq. (5.44) which gives the spin ratchet current through the hopping matrix elements is now replaced with the following one,

$$\bar{J}^{\infty}_{\mathrm{S}} = 2L\frac{|\Delta^{\mathrm{inter,f}}_{\gamma;1,4}(m)|^4 J^{\mathrm{inter,f}}_{\gamma;1,4}J^{\mathrm{inter,b}}_{\gamma;4,1} - |\Delta^{\mathrm{inter,f}}_{\gamma;4,1}(m)|^4 J^{\mathrm{inter,f}}_{\gamma;4,1}J^{\mathrm{inter,b}}_{\gamma;1,4}}{|\Delta^{\mathrm{inter,f}}_{\gamma;1,4}(m)|^2\big(J^{\mathrm{inter,f}}_{\gamma;1,4} + J^{\mathrm{inter,b}}_{\gamma;4,1}\big) + |\Delta^{\mathrm{inter,f}}_{\gamma;4,1}(m)|^2\big(J^{\mathrm{inter,f}}_{\gamma;4,1} + J^{\mathrm{inter,b}}_{\gamma;1,4}\big)}. \tag{5.69}$$

Remarkably, Eqs. (5.68) and (5.69) tell us that at low temperatures the ratchet charge and spin transport in the system exists just because of spin flip processes. Whereas it looks natural for the spin current, it is a quite unexpected and important result for the charge current. This current emerges because the magnetic driving changes the charge dynamics. In this case the spin-orbit interaction plays a role inverse to the one which it plays for the electric driving: the magnetic field exciting spin dynamics induces orbital dynamics through the spin-orbit interaction. The corresponding charge flow, originating just due to the spin-orbit interaction, is finite even when only one energy band contributes to transport.

5.3.3 Charge and spin ratchet effects: analytical analysis

The situation, however, is highly non-trivial and the final conclusions about the existence of the ratchet charge and spin flows cannot be based only on the presence of spin-orbit interactions. There are also external time-dependent fields driving the system and internal quantum dissipative processes. The mutual driving-dissipation effect is incorporated in the integrals, Eq. (5.64). Therefore, a further analysis is required:

one should additionally take into consideration the properties of the integrals from Eq. (5.64) and the properties of the static periodic potential with respect to the spatial inversion symmetry.

There are twelve different cases, shown in Table 5.1, to check whether the charge and spin ratchet effects can take place in the corresponding physical situations. Only those four of them which are given by the row with $F \neq 0$, $H = 0$ have been studied in the thesis up to this point. The other eight possibilities have not been investigated yet.

Table 5.1: Existence of the charge and spin ratchet effects

	$\gamma = 0$		$\gamma \neq 0$	
	$U(x) \neq U(-x)$	$U(x) = U(-x)$	$U(x) \neq U(-x)$	$U(x) = U(-x)$
$F \neq 0$ $H = 0$	$J_{\mathrm{C}} = 0$ $J_{\mathrm{S}} = 0$	$J_{\mathrm{C}} = 0$ $J_{\mathrm{S}} = 0$	$J_{\mathrm{C}} = 0$ $J_{\mathrm{S}} \neq 0$	$J_{\mathrm{C}} = 0$ $J_{\mathrm{S}} = 0$
$F = 0$ $H \neq 0$	$J_{\mathrm{C}} = 0$ $J_{\mathrm{S}} = 0$	$J_{\mathrm{C}} = 0$ $J_{\mathrm{S}} = 0$	$J_{\mathrm{C}} = 0$ $J_{\mathrm{S}} \neq 0$	$J_{\mathrm{C}} = 0$ $J_{\mathrm{S}} = 0$
$F \neq 0$ $H \neq 0$	$J_{\mathrm{C}} \neq 0$ $J_{\mathrm{S}} \neq 0$	$J_{\mathrm{C}} \neq 0$ $J_{\mathrm{S}} \neq 0$	$J_{\mathrm{C}} \neq 0$ $J_{\mathrm{S}} \neq 0$	$J_{\mathrm{C}} \neq 0$ $J_{\mathrm{S}} \neq 0$

The results presented in Table 5.1 are easily obtained from Eqs. (5.68) and (5.69) if one takes into account that for $\gamma = 0$ or $U(x) = U(-x)$ the difference (4.36) is equal to zero (see Subsection 5.2.9) and for $F = 0$ or $H = 0$ one makes use of the equality $J^{\mathrm{inter,f}}_{\gamma;\xi',\xi} = J^{\mathrm{inter,b}}_{\gamma;\xi',\xi}$ which follows from Eq. (5.64).

The principal feature of the physics taking place when $F \neq 0$ and $H \neq 0$ is that the existence of the ratchet effects is *not* dictated only by properties of the isolated system as it was the case in Section 5.2. The physical picture is now more intricate. In the charge and spin currents one cannot find clear traces of either driving and dissipation or the isolated system. The two imprints are not separable and the charge and spin ratchet mechanisms are determined by the whole system-plus-bath complex.

5.3.4 Charge and spin ratchet effects: numerical analysis

Numerical calculations based on Eqs. (5.68), (5.69) and (5.64) have been performed to obtain the dependence of the ratchet currents on F and H. Figure 5.6 shows the situation with $\gamma = 0$. The superlattice is modeled by the potential $U(x) = V_0 + \sum_{l=1}^{2} V_l \cos(2\pi l x/L - \phi_l)$ with $V_0 = -V_1 = 2.6\hbar\omega_0$, $V_2 = 1.9\hbar\omega_0$, $\phi_1 = 1.9$, $\phi_2 = 0$ for the asymmetric case while for the symmetric one $V_0 = -V_1 = 2.6\hbar\omega_0$, $V_2 = 0$, $\phi_1 = \phi_2 = 0$. The period is $L = 2.5\sqrt{\hbar/m\omega_0}$ which gives $k_{\mathrm{so}}L \approx 0.368\pi$. The driving frequency of the electric and magnetic fields is $\Omega = \sqrt{3}\omega_0/4$. The bath is Ohmic with the exponential cut-off at $\omega_c = 10\omega_0$: $J(\omega) = \eta\omega \exp(-\omega/\omega_c)$. The viscosity coefficient is $\eta = 0.1$ and the temperature is $k_{\mathrm{B}}T = 0.5\hbar\omega_0$. As theoretically expected the ratchet effects exist even when the periodic potential is symmetric, Figs. 5.6a and 5.6c. However, the currents of these intrinsic ratchet effects are much smaller than the

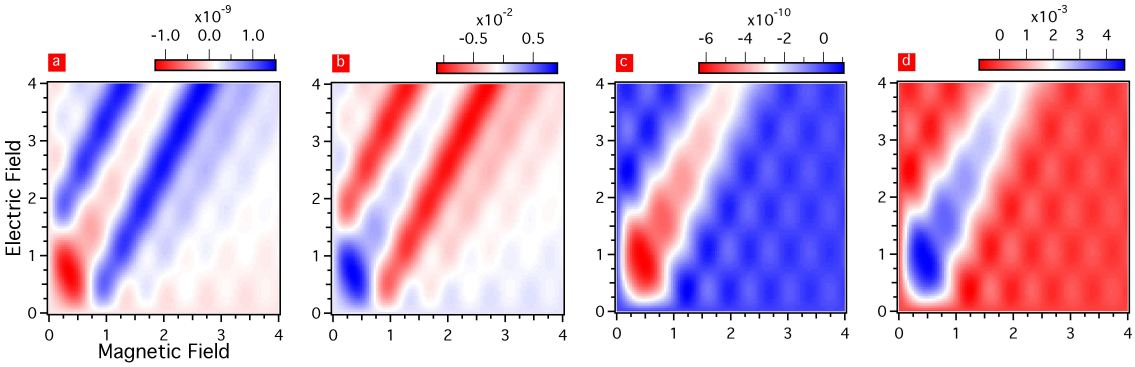

Figure 5.6: The charge and spin ratchet currents as functions of the amplitudes of the electric and magnetic fields. a,b, Spin current for the symmetric and asymmetric cases, respectively. c,d, Charge current for the symmetric and asymmetric cases, respectively. The amplitudes of the electric, FL, and magnetic, $g\mu_{\mathrm{B}}H$, fields are in units of $\hbar\omega_0$. The currents are in units of $L\omega_0$. The orbit-orbit coupling is absent, $\gamma = 0$, but the spin current is finite in the symmetric case when both of the fields are present. The charge current is excited when both the electric and magnetic fields simultaneously drive the system. In the intrinsic ratchet response (a and c) the magnitude of the charge and spin currents is strongly suppressed by the symmetry of the periodic potential while in the extrinsic ratchet response (b and d) the charge and spin currents are enhanced by the spatial asymmetry of the system.

corresponding currents of the extrinsic ones, Fig. 5.6b and 5.6d. What is surprising in the case when both of the driving fields are present is that the orbit-orbit coupling has a weak effect on the ratchet spin current as it is demonstrated in Fig. 5.7. At the same time when $H = 0$ the orbit-orbit coupling is responsible for the existence of the pure spin ratchet effect (see Subsection 5.2.9) as one can see in the inset of Fig. 5.7a. Physically it is explained by the increased contribution from the spin torque to the spin current. When $H \neq 0$, the high-frequency magnetic field flips periodically the electron spins. Since this field is uniform the difference (which is created by the orbit-orbit coupling) between the group velocities of the electrons moving in the center of the wire and closer to its edges is not decisive for the ratchet effect. The contribution to the spin current coming from the group velocity is now smaller than the one due to the spin torque and as a result the orbit-orbit coupling has a little impact on the spin current.

5.4 Conclusion

In this chapter, we have studied averaged stationary quantum transport in an electrically and magnetically driven dissipative periodic quasi-1D system with RSOI assuming moderate-to-strong dissipation.

For the case of an ac electric driving the system has additionally been placed in a transverse in-plane uniform stationary magnetic field. It has been shown that in this case the averaged stationary charge transport is well suppressed as soon as it is restricted within the Bloch sub-bands grown out of the same Bloch band of the corresponding truly 1D problem without RSOI. However in the same situation the averaged stationary spin transport is activated. The analytical expression for the spin

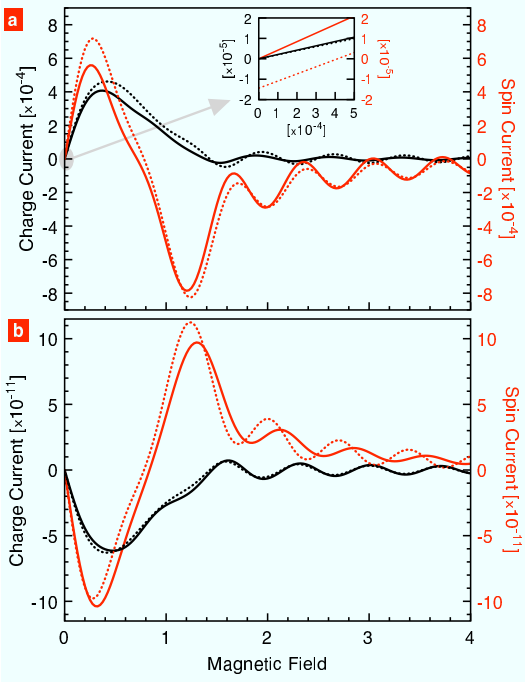

Figure 5.7: The charge and spin ratchet currents as functions of the magnetic field amplitude. The magnetic amplitude, $g\mu_B H$, is in units of $\hbar\omega_0$. The electric amplitude is fixed, $FL = \hbar\omega_0$. The solid curves correspond to $\gamma = 0$. The dotted curves correspond to $\gamma = 0.1$. a, Asymmetric case. The inset shows a vicinity of the point $H = 0$ at which the pure spin ratchet response takes place for $\gamma \neq 0$. b, Symmetric case.

current has been derived and its behavior as a function of the driving parameters, dissipation, RSOI strength, orbit-orbit coupling strength and a transverse in-plane uniform stationary magnetic field has been analyzed. Our results on the spin transport in the system have been presented and thoroughly discussed. It has been found that the spin current as a function of the magnetic field shows a highly non-trivial dependence for different values of the dissipation and driving parameters. In particular, increasing the magnitude of the magnetic field does not always lead to a monotonous response in the magnitude of the spin current. The magnitude of the spin current can have maxima after which its dependence on the magnitude of the magnetic field changes to the opposite one. Moreover, the spin current as a function of the amplitude of an external longitudinal ac electric field has reversals of its direction when the system is placed in a finite transverse in-plane uniform stationary magnetic field. Also as a function of this magnetic field the spin current changes its direction at finite values of the amplitude of the ac electric field. Such behavior is undoubtedly related to a deep correlation between the dissipative processes and magnetic field effects in the system.

When additionally an ac magnetic driving has been included in the problem, we have shown that the existence of spin flip processes in a dissipative system is already sufficient to produce the charge ratchet effect even if the periodic potential is space-symmetric and the system is driven by time-symmetric fields. The charge ratchet current has been found to have a purely spin flip origin. Space asymmetry of the periodic potential and time asymmetry of the driving fields have not been necessary.

Although we have considered RSOI as a mechanism for the electron spin flip, the result can be more general: the charge ratchet mechanism resulting from spin flip processes (not necessarily due to RSOI) may take place when the periodic potential is space-symmetric and driving fields are time-symmetric.

Chapter 6

Conclusion - Zusammenfassung

In this thesis we have studied the charge and spin ratchet dynamics in a dissipative system with spin-orbit interactions. More exactly, we have investigated the possibility to implement an incoherent space rocked charge and spin ratchet mechanisms in the form of a Brownian charge and spin motor resulting from a dissipative coupling of a quasi-1D system formed in a 2DEG with RSOI to an external environment. Our research has involved the following steps and results.

In Chapter 3 we have first performed a general analysis of the energy spectrum of a superlattice based on a 2DEG with RSOI. The superlattice has been formed by means of a longitudinal periodic potential of a general shape and by a transverse potential of a totally arbitrary form. A general eigenvalue problem has been formulated. Afterwards assuming the case of a harmonic confinement and taking into account only the first two transverse modes we have found the structure of the eigenenergies and eigenstates. Finally, a generalization to include a transverse in-plane static magnetic field and orbit-orbit coupling has been performed.

In Chapter 4 we have used the eigenstates obtained in Chapter 3 to find a basis diagonalizing the coordinate and spin operators. This basis, so-called σ-DVR basis, has been found and used to construct an effective low temperature tight-binding model of the RSOI superlattice from Chapter 3. This tight-binding model has been derived assuming that at low temperatures only the first four Bloch sub-bands are populated with electrons.

In Chapter 5 the superlattice from Chapter 3 was coupled to an external environment within the model of Caldeira and Leggett. Additionally, the superlattice has been externally driven. We have used two types of this driving: 1) by pure electric field; 2) by electric and magnetic fields. Both asymmetric and symmetric shapes of the superlattice periodic potential have been considered. Using the effective σ-DVR tight-binding model from Chapter 4 the charge and spin ratchet mechanisms have been explored both analytically and numerically. It has been shown that for the case of pure electric driving the charge ratchet mechanism is absent while the spin ratchet mechanism exists only when the periodic potential of the superlattice is asymmetric and both the spin-orbit and orbit-orbit coupling strengths are finite. For the case of electric and magnetic driving it has been demonstrated that the charge and spin

ratchet mechanisms exist for both symmetric and asymmetric shapes of the superlattice periodic potential. A remarkable result in this case is that the charge ratchet current flows only because of the coexistence of quantum dissipative processes with spin flip processes induced by RSOI. This current is thus of pure spin-orbit nature and as a result it is absent in the corresponding systems without RSOI.

Chapter 7

Acknowledgement - Dankeschön

I would like to thank Prof. Milena Grifoni and Prof. Klaus Richter for sharing their excellent knowledge of condensed matter theory with me during my PhD study. I am grateful to Dr. Dario Bercioux for working with me and especially for his professional support in the computational part of our research. The regular and fruitful discussions with Milena, Klaus and Dario always stimulated me and resulted in a productive collaboration. Additionally, I thank Dario for the Capri Spring School on Transport in Nanostructures 2009 in which his contribution produced a very warm and friendly atmosphere pervading this excellent school which definitely left a trace in my scientific views and not only.

A discussion on coherent and incoherent transport with Dr. Andrea Donarini was very helpful in the corresponding classification of the charge and spin ratchets mechanism in Chapter 1.

For many different discussions on the subject of the thesis and on modern condensed matter theory in general which I had during my PhD study I thank my colleagues, Georg Begemann, Marco Boselli, Björn Erbe, Johannes Hausinger, Sonja Koller, Magdalena Marganska and Carmen Vierheilig, as well as my former colleagues, Leonhard Mayrhofer, Francesco Nesi and Shidong Wang.

* * *

Support from the DFG under the program SFB 689 is acknowledged.

Bibliography

[1] R. Brown. A brief account of microscopical observations made in the months of June, July and August, 1827, on the particles contained in the pollen of plants; and on the general existence of active molecules in organic and inorganic bodies. *Edinburgh New Phil. J.*, 5:358, 1828.

[2] R.D. Astumian and P. Hänggi. Brownian motors. *Phys. Today*, 55:33, 2002.

[3] M. Smoluchowski. Experimentell nachweisbare der üblichen thermodynamik widersprechende molekularphänomene. *Phys. Z.*, 13:1069, 1912.

[4] M.O. Magnasco. Forced thermal ratchets. *Phys. Rev. Lett.*, 71:1477, 1993.

[5] P. Jung, J.G. Kissner, and P. Hänggi. Regular and chaotic transport in asymmetric periodic potentials: Inertia ratchets. *Phys. Rev. Lett.*, 76:3436, 1996.

[6] J.L. Mateos. Chaotic transport and current reversal in deterministic ratchets. *Phys. Rev. Lett.*, 84:258, 2000.

[7] J.L. Mateos. Current reversals in chaotic ratchets: the battle of the attractors. *Physica A*, 325:92, 2003.

[8] M. Borromeo, G. Costantini, and F. Marchesoni. Deterministic ratchets: Route to diffusive transport. *Phys. Rev. E.*, 65:041110, 2002.

[9] L. Machura, M. Kostur, P. Talkner, J. Luczka, and P.änggi. Absolute negative mobility induced by thermal equilibrium fluctuations. *Phys. Rev. Lett.*, 98:040601, 2007.

[10] L. Machura, M. Kostur, P. Talkner, J. Luczka, F. Marchesoni, and P. Hänggi. Brownian motors: Current fluctuations and rectification efficiency. *Phys. Rev. E*, 70:061105, 2004.

[11] F. Marchesoni, S. Savel'ev, and F. Nori. Achieving optimal rectification using underdamped rocked ratchets. *Phys. Rev. E*, 73:021102, 2006.

[12] S. Flach, O. Yevtushenko, and Y. Zolotaryuk. Directed current due to broken time-space symmetry. *Phys. Rev. Lett.*, 84:2358, 2000.

[13] A. Lorke, S. Wimmer, B. Jager, J.P. Kotthaus, W. Wegscheider, and M. Bichler. Far-infrared and transport properties of antidot arrays with broken symmetry. *Physica B*, 249-251:312, 1998.

[14] S. Sassine, Yu. Krupko, J.-C. Portal, Z.D. Kvon, R. Murali, K.P. Martin, G. Hill, and A.D. Wieck. Experimental investigation of the ratchet effect in a two-dimensional electron system with broken spatial inversion symmetry. *Phys. Rev. B*, 78:045431, 2008.

[15] A.D. Chepelianskii, M.V. Entin, L.I. Magarill, and D.L. Shepelyansky. Ratchet transport of interacting particles. *Phys. Rev. E*, 78:041127, 2008.

[16] Y.M. Blanter and M. Büttiker. Rectification of fluctuations in an underdamped ratchet. *Phys. Rev. Lett.*, 81:4040, 1998.

[17] P. Reimann. Brownian motors: noisy transport far from equilibrium. *Phys. Rep.*, 361:57, 2002.

[18] P. Olbrich, E.L. Ivchenko, R. Ravash, T. Feil, S.D. Danilov, J. Allerdings, D. Weiss, D. Schuh, W. Wegscheider, and S.D. Ganichev. Ratchet effects induced by terahertz radiation in heterostructures with a lateral periodic potential. *Phys. Rev. Lett.*, 103:090603, 2009.

[19] F. Jülicher, A. Ajdari, and J. Prost. Modeling molecular motors. *Rev. Mod. Phys.*, 69:1269, 1997.

[20] P. Hänggi and F. Marchesoni. Artificial Brownian motors: Controlling transport on the nanoscale. *Rev. Mod. Phys.*, 81:387, 2009.

[21] P. Reimann, M. Grifoni, and P. Hänggi. Quantum ratchets. *Phys. Rev. Lett.*, 79:10, 1997.

[22] J.B. Majer, J. Peguiron, M. Grifoni, M. Tusveld, and J.E. Mooij. Quantum ratchet effect for vortices. *Phys. Rev. Lett.*, 90:056802, 2003.

[23] H. Linke, T.E. Humphrey, A. Löfgren, A.O. Sushkov, R. Newbury, R.P. Taylor, and P. Omling. Experimental tunneling ratchets. *Science*, 286:2314, 1999.

[24] R. Roncaglia and G.P. Tsironis. Discrete quantum motors. *Phys. Rev. Lett.*, 81:10, 1998.

[25] S. Scheidl and V.M. Vinokur. Quantum Brownian motion in ratchet potentials. *Phys. Rev. B*, 65:195305, 2002.

[26] J. Lehmann, S. Kohler, P. Hänggi, and A. Nitzan. Molecular wires acting as coherent quantum ratchets. *Phys. Rev. Lett.*, 88:228305, 2002.

[27] L. Machura, M. Kostur, P. Hänggi, P. Talkner, and J. Luczka. Consistent description of quantum Brownian motors operating at strong friction. *Phys. Rev. E*, 70:031107, 2004.

[28] M. Grifoni, M.S. Fereira, J. Peguiron, and J.B. Majer. Quantum ratchets with few bands below the barrier. *Phys. Rev. Lett.*, 89:146801, 2002.

[29] J. Peguiron and M. Grifoni. Duality relation for quantum ratchets. *Phys. Rev. E*, 71:010101(R), 2005.

[30] J. Rammer. *Quantum Transport Theory.* Perseus Books, Reading, Massachusetts, 1998.

[31] U. Weiss. *Quantum Dissipative Systems.* World Scientific, Singapore, 3 edition, 2008.

[32] S. Datta. *Electronic Transport in Mesoscopic Systems.* Cambridge University Press, Cambridge, UK, 1995.

[33] A.O. Caldeira and A.J. Leggett. Influence of dissipation on quantum tunneling in macroscopic systems. *Phys. Rev. Lett.*, 46:211, 1981.

[34] I. Goychuk and P. Hänggi. Quantum rectifiers from harmonic mixing. *EPL*, 43:503, 1998.

[35] I. Goychuk and P. Hänggi. Minimal quantum Brownian rectifiers. *J. Phys. Chem.*, 105:6642, 2001.

[36] D.O. Harris, G.G. Engerholm, and W.D. Gwinn. Calculation of matrix elements for one-dimensional quantum-mechanical problems and the application to anharmonic oscillators. *J. Chem. Phys.*, 43:1515, 1965.

[37] M. Grifoni, M. Sassetti, and U. Weiss. Exact master equations for driven dissipative tight-binding models. *Phys. Rev. E*, 53:R2033, 1996.

[38] M. Grifoni and P. Hänggi. Driven quantum tunneling. *Phys. Rep.*, 304:229, 1998.

[39] L. Hartmann, M. Grifoni, and P. Hänggi. Dissipative transport in dc-ac-driven tight-binding lattices. *EPL*, 38:497, 1997.

[40] I. Goychuk and P. Hänggi. Quantum dynamics in strong fluctuating fields. *Adv. Phys.*, 54:525, 2005.

[41] I. Goychuk, M. Grifoni, and P. Hänggi. Nonadiabatic quantum Brownian rectifiers. *Phys. Rev. Lett.*, 81:649, 1998.

[42] V.S. Khrapai, S. Ludwig, J.P. Kotthaus, H.P. Tranitz, and W. Wegscheider. Double-dot quantum ratchet driven by an independently biased quantum point contact. *Phys. Rev. Lett.*, 97:176803, 2006.

[43] A. Vidan, R.M. Westervelt, M. Stopa, M. Hanson, and A.C. Gossard. Triple quantum dot charging rectifier. *Appl. Phys. Lett.*, 85:3602, 2004.

[44] H. Linke, W. Sheng, A. Löfgren, H. Xu, P. Omling, and P.E. Lindelof. A quantum dot ratchet: Experiment and theory. *EPL*, 44:341, 1998.

[45] J. Lehmann, S. Kohler, and P. Hänggi. Rectification of laser-induced electronic transport through molecules. *J. Chem. Phys.*, 118:3283, 2003.

[46] F.D.M. Haldane. 'Luttinger liquid theory' of one-dimensional quantum fluids: I. Properties of the Luttinger model and their extension to the general 1D interacting spinless Fermi gas. *J. Phys. C: Solid State Phys.*, 14:2585, 1981.

[47] T. Giamarchi. *Quantum Physics in One Dimension.* Oxford University Press, New York, US, 2003.

[48] D.E. Feldman, S. Scheidel, and V.M. Vinokur. Rectification in Luttinger liquids. *Phys. Rev. Lett.*, 94:186809, 2005.

[49] S. Denisov, L. Morales-Molina, S. Flach, and P. Hänggi. Periodically driven quantum ratchets: Symmetries and resonances. *Phys. Rev. A*, 75:063424, 2007.

[50] D. Poletti, G.G. Carlo, and B. Li. Current behavior of a quantum Hamiltonian ratchet in resonance. *Phys. Rev. E*, 75:011102, 2007.

[51] A. Kenfack, J. Gong, and A.K. Pattanayak. Controlling the ratchet effect for cold atoms. *Phys. Rev. Lett.*, 100:044104, 2008.

[52] J. Wang and J. Gong. Quantum ratchet accelerator without a bichromatic lattice potential. *Phys. Rev. E*, 78:036219, 2008.

[53] I. Dana, V. Ramareddy, I. Talukdar, and G.S. Summy. Experimental realization of quantum-resonance ratchets at arbitrary quasimomenta. *Phys. Rev. Lett.*, 100:024103, 2008.

[54] L. Morales-Molina and S. Flach. Resonant ratcheting of a Bose-Einstein condensate. *New J. Phys.*, 10:013008, 2008.

[55] J. Pelc, J. Gong, and P. Brumer. Chaos and correspondence in classical and quantum Hamiltonian ratchets: A Heisenberg approach. *Phys. Rev. E*, 79:066207, 2009.

[56] L.D. Landau and E.M. Lifshitz. *Course of Theoretical Physics, Quantum Mechanics (Non-Relativistic Theory)*, volume 3. Butterworth-Heinemann, Oxford, UK, 1981.

[57] E.I. Rashba. Spin currents in thermodynamic equilibrium: The challenge of discerning transport currents. *Phys. Rev. B*, 68:241315(R), 2003.

[58] E.B. Sonin. Proposal for measuring mechanically equilibrium spin currents in the Rashba medium. *Phys. Rev. Lett.*, 99:266602, 2007.

[59] J. Shi, P. Zhang, D. Xiao, and Q. Niu. Proper definition of spin current in spin-orbit coupled systems. *Phys. Rev. Lett.*, 96:076604, 2006.

[60] P. Zhang, Z. Wang, J. Shi, D. Xiao, and Q. Niu. Theory of conserved spin current and its application to a two-dimensional hole gas. *Phys. Rev. B*, 77:075304, 2008.

[61] M. Scheid, M. Wimmer, D. Bercioux, and K. Richter. Zeeman ratchets for ballistic spin currents. *Phys. Stat. Sol. (c)*, 3:4235, 2006.

[62] M. Scheid, D. Bercioux, and K. Richter. Zeeman ratchets: pure spin current generation in mesoscopic conductors with non-uniform magnetic fields. *New J. Phys.*, 9:401, 2007.

[63] E.I. Rashba. Properties of semiconductors with an extremum loop I. Cyclotron and combinational resonance in a magnetic field perpendicular to the plane of the loop. *Fiz. Tverd. Tela (Leningrad)*, 2:1224, 1960. [Sov. Phys. Solid State 2, 1109 (1960)].

[64] M. Scheid, A. Pfund, D. Bercioux, and K. Richter. Coherent spin ratchets: A spin-orbit based quantum ratchet mechanism for spin-polarized currents in ballistic conductors. *Phys. Rev. B*, 76:195303, 2007.

[65] M. Scheid, A. Lassl, and K. Richter. Resonant-tunneling-based spin ratchets. *EPL*, 87:17001, 2009.

[66] S. Smirnov, D. Bercioux, and M. Grifoni. Bloch's theory in periodic structures with Rashba's spin-orbit interaction. *EPL*, 80:27003, 2007.

[67] S. Smirnov, D. Bercioux, M. Grifoni, and K. Richter. Quantum dissipative Rashba spin ratchets. *Phys. Rev. Lett.*, 100:230601, 2008.

[68] M.E. Flatte. A one-way street for spin current. *Nature Physics*, 4:587, 2008.

[69] S. Smirnov, D. Bercioux, M. Grifoni, and K. Richter. Interplay between quantum dissipation and an in-plane magnetic field in the spin ratchet effect. *Phys. Rev. B*, 78:245323, 2008.

[70] S. Smirnov, D. Bercioux, M. Grifoni, and K. Richter. *arXiv:0903.2765v1.*

[71] D. Stein, K. v. Klitzing, and G. Weimann. Electron spin resonance on GaAs-$Al_xGa_{1-x}As$ heterostructures. *Phys. Rev. Lett.*, 51:130, 1983.

[72] H. L. Stormer, Z. Schlesinger, A. Chang, D. C. Tsui, A. C. Gossard, and W. Wiegmann. Energy structure and quantized Hall effect of two-dimensional holes. *Phys. Rev. Lett.*, 51:126, 1983.

[73] Yu. A. Bychkov and E.I. Rashba. Oscillatory effects and the magnetic susceptibility of carriers in inversion layers. *J. Phys. C: Solid State Phys.*, 17:6039, 1984.

[74] A. B. Fowler, F. F. Fang, W. E. Howard, , and P. J. Stiles. Magneto-oscillatory conductance in silicon surfaces. *Phys. Rev. Lett.*, 16:901, 1966.

[75] G. Dresselhaus. Spin-orbit coupling effects in zinc blende structures. *Phys. Rev.*, 100:580, 1955.

[76] E. A. de Andrada e Silva, G. C. La Rocca, and F. Bassani. Spin-split subbands and magneto-oscillations in III-V asymmetric heterostructures. *Phys. Rev. B*, 50:8523, 1994.

[77] E. A. de Andrada e Silva, G. C. La Rocca, and F. Bassani. Spin-orbit splitting of electronic states in semiconductor asymmetric quantum wells. *Phys. Rev. B*, 55:16293, 1997.

[78] J. Nitta, T. Akazaki, H. Takayanagi, and T. Enoki. Gate control of spin-orbit interaction in an inverted $In_{0.53}Ga_{0.47}As/In_{0.52}Al_{0.48}As$ heterostructure. *Phys. Rev. Lett.*, 78:1335, 1997.

[79] Th. Schäpers, G. Engels, J. Lange, Th. Klocke, M. Hollfelder, and H. Lüth. Effect of the heterointerface on the spin splitting in modulation doped $In_xGa_{1-x}As/InP$ quantum wells for $B \to 0$. *J. App. Phys.*, 83:4324, 1998.

[80] D. Grundler. Large Rashba splitting in InAs quantum wells due to electron wave function penetration into the barrier layers. *Phys. Rev. Lett.*, 84:6074, 2000.

[81] Patrick A. Lee and T. V. Ramakrishnan. Disordered electronic systems. *Rev. Mod. Phys.*, 57:287, 1985.

[82] J. B. Miller, D. M. Zumbühl, C. M. Marcus, Y. B. Lyanda-Geller, D. Goldhaber-Gordon, K. Campman, and A. C. Gossard. Gate-controlled spin-orbit quantum interference effects in lateral transport. *Phys. Rev. Lett.*, 90:076807, 2003.

[83] S.D. Ganichev, V.V. Bel'kov, L.E. Golub, E.I. Ivchenko, Petra Schneider, S. Giglberger, J. Eroms, J. De Boeck, G. Borchs, W. Wegscheider, D. Weiss, and W. Prettl. Experimental separation of Rashba and Dresselhaus spin splittings in semiconductor quantum wells. *Phys. Rev. Lett.*, 92:256601, 2004.

[84] S.D. Ganichev, E.L. Ivchenko, V.V. Bel'kov, S.A. Tarasenko, M. Sollinger, D. Weiss, W. Wegscheider, and W. Prettl. Spin-galvanic effect. *Nature*, 417:153, 2002.

[85] B.A. Bernevig, J. Orenstein, and S.-C. Zhang. Exact SU(2) symmetry and persistent spin helix in a spin-orbit coupled system. *Phys. Rev. Lett.*, 97:236601, 2006.

[86] J.D. Koralek, C.P. Weber, J. Orenstein, B.A. Bernevig, S.-C. Zhang, S. Mack, and D.D. Awschalom. Emergence of the persistent spin helix in semiconductor quantum wells. *Nature*, 458:610, 2009.

[87] J. Fabian. Spin's lifetime extended. *Nature*, 458:580, 2009.

[88] Supriyo Datta and Biswajit Das. Electronic analog of the electro-optic modulator. *Appl. Phys. Lett.*, 56:665, 1990.

[89] A.V. Moroz and C.H.W. Barnes. Effect of the spin-orbit interaction on the band structure and conductance of quasi-one-dimensional systems. *Phys. Rev. B*, 60:14272, 1999.

[90] A.V. Moroz and C.H.W. Barnes. Spin-orbit interaction as a source of spectral and transport properties in quasi-one-dimensional systems. *Phys. Rev. B*, 61:R2464, 2000.

[91] M. Governale and U. Zülicke. Spin accumulation in quantum wires with strong Rashba spin-orbit coupling. *Phys. Rev. B*, 66:073311, 2002.

[92] C.A. Perroni, D. Bercioux, V.M. Ramaglia, and V. Cataudella. Rashba quantum wire: exact solution and ballistic transport. *J.Phys.: Condens. Matter*, 19:186227, 2007.

[93] P. Kleinert, V.V. Bryksin, and Bleibaum. Spin accumulation in lateral semiconductor superlattices induced by a constant electric field. *Phys. Rev. B*, 72:195311, 2005.

[94] V. Ya. Demikhovskii and D.V. Khomitsky. Spin-orbit lateral superlattices: energy bands and spin polarization in 2deg. *Pis'ma Zh. Eksp. Teor. Fiz.*, 83:399, 2006.

[95] V. Ya. Demikhovskii and A.A. Perov. Harper-hofstadter problem for a 2DEG. *EPL*, 76:477, 2006.

[96] N.W. Ashcroft and N.D. Mermin. *Solid State Physics*. Saunders College, Philadelphia, 1976.

[97] L.D. Landau, E.M. Lifshitz, and L.P. Pitaevskii. *Course of Theoretical Physics, Statistical Physics. Part 2: Theory of the condensed state*, volume 9. Butterworth-Heinemann, Oxford, UK, 2002.

[98] J. Luo and P.J. Stiles. Effects of inversion asymmetry on electron energy band structures in GaSb/InAs/GaSb quantum wells. *Phys. Rev. B*, 41:7685, 1990.

[99] V. Sih, R.C. Myers, Y.K. Kato, W.H. Lau, A.C. Gossard, and D.D. Awschalom. Spatial imaging of the spin hall effect and current-induced polarization in two-dimensional electron gases. *Nature Physics*, 1:31, 2005.

[100] Y.K. Kato, R.C. Myers, A.C. Gossard, and D.D. Awschalom. Current-induced spin polarization in strained semiconductors. *Phys. Rev. Lett.*, 93:176601, 2004.

[101] P. Kotissek, M. Bailleul, M. Sperl, A. Spitzer, D. Schuh, W. Wegscheider, C.H. Back, and G. Bayreuther. Cross-sectional imaging of spin injection into a semiconductor. *Nature Physics*, 3:872, 2007.

[102] L.V. Keldysh. Diagram technique for nonequilibrium processes. *Sov. Phys. JETP*, 20:1018, 1965.

[103] T. Schäpers, J. Knobbe, and V.A. Guzenko. Effect of Rashba spin-orbit coupling on magnetotransport in InGaAs/InP quantum wire structures. *Phys. Rev. B*, 69:235323, 2004.

[104] O. Madelung. *Semiconductors: Data Handbook*. Springer, Berlin, 2003.

[105] J. Steinshnider, J. Harper, M. Weimer, C.-H. Lin, S.S. Pei, and D.H. Chow. Origin of antimony segregation in GaInSb/InAs strained-layer superlattices. *Phys. Rev. Lett.*, 85:4562, 2000.